Dissertation

Elucidating the consequences of loss of *MMP-12* in lysosomal acid lipase deficiency

submitted by

Martin Bürger MSc. BSc.

for the academic degree of

Doctor of Philosophy (PhD)

at the

Medical University of Graz

Gottfried Schatz Research Center

Molecular Biology and Biochemistry

under the supervision of

Univ.-Prof. Mag. Dr.rer.nat. Dagmar Kratky

2025

Declaration of Academic Integrity

I hereby confirm that the present diploma thesis is the result of my own independent scholarly work. I also confirm that in all cases, where material from the work of others (in books, articles, essays, dissertations, and on the internet) is acknowledged, quotations and paraphrases are clearly indicated. No material other than that cited in the reference list has been used. I have read and understood the Medical University's regulations and procedures concerning plagiarism.

Furthermore, I hereby declare that if artificial intelligence (AI) tools were used for the generation and/or correction of certain text passages in the creation of this work, such employment was conducted in compliance with ethical principles, academic integrity, and the regulations of my university. Additionally, it was ensured that this usage was transparently disclosed and appropriately attributed.

Martin Bürger Graz, 03.06.2025

Disclosure

Please note that parts of this thesis have been published and/or are under consideration for future publications:

Limited Alleviation of Lysosomal Acid Lipase Deficiency by Deletion of Matrix Metalloproteinase 12.

M. Buerger, M. Amor, A. Akhmetshina, V. Bianco, B. Perfler, A. Zebisch, T. Weichhart, D. Kratky; Int. J. Mol. Sci. 2024, 25, 11001. https://doi.org/10.3390/ijms25201100

Additional co-authors who contributed to this thesis:
ELISA and lipid measurements were performed by A. Ibovnik

All co-authors were contacted for their permission to use the data in this thesis. They all agreed to the use in written statements that were sent to the study management unit of the Medical University of Graz.

During my dissertation studies, I have contributed to the following publications:

Bianco, V; Svecla, M; Vingiani, GB; Kolb, D; Schwarz, B; **Buerger, M**; Beretta, G; Norata, GD; Kratky, D. - *Regional Differences in the Small Intestinal Proteome of Control Mice and of Mice Lacking Lysosomal Acid Lipase.* J Proteome Res. 2024; 23(4): 1506-1518. Doi: 10.1021/acs.jproteome.4c00082

Amor, M; Bianco, V; **Buerger, M**; Lechleitner, M; Vujić, N; Dobrijević, A; Akhmetshina, A; Pirchheim, A; Schwarz, B; Pessentheiner, AR; Baumgartner, F; Rampitsch, K; Schauer, S; Klobučar, I; Degoricija, V; Pregartner, G; Kummer, D; Svecla, M; Sommer, G; Kolb, D; Holzapfel, GA; Hoefler, G; Frank, S; Norata, GD; Kratky, D. - *Genetic deletion of MMP12 ameliorates cardiometabolic disease by improving insulin sensitivity, systemic inflammation, and atherosclerotic features in mice*. Cardiovasc Diabetol. 2023; 22(1): 327 Doi: 10.1186/s12933-023-02064-3

Bianco, V; Korbelius, M; Vujic, N; Akhmetshina, A; Amor, M; Kolb, D; Pirchheim, A; Bradic, I; Kuentzel, KB; **Buerger, M**; Schauer, S; Phan, HTT; Bulfon, D; Hoefler, G; Zimmermann, R; Kratky, D. - *Impact of (intestinal) LAL deficiency on lipid metabolism and macrophage infiltration.* Mol Metab. 2023; 73: 101737 Doi: 10.1016/j.molmet.2023.101737.

“The more we learn about the world, and the deeper our learning, the more conscious, specific, and articulate will be our knowledge of what we do not know”

- Karl Popper

Acknowledgements

Most importantly, I would like to express my deepest appreciation and gratitude to my supervisor Dagmar Kratky. You are not only leading this team by example but also inspire everyone around you to rise to your level. Your guidance as my mentor and the support and patience you have displayed were essential for this project's success. I am grateful for the freedom you have given me to steer this project into unexpected territories far off its initial plan.

I am sincerely thankful to the godmother of my dissertation, Melina Amor. I am grateful for your support and care, and I am glad to have shared MMP-12 with you.

I want to acknowledge my thesis committee Sasa Frank, Tarek Moustafa and Branislav Radovic, for their rigorous input and valuable help.

I am grateful to our collaborators Armin Zebisch and Bianca Perfler for sharing their expertise and answering an uncountable number of questions. Your support was instrumental for the success of this project.

During my research stay I was fortunate to join Thomas Weichhart and his group. Thank you, Mario, Paul, Alishan, Piyal, Jayne and Tayeba for their help and company.

I want to express my appreciation for the funding institutions FWF, SFB Lipid Hydrolysis, Medical University of Graz, as well as the international PhD program "Metabolic and Cardiovascular Diseases", particularly acknowledging Karin Osibow for her support and management of student affairs.

I want to thank all the current and former members of the Kratky Lab, Anton, Valentina, Alena, Anja, Melanie, Nemo, Ivan, Kathi, Anita, Silvia, Birgit, Helga, Irmi, Stefan, Laszlo, Suravi, Malena and Vanessa. I count myself lucky to have been part of this family!

A sincere thank you to my parents. You never stopped believing in me and supported me for as long as I remember no matter the endeavor.

Last but not least, I want to thank my fiancé, Theresa. Your support and encouragement throughout this difficult journey have been invaluable to me!

Table of Contents

Abbreviations

ALT	Alanine aminotransferase
AST	Aspartate aminotransferase
AT	Adipose tissue
BAT	Brown adipose tissue
BMDMs	Bone marrow-derived macrophages
CE	Cholesteryl esters
CEACAM-1	Carcinoembrionic antigen-related cell adhenison molecule 1
CESD	Cholesteryl ester storage disease
CLP	Common lymphoid progenitors
CMP	Common myeloid progenitors
DKO	Double knockout
ECM	Extracellular matrix
ERT	Enzyme replacement therapy
eWAT	Epididymal white adipose tissue
Elane	Neutrophil elastase
FC	Free cholesterol
FFA	Free fatty acids
GMPs	Granulocyte-macrophage-progenitor cells
GRA	Granulocyte count
H&E	Hematoxylin and eosin
HCT	Hematocrit
HFD	High fat diet
HGB	Hemoglobin concentration
hLAL	Human lysosomal acid lipase
KO	Knockout
LAL	Lyosomal acid lipase
LAL-D	Lysosomal acid lipase deficiency
LDL	Low-density lipoprotein
LK	Lin- c-Kit+
LSK	Lin- Sca-1+ c-Kit+
LYM	Lymphocyte count
Lin-	Lineage negative

mTOR	Mammalian target of rapamycin
MAFLD	Metabolic dysfunctin-associated fatty liver disease
MCH	Mean corpuscular hemoglobin
MCHC	Mean corpuscular hemoglobin concentration
MCV	Mean corpuscular volume
MDSC	Myeloid-derived suppressor cells
MEP	Megakaryocyte-erythrocyte progenitors
MMP-12	Matrix metalloproteinase 12
MON	Monocyte count
MPV	Mean platelet volume
NASH	Non-alcoholic steatohepatitis
NET	Neutrophil extracellular trap
NO	Nitric oxide
PCT	Procalcitonin
PDW	Platelet distribution width
PGE2	Prostaglandin E2
PLA	Platelet-leukocyte aggregate
PLT	Platelet (thrombocyte) count
PMN	Polymorphonuclear
PPARα/ɣ	peroxisome proliferator-activated receptor α/ɣ
RBC	Red blood cells (erythrocytes)
% RDW	Red blood cell distribution width %
ROS	Reactive oxygen species
SAA	Serum amyloid A
sEDP	Soluble elastin-derived peptides
sWAT	Subcutaneous white adipose tissue
TAG	Triacylglycerol
TC	Total cholesterol
TIMP	Tissue inhibitor of MMPs
VLDL	Very low-density lipoprotein
WBC	White blood cell count
WT	Wild type

Zusammenfassung

Hintergrund: Die lysosomale saure Lipase-Defizienz (LAL-D) ist eine seltene lysosomale Speicherkrankheit, die durch eine gestörte Spaltung von Cholesterinestern und Triglyceriden gekennzeichnet ist und chronische Entzündungen sowie eine Dysfunktion des Immunsystems verursacht. Studien zeigten eine deutlich erhöhte Expression der Matrix-Metalloproteinase-12 (MMP-12) in LAL-D Mäusen (*Lal* KO), hauptsächlich sekretiert von Makrophagen. Zusätzlich führte eine Überexpression von MMP-12 in Zellen einer myeloiden Abstammung zu einer Lymphozyten-Dysfunktion, einer systemischen Expansion myeloider Zellen (CD11b+Gr-1+) sowie pathologischen Veränderungen ähnlich denen der *Lal* KO Mäuse. Daraus wurde abgeleitet, dass MMP-12 eine bedeutende Rolle bei der Immunpathologie im Kontext von LAL-D einnimmt.

Ziele: Diese Arbeit zielte darauf ab, den pathologischen Beitrag von MMP-12 zur Immunstörung bei LAL-D zu klären, indem *Lal/Mmp12* Doppelknockout-Mäuse (DKO) generiert und umfassend charakterisiert wurden. Insbesondere sollte untersucht werden, ob die genetische Deletion von MMP-12 wesentliche entzündliche und immunologische Phänotypen der *Lal* KO Mäuse verbessern kann.

Ergebnisse: Trotz stark erhöhter Expression von MMP-12 bei *Lal* KO Mäusen zeigten DKO Mäuse keine Verbesserungen zentraler pathologischer Merkmale wie Hepatosplenomegalie, Makrophagenakkumulation sowie dem Verlust des Fettgewebes. Dennoch stellten wir subtile, aber signifikante Verbesserungen immunologischer Parameter fest. Blutbildanalysen zeigten teilweise normalisierte Lymphozytenzahlen und eine Abschwächung der lymphoiden zu myeloiden Verschiebung im peripheren Blut, Knochenmark und der Milz in DKO Mäusen. Zusätzlich waren thymische Atrophie und gestörte thymische Morphologie, charakteristisch für *Lal* KO Mäuse, bei DKO Mäusen deutlich verbessert. Ich konnte jedoch keine Veränderungen im hämatopoetischen Vorläufer-Kompartiment oder in der Efferozytose-Kapazität der Makrophagen beobachtet. Bemerkenswert war eine moderate Reduktion der Überlebensfähigkeit von Neutrophilen und deren Neigung zur Bildung neutrophiler extrazellulärer Fallen (NETs) in DKO Mäusen zu beobachten.

Schlussfolgerung: Obwohl die myeloid-spezifische Überexpression von MMP-12 viele der inflammatorischen und immunologischen Dysfunktionen von LAL-D reproduzieren konnte, führte die genetische Deletion von *Mmp12* lediglich zu begrenzten Verbesserungen. Diese Ergebnisse deuten darauf hin, dass MMP-12 zwar zur Immundysregulation bei LAL-D beiträgt, jedoch keinen zentralen Beitrag zur Pathologie leistet und daher kein geeignetes therapeutisches Ziel darstellt.

Abstract

Background: Lysosomal acid lipase-deficiency (LAL-D) is a rare lysosomal storage disorder characterized by impaired degradation of cholesteryl esters and triglycerides, resulting in chronic inflammation and immune system dysfunction. Previous studies have demonstrated significantly elevated expression of Matrix Metalloproteinase-12 (MMP-12) in LAL-D mice (*Lal* KO), predominantly secreted by macrophages, and associated with severe inflammatory phenotypes. Furthermore, myeloid lineage-specific overexpression of MMP-12 resulted in lymphocyte dysfunction and systemic expansion of myeloid cells (CD11b+Gr-1+) similar to *Lal* KO mice. Therefore, we hypothesized that MMP-12 plays a substantial role in the immunopathology observed in LAL-D.

Aims: This thesis aimed to clarify the pathological contribution of MMP-12 to the immune dysfunction in LAL-D by generating and characterizing *Lal/Mmp12* double knockout (DKO) mice. Specifically, the study sought to determine whether genetic ablation of MMP-12 could ameliorate key inflammatory and immunological phenotypes of *Lal* KO mice.

Results: Despite significantly elevated MMP-12 expression in *Lal* KO mice, *Lal/Mmp12* DKO mice exhibited minimal improvements in major pathological features, including hepatosplenomegaly, hepatic inflammation, macrophage accumulation, and adipose tissue loss. Nevertheless, we observed subtle yet significant improvements in immune parameters. Complete blood counts revealed partially restored lymphocyte numbers and an amelioration of the lymphoid-to-myeloid shift in peripheral blood, bone marrow, and spleen. Additionally, thymic atrophy and disrupted thymic architecture characteristic of *Lal* KO mice were noticeably improved in DKO mice. However, we observed no alterations in hematopoietic progenitor compartments or in macrophage-mediated efferocytosis capacity. Notably, neutrophil viability and neutrophil extracellular trap (NET) formation were moderately reduced in the absence of MMP-12.

Conclusion: Although myeloid-specific overexpression of MMP-12 recapitulated multiple inflammatory and immune cell dysfunctions associated with LAL-D, genetic deletion of *Mmp12* had only limited beneficial effects. These results suggest that while MMP-12 contributes to immune dysregulation in LAL-D, it is not a central contributor to the disease pathology, and thus not a viable therapeutic target.

1. Introduction

1.1. Lysosomal acid lipase

Lysosomal acid lipase (LAL), encoded by the *Lipa* gene, is the only known lipase active at an acidic pH. Traditionally, acidic (lysosomal) lipolysis was exclusively considered to degrade exogenous lipids derived from plasma lipoproteins. Following the endocytosis and delivery of triacylglyceride (TAG)-rich very low-density lipoprotein (VLDL), cholesteryl ester (CE)-rich low-density lipoprotein (LDL) and other lipoproteins to the lysosome, LAL hydrolyzes CE, TAG, diacylglycerols (1, 2) and retinyl esters (3), thereby generating free fatty acids (FFA), free cholesterol (FC) and retinol, as reviewed in (4). However, LAL was also shown to hydrolyze neutral lipids within lipid droplets through the lysosome-dependent autophagy of lipid droplets, known as lipophagy. In addition, acidic lipolysis is also responsible for the degradation of lipids derived from apoptotic bodies (5).

1.1.1. Molecular characteristics of LAL

In humans, LAL is a 46-kDa glycoprotein encoded by the *LIPA* gene located on chromosome 10p23.2-q23.3 (6). Human (h)LAL is synthesized with a signal peptide (7) and pro region central for correct folding, stability and secretion (8). Similarly, a systematic mutagenesis of the 6 known glycosylation sites demonstrated two individual mutant enzymes (N134Q and N246Q) without lipolytic activity, attributed to a defective protein secretion (1). The core domain of LAL belongs to the α/β hydrolase-fold family with its active site composed of the classical catalytic triad of Ser-153, His-353, and Asp-324 (9). The structure of hLAL is closely related to that of the human gastric lipase, with both enzymes displaying a 58% sequency identity (10). The murine and human LAL share a 75% sequence identity and 91% similarity (11). In mice, LAL was shown to exhibit a significantly lower CE hydrolase activity compared to humans.

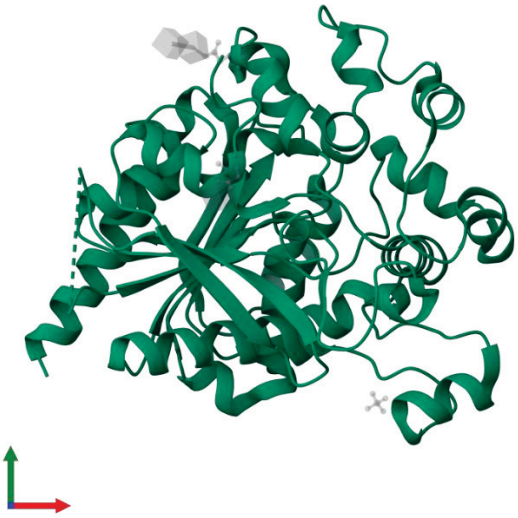

Figure 1: Crystal structure of human LAL (PDB ID: 6V7N), obtained from the Protein Data Bank and originally reported in (9).

1.1.2. Biochemical characteristics of LAL

The enzymatic activity of LAL does not depend on cofactors, unlike the rate-limiting enzyme in neutral lipolysis, adipose triglyceride lipase, which requires the coactivator CGI-58. Instead, LAL activity is primarily regulated at the transcriptional level and has been reviewed in detail in (4). In short, following nutrient starvation the mammalian target of rapamycin (mTOR) and AMP-activated protein kinase (AMPK) lead to the nuclear translocation of transcription factors EB (TFEB), forkhead box O 1(FOXO1), and the peroxisome proliferator-activated receptor ɣ (PPARɣ) co-activator 1α (PGC1α)-PPARα complex, and induction of *Lipa* expression (12-14). Additionally, in macrophages, LAL activity has been shown to be modulated post-transcriptionally by changes in lysosomal pH induced by the uptake of oxidized LDL (15, 16).

LAL-derived degradation products serve multiple critical functions: they provide essential structural components for cell membranes, such as free cholesterol, are a key source of FFAs for energy production via fatty acid oxidation, and regulate the activity of important nuclear receptors like PPARα, PPARɣ (17-19), and LXR (20). For example, PPARɣ suppresses the expression of pro-inflammatory cytokines, thereby promoting the polarization of immune cells towards an anti-inflammatory phenotype (21, 22). In addition, they act as precursors for the synthesis of important lipid mediators (23), including oxysterols and steroid hormones derived from cholesterol, as well as eicosanoids (e.g., prostaglandins) and sphingolipids (e.g., ceramides) derived from FFAs, reviewed in (24) and (25).

1.2. Lysosomal acid lipase deficiency in humans

Both clinical and animal studies have demonstrated the indispensable role of LAL in lysosomal lipid degradation. Defective acidic lipolysis results in progressive lysosomal accumulation of CE and TAG, along with a depletion of essential degradation products. Reduced cytosolic FFA levels impair fatty acid oxidation, TAG re-esterification, and VLDL secretion (26).

Combined with the gradual loss of white adipose tissue (WAT), these changes trigger systemic metabolic adaptations that increase glucose utilization (24). The resulting decrease in cytosolic FC concentration in hepatocytes impairs ABCA1/G1-mediated cholesterol efflux and activates SREBP2, leading to elevated endogenous cholesterol synthesis and upregulation of the LDL receptor - further exacerbating hepatic lipid accumulation (26). The liver, spleen, macrophages, and intestine are among the tissues most affected by ectopic lysosomal lipid accumulation.

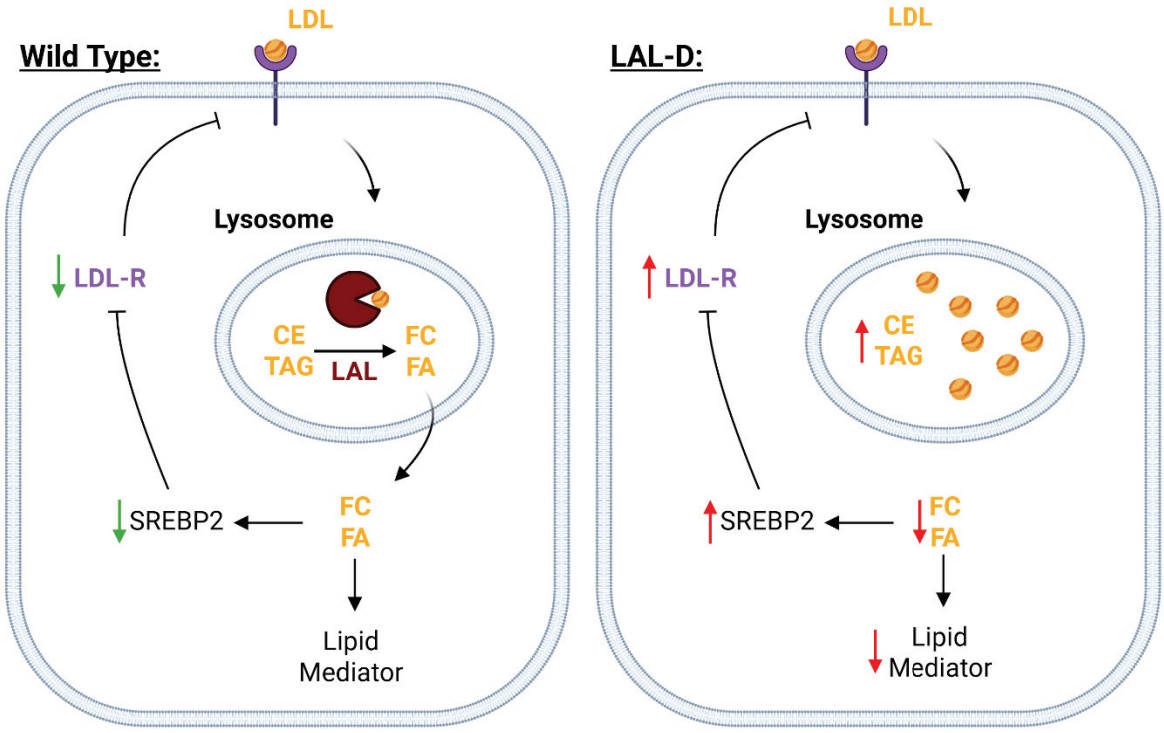

Figure 2: Schematic comparison between acidic lipolysis under physiological conditions and LAL-deficiency. (Wild type) Endocytosis and transport of low-density lipoprotein to the lysosome, followed by the hydrolysis of cholesteryl esters (CE) and triacylglycerol (TAG) by LAL, liberating free cholesterol (FC) and free fatty acids (FFA). Cytosolic free cholesterol inhibits SREBP2 activity, suppressing LDL receptor expression. LAL-derived degradation products are important signaling molecules (e.g. activate PPARγ). (LAL-D) The absence of LAL causes an accumulation of CE and TAG in the lysosome. Depleted levels of FC and FFA activate SREBP2, leading to increased LDL receptor expression. (Created with BioRender.com).

Traditionally, LAL-D has been classified into two distinct pathologies based on differences in symptom onset and severity (27). With residual LAL activity of ~5-10%, patients develop the less severe cholesteryl ester storage disease (CESD), characterized by late-onset pathology and a broad clinical phenotype, including hepatomegaly, premature atherosclerosis, hyperlipidemia, elevated transaminase levels, and reduced life expectancy. CESD is often misdiagnosed (28) and typically identified at a more advanced disease stage with more evident pathological features. In contrast, at <1-5% residual LAL activity, the early-infantile onset of the Wolman's disease manifests, reducing life expectancy to approximately 6 months. Following EMA approval of enzyme replacement therapy (ERT) for LAL-D, both forms have been unified under a single diagnosis (29).

To date, over 100 loss-of-function mutations in the *LIPA* gene have been predicted to cause this rare autosomal recessive lysosomal storage disorder. Of those, 98 mutations have been confirmed, leading to an estimated prevalence ranging from 1 in 40,000 to 1 in 300,000 people (30, 31) varying by region and ethnicity. The diagnosis of late-onset LAL-D is complicated by shared pathology with several other cardiovascular, hepatic and metabolic diseases (31) and is therefore commonly misdiagnosed as heterozygous familial and polygenetic hypercholesterolemia (32), familial defective ApoB (33), and familial hyperlipidemia (34). Besides a detailed analysis of the family history to distinguish an autosomal dominant disorder (e.g. familial hypercholesterolemia) from an autosomal recessive disorder like LAL-D, a minimally invasive, rapid and cost-effective dried-blood spot test was established as the gold standard for the diagnosis of LAL-D (35, 36)

Therapeutic approaches for LAL-D vary greatly depending on the disease severity, with early-onset LAL-D necessitating immediate intervention, since the hepatic pathology already manifests in LAL-D fetuses (37). The use of lipid-lowering drugs (e.g. statins) were early attempts at mitigating elevated LDL-cholesterol and were shown to reduce plasma lipid parameters (38). However, blocking de novo cholesterol synthesis, lead to a reduction in cytosolic FC levels which in turn stimulated the upregulation of LDLR expression (39) exacerbating hepatic lipid accumulation (40). Early attempts at bone marrow transplantations provided mixed outcomes, including increased liver toxicity by chemotherapeutics and graft rejections. However, some cases demonstrated a complete remission of the systemic pathology in infants (41, 42). In contrast, greater success was observed for liver transplants in adult LAL-D patients, yielding immediate improvements of the lipoprotein profile and systemic phenotype (43, 44). Upon the development of human recombinant LAL, known under the brand

names Sebelipase alfa and Kanuma®, ERT has become a viable strategy for the treatment of LAL-D (29). In late-onset LAL-D patients, ERT has resulted in markedly reduced liver transaminase and LDL-cholesterol levels (45, 46). Unfortunately, the response of patients varied greatly with some cases of ERT worsening hepatic fibrosis and inflammation (47, 48). Albeit very common, adverse effects of ERT were of only mild to moderate severity and are most likely arising due to a frequent development of neutralizing antibodies by the patient (47). Notably, the treatment costs of ERT are exceedingly high, leading to some insurers refusing coverage. Despite this, ERT was able to greatly increase the survival rate of early-onset LAL-D patients for up to 10 years (49, 50). In the future, the use of vector-based gene therapy has been proposed as a viable therapy alternative and is currently being tested on *Lal* KO mice (51).

For the study of LAL-D, *Lal* KO mice remain the most widely used model system. In addition, pharmacological inhibitors of LAL (Lalistat-1 and 2) have been successfully employed *in vitro* (52, 53). However, a recent publication revealed off-target effects of these compounds on key hydrolases of neutral lipolysis at commonly used concentrations (54).

The first LAL-D mouse model was generated by Du et al. in 1998 (55) on a mixed background of 129Sv and CDF-1. Surprisingly, a homozygous knockout of the *Lipa* gene in mice only caused a phenotype resembling the less severe CESD in humans. Nonetheless, *Lal* KO mice displayed a life expectancy reduced to 6-8 months and infertility, necessitating heterozygous breedings (56). These mice also developed classic LAL-D features, including loss of adipose tissue, emphysema, and hepatosplenomegaly (56). The same group later demonstrated a partially rescued *Lal* KO phenotype by an adenovirus-mediated gene transfer, substantially reducing splenomegaly and hepatic lipid accumulation (57). This demonstrated the potential of gene therapy for the treatment of CESD.

1.3. The immune cell dysfunction in LAL deficiency

A major hallmark of the LAL-D phenotype is the progressive accumulation of lipid-laden macrophages across the liver, small intestine, spleen, and bone marrow (56, 58). Histological examinations demonstrated massive granuloma-like aggregates of macrophages filled with CE and TAG. The extent of hepatomegaly is directly connected to the extent of macrophage accumulation, exemplified by these aggregates accounting for more than 50% of the area of a liver section from a 30-week-old *Lal* KO mouse.

The central importance of LAL for the homeostasis of the entire immune system is exemplified by a progressive expansion of CD11b+Gr1+ myeloid cells across the immune cell compartments of the bone marrow, spleen, and peripheral blood (59). The analysis of the bone marrow progenitor cell compartment revealed an increase in Lin-Sca-1+c-Kit+ (LSK) cells and granulocyte-macrophage-progenitor cells (GMPs), skewing bone marrow hematopoiesis towards the myeloid lineage. A series of bone marrow transplantations between WT and *Lal* KO mice demonstrated that the myeloid expansion mainly originated from a cell autonomous defect in myeloid progenitor cells and to a lesser extent from the bone marrow microenvironment itself (60).

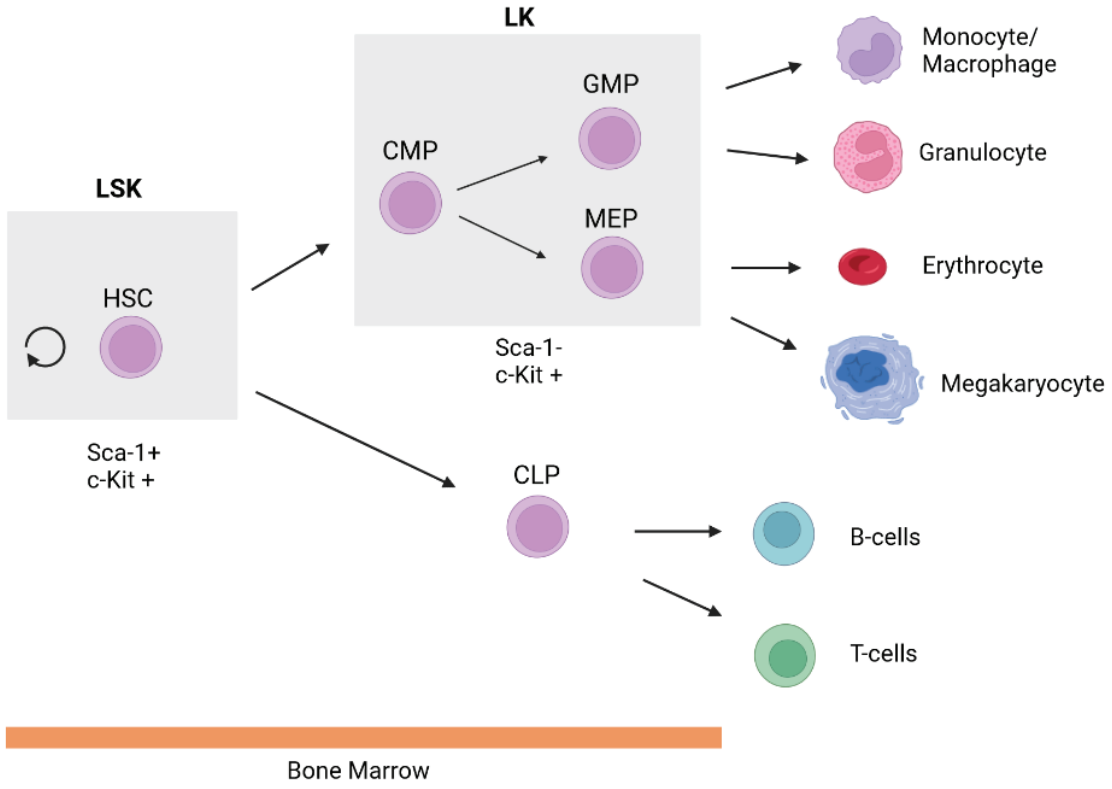

Figure 3: Overview of hematopoietic lineage differentiation in the bone marrow. Hematopoietic stem cells (HSCs) identified as Lin$^-$ Sca-1+ c-Kit+ (LSK) cells, give rise to lineage-committed progenitors. Common myeloid progenitors (CMPs) further differentiate into granulocyte-macrophage progenitors (GMPs) and megakaryocyte-erythrocyte progenitors (MEPs), which give rise to monocytes/macrophages, granulocytes, erythrocytes, and megakaryocytes, respectively. Common lymphoid progenitors (CLPs) differentiate into B-cells and T-cells. (Created with BioRender.com)

Complementing the defects in myelopoiesis, *Lal* KO mice also display severely impaired lymphopoiesis. Upon the differentiation of common lymphoid progenitors (CLP) to early T-cell progenitors, they migrate via the bloodstream to the most important organ in T-cell maturation, the thymus (61). As a primary lymphoid organ, the thymus exclusively facilitates the development of T-lymphocytes. LAL was shown to be indispensable for the development and function of T lymphocytes (60, 62) and leads to an abnormal morphology of the thymus. The authors observed a strong decrease in peripheral blood lymphocytes, originating from both decreased proliferation and increased apoptosis in the thymus (60, 62).

The substantial decline in lymphocyte counts in *Lal* KO mice originated from immunosuppressive properties of myeloid cells (59). A co-culture experiment between WT lymphocytes and *Lal* KO CD11b+/Gr-1+ cells demonstrated a strong decrease in T-cell proliferation (59). In addition, their lymphokine production was significantly reduced, suggesting a functional impairment of *Lal* KO T-lymphocytes (59, 62).

Several rescue strategies have demonstrated the critical role of LAL in maintaining immune and hematopoietic homeostasis. A macrophage-specific reconstitution of LAL activity was sufficient to significantly reduce lipid accumulation, neutrophil infiltration, and tissue inflammation in multiple organs, including the liver, intestine, and lung (63). Moreover, the expression of several pro-inflammatory cytokines, chemokines, and MMPs were normalized, and the lung emphysema phenotype was markedly improved. However, the correction was limited to macrophage-driven pathology, as lipid accumulation in hepatocytes and infertility remained unaffected, emphasizing the importance of LAL activity in non-myeloid cells for full phenotypic rescue. Similarly, defective myelopoiesis and lymphopoiesis of *Lal* KO mice were successfully rescued by myeloid-specific expression of human LAL. This intervention led to a reduced systemic expansion of CD11b+Gr-1+ cells, originating from a bone marrow progenitor compartment that more closely resembled that of WT mice (64). Additionally, the thymic architecture was partially restored, accompanied by improved T-lymphocyte proliferation and function, underscoring the essential role of LAL in hematopoietic development and immune competence.

1.4. Myeloid-derived suppressor cells

Chronic unresolved inflammation is known to result in the development of immunosuppressive CD11b+/Gr-1+ cells, known as myeloid-derived suppressor cells (MDSCs). MDSCs are phenotypically indistinguishable from other myeloid cells like neutrophils and monocytes (65). To date, no MDSC-specific cell surface markers have been discovered. MDSCs may only be identified by their unique gene expression profile and immunosuppressive properties, which have been extensively reviewed in (66). In short, MDSCs can be divided into neutrophil-like MDSCs, termed polymorphonuclear (PMN)-MDSCs, and monocyte-like MDSCs, termed monocytic (M)-MDSCs. All MDSCs display an immature phenotype and morphology, comparatively weak phagocytic activity, increased levels of reactive oxygen species (ROS) and nitric oxide production, higher expression of arginase, PGE-2, and multiple anti-inflammatory cytokines (e.g. IL-10 (67), and TGFβ (65, 68).

Table 1: Functional and molecular properties of neutrophils, monocytes, and myeloid-derived suppressor cells (MDSCs), as reviewed in (65).

	Neutrophils	**PMN-MDSCs**	**Monocytes**	**M-MDSCs**
Surface Phenotype	$CD11b^{+}Ly6G^{+}$	$CD11b^{+}Ly6G^{+}$	$CD11b^{+}Ly6G^{-}$	$CD11b^{+}Ly6G^{-}$
Immune Suppression	-	+	-	+
ROS	- and +	++	- and +	++
NO	-	+	-	+
ARG1	-	++	+	++
PGE2	-	++	-	+
Stat3	- and +	++	- and +	++
CEBPβ	- and +	++	- and +	++

In *Lal* KO mice, CD11b+/Gr-1+ cells have been demonstrated to exhibit the gene expression signature of MDSCs (69). An overactivation of the mTOR pathway was shown to drive the development and function of *Lal* KO MDSCs (70). mTOR is the catalytic subunit of the mTORC1 complex and localizes to the lysosomal membrane upon activation. It senses the availability of cellular nutrients, oxygen, and energy and is instrumental in the regulation of protein synthesis, cellular metabolism, as well as autophagy and lysosomal biogenesis, as comprehensively reviewed in (71). The injection of the mTOR inhibitor rapamycin was able to significantly ameliorate the systemic expansion of CD11b+Ly6G+ cells, reduce their proliferation and increase apoptosis, as well as ameliorate their immunosuppressive functions on lymphocytes (70). In addition, several enzymes of glycolysis (hexokinase, glyceraldehyde-

3 phosphate dehydrogenase and pyruvate kinase) and the citric acid cycle (isocitrate dehydrogenase 1 and succinate dehydrogenase) were markedly upregulated in *Lal* KO MDSCs (60, 69). Interestingly, an elevated expression of lactate dehydrogenase A and B was observed (69), indicating activation of a metabolic pathway typically associated with cancer cells - the Warburg effect (72). In addition, some enzymes involved in glycogen synthesis and the pentose pathway exhibited increased expression in *Lal* KO MDSC (69). Despite impaired mitochondrial function, *Lal* KO bone marrow MDSCs exhibited elevated expression of enzymes involved in the respiratory chain (NADH dehydrogenase, cytochromes and ATPases) as well as higher ATP levels (69), compared to WT bone marrow cells (69). Unfortunately, these changes in *Lal* KO MDSCs were obtained by comparison with WT bone marrow cells. Therefore, unique characteristics differentiating *Lal* KO MDSCs from WT MDSCs have not been elucidated and remain unknown.

1.5. MMP-12 and its connection to LAL-D

The destruction of lung tissue constitutes another major well characterized pathology of *Lal* KO mice (73, 74). As a direct consequence to blocking TAG and CE degradation, *Lal* KO mice develop a severe lung pathology, including extensive neutrophil infiltration, the accumulation of lipid-laden macrophages, tumor formation, and emphysema (74, 75). A microarray analysis of whole lung tissue identified matrix metalloproteinase-12 (MMP-12) as the single most dysregulated gene in 6-months old *Lal* KO mice, as compared to age-matched WT littermates (74). This also translated to a massive increase in MMP-12 protein expression in the bronchoalveolar lavage and alveolar type II cells (74). The application of the LAL-degradation product and PPARɣ agonist 9-HODE suppressed the mRNA expression of *Mmp12*, thereby demonstrating a novel transcriptional regulation of *Mmp12*.

In humans, MMP-12 belongs to the matrix metalloproteinase family of 23 zinc-containing endopeptidases. Each family member was shown to process an overlapping array of different extracellular matrix (ECM) components, e.g. collagens, gelatin, elastins, glycoproteins, and proteoglycans (76, 77). Furthermore, several different cell types were shown to produce MMPs, including macrophages, neutrophils, lymphocytes, fibroblasts, osteoblasts, and endothelial cells. Most MMPs are secreted in an inactive form, called zymogens (pro-MMP), and require proteolytic cleavage for activation (76). Under physiological conditions, the expression, secretion, activation and activity of MMPs is tightly regulated. Upon secretion and activation, endogenous inhibitors called tissue inhibitors of metalloproteinases (TIMPs) provide an additional spatially dependent layer of regulation(78).

MMP-12 was first described as an extracellular matrix degrading enzyme secreted by macrophages called macrophage metalloelastase (79). Since then, the broader involvement of MMP-12 in the following biological functions was demonstrated.

1.6. ECM degradation by MMP-12

Elastin fibers are a central component of the ECM, providing resilience and elasticity to several tissues such as skin, lung, and blood vessels. These fibers are remarkably resistant to proteolytic degradation, resulting in extremely low turnover under physiological conditions. However, in multiple chronic inflammatory conditions, elastin integrity is compromised due to aberrant expression of proteolytic enzymes such as MMP-12 (80). The exposure of skin to UV irradiation induces the expression of both MMP-12 and tropoelastin (80). Elevated expression of MMP-12 is not only able to damage the ECM but also impairs its repair by degrading tropoelastin, leading to sustained tissue damage.

The degradation of ECM components is known to liberate ECM-derived peptides, termed matrikines (81). The degradation of elastin by MMP-12 was shown to generate elastin-derived peptides (EDPs) containing different lengths of the Val-Gly-Val-Ala-Pro-Gly (VGVAPG) hexapeptide repeats (82). The VGVAPG peptide sequence has high binding affinity to the elastin-binding protein (EBP) (82), a catalytically inactive splicing variant of the β-galactosidase gene *GLB1*, which, together with cathepsin A and neuraminidase, forms the elastin receptor complex *(83)*. Matrikines, such as EDPs, were shown to possess chemoattractant properties that lead to monocyte infiltration (84), mediate inflammation and promote NASH (85), and affect insulin sensitivity (86). The elastin receptor complex is located on the cell surface of several types of immune cells (83). The binding of EDPs has been shown to stimulate proliferation in multiple human cell types, thereby linking elastin degradation not only to ECM remodeling but also to downstream signaling events with potential implications for inflammation, tissue remodeling, and disease progression (83).

1.7. Transcription factor properties of MMP-12

Independent of its proteolytic activity, MMP-12 has been shown to exhibit transcription factor-like properties by translocating to the nucleus of fibroblasts, binding to the promoter of *IκBα*, and inducing its expression (19). Loss of MMP-12 impaired IFN-α secretion and led to elevated viral burden in infected cells, underscoring an essential intracellular function beyond its array of proteolytic functions. Altered *IκBα* expression has broad implications due to the complexity of NF-κB signaling and its regulation of numerous downstream biological processes (87).

Similarly, in the intestinal epithelium of obese mice fed a high-fat diet, siRNA-mediated knockdown of MMP-12 reduced lipid transport, bile acid reabsorption, and inflammation. Mechanistically, MMP-12 was found to bind to the promoter of *Fabp4* and induce its expression via epigenetic modification (88). These nuclear functions occurred independently of MMP-12's catalytic domain, further supporting its non-proteolytic role in gene regulation. The authors concluded that the inhibition of MMP-12 led to marked improvements in high-fat diet-induced metabolic dysfunction and restoration of intestinal homeostasis.

1.8. The role of MMP-12 in regulating immune cells

Notably, several reports have demonstrated that the substrate specificity of MMP-12 is not limited to ECM proteins but also includes various cytokines and cell surface receptors (89, 90). MMP-12 has been shown to cleave multiple chemokines, including CXCL1, -2, -3, -5, and -8, as well as CCL2, -7, -8, and -13, and the murine IL-8 homologues mCXCL1, -2, and -3 (89). This proteolytic activity contributes to the regulation of immune cell recruitment, as evidenced by reduced monocyte and neutrophil infiltration in the bronchoalveolar lavage of *Mmp12* KO mice following lipopolysaccharide injection (89).

In line with this, *Mmp12* deficiency was also shown to dampen cigarette smoke–induced emphysema by reducing neutrophil and monocyte infiltration and limiting granuloma formation (59). To further investigate the role of MMP-12 in pulmonary pathology, MMP-12 has been overexpressed in lung epithelial cells, resulting in spontaneous emphysema, inflammatory cell infiltration, and the development of bronchioalveolar adenocarcinoma (91). Similarly, the application of an MMP-12 inhibitor worsened post-myocardial infarction by delaying the resolution of inflammation. Together with other studies linking MMP-12 expression to chronic obstructive pulmonary disease (COPD) and lung cancer in patients (75, 92), these findings strongly support the role of MMP-12 as a potent pro-inflammatory factor, likely contributing to the pulmonary pathology observed in *Lal* KO mice.

1.9. Platelets and platelet-leukocyte-aggregates

Thrombocytes together with coagulation factors form the basis of blood coagulation (93). Following a vascular injury or insult, thrombocytes are activated and adhere to extracellular matrix antigens revealed from beneath the endothelium to form a platelet plug. One notable epitope resulting in the activation of platelets is collagen and is therefore commonly used in collage-induced platelet coagulation assays. Changes in platelet activation have implications

for thrombose formation and atherosclerosis (94), as well as bleeding disorders causing prolonged bleeding times and excessive blood loss from injuries (95).

The involvement of platelets outside of hemostasis and thrombosis has been increasingly recognized. Platelets are now well understood to exert a regulatory function on both innate and adaptive immune cells (96, 97). Under certain pro-inflammatory or pro-thrombotic conditions, platelets can form platelet-leukocyte aggregates (PLAs), mainly with monocytes and macrophages, and to a lesser extent with neutrophils and lymphocytes (94, 98). Upon the formation of PLAs, platelets are capable of both diminishing and enhancing the function of leukocytes (99) and alter their cytokine secretion profile during an injury or infection (98). Interestingly, the platelet-leukocyte interaction also has implications for leukocyte extravasation, tissue infiltration, and differentiation (98). In addition, platelet-neutrophil aggregates are able to induce ROS production, promote NETosis (100), and delay apoptosis during sepsis (101).

MMPs are well understood to modulate the function and pathology of thrombocytes. MMP-1 and 13 were shown to activate the thrombin receptor protease activated receptor-1 (PAR-1) (102) leading to a unique form of thrombocyte signaling distinct from the classical thrombin induced activation (103). Interestingly, MMP-12 was shown to cleave surface CEACAM-1, thereby increasing type I collagen induced platelet activation (104). This demonstrated a direct involvement of MMP-12 in blood coagulation with implications beyond hemostasis, offering a means by which MMP-12 may alter the function and survival of immune cell.

1.10. Neutrophils

Neutrophils are polymorphonuclear (PMN) leukocytes best known for their essential host defense role against invading pathogens, in particular bacteria and fungi (105). Upon inflammation, neutrophils are rapidly mobilized and migrate to the site of injury as first-line responders (106). In humans, four distinct groups of chemoattractants act on neutrophils, 1) chemotactic lipids (e.g. leukotriene B_4, LTB_4) (107), 2) chemokines (CXCL1 to 3 and CXCL 5 to 8) (108), 3) complement anaphylatoxins (C3a and C5a) (109) and 4) formyl peptides (110) activate dedicated G-protein coupled receptors. All groups have overlapping functions yet cooperate in a nonredundant manner allowing fine control of neutrophil trafficking (111). Upon mobilization into the bloodstream by chemokines such as granulocyte colony-stimulating factor (G-CSF) (112), neutrophils are captured by selectin receptors (e.g., E-selectin and P-selectin) expressed on activated endothelial cells (113). This interaction initiates a rolling phase along

the vascular wall, during which neutrophils are further activated by chemokines presented on the endothelial surface. Subsequently, neutrophil integrins undergo conformational changes enabling the binding to endothelial integrin receptors. This firm adhesion leads to the arrest of neutrophil movement, followed by transmigration across the endothelium into the inflamed tissue (114), where they exert their antimicrobial roles.

Neutrophils can kill pathogens via the release of cytotoxic proteins, peptides, and enzymes through a process called exocytosis (115). In addition, a membrane-bound NADPH-oxidase can produce superoxide anions (e.g. O_2^-), leading to the formation of antimicrobial hydrogen peroxides and other reactive oxygen species (116). Both mechanisms can also be used to neutralize microbes following efferocytosis, upon the fusion of the phagosome with granules (117). These defensive functions are enhanced by both host-derived factors like G-CSF, GM-CSF, IFNɣ, TNF, as well as pathogen-derived products like LPS and specific nucleic acid sequences (118). All these factors prolong neutrophil survival by doubling their lifespan and inhibiting apoptosis (118). However, the anti-bacterial properties of neutrophils also contribute to several inflammatory diseases, ranging from acute lung injury (119), sepsis, COPD to arthritis (120). Proper activation, migration and survival of neutrophils are essential for their physiological function and to prevent neutrophil-mediated tissue injury. Mechanisms by which neutrophils cause tissue damage (121) (e.g. unwarranted degranulation) have been well documented in other diseases (122-124) but have not yet been investigated in *Lal* KO mice and remain unknown.

Under physiological conditions, neutrophils typically survive for h to days. In mice, the half-life of neutrophils circulating in the peripheral blood was estimated to be between 9-18 h, whereas in humans, a lifespan of up to several days has been reported (105, 125). Apoptotic and aged neutrophils are removed by migrating to the bone marrow, liver and spleen, where they are recognized by macrophages and dendritic cells followed by efferocytosis. Neutrophils can undergo a specialized form of cell death called NETosis (126), resulting in the formation of neutrophil extracellular traps (NETs) (127). NETs are traditionally only produced in response to microbial infections with the intention to trap, neutralize and kill pathogens, including bacteria, fungi, viruses, and parasites (128-130). In addition, NETs can be artificially induced by phorbol 12-myristate 13-acetate (PMA) (131) and bacterial toxins like ionomycin (132) and nigericin (133). Mechanistically, NET formation involves activation of NADPH oxidase and the generation of ROS, which act as key intracellular signals (134). This is followed by chromatin decondensation, histone citrullination by PAD4 (135, 136), and rupture of the nuclear and cell

membrane, releasing a dense extracellular network composed of neutrophil DNA coated with cytotoxic granule proteins, including neutrophil elastase and myeloperoxidase (127, 137). While NETs are an important antimicrobial defense mechanism, dysregulated or excessive NET formation has been observed in the absence of infection and can contribute to collateral tissue injury and sustained inflammation (138).

1.11. Efferocytosis

Under physiological conditions, apoptotic neutrophils are removed by phagocytes, e.g. macrophages and dendritic cells, in a process called efferocytosis. This process is essential for resolving inflammation and mitigating the effect of pro-inflammatory content released from dead cells. The clearance of apoptotic cells by efferocytosis is considered non-inflammatory and immunologically silent.

Efferocytosis is a tightly regulated, multi-step process that involves the recognition, engulfment, and degradation of apoptotic cells (139). They are recognized by recruited phagocytes (140) based on the externalization of phosphatidylserine, which is only found on the inner membrane of viable cells. Beyond the simple clearance of dead cell and cell debris, efferocytosis exerts profound effects on the immune response (141). Engulfment of apoptotic cells induces an anti-inflammatory transcriptional program in macrophages, promoting the release of TGF-β and IL-10, and suppressing pro-inflammatory cytokines such as TNF and IL-1β (139, 141). In this context, efferocytosis is critical for resolving inflammation and preventing chronic immune activation. Its dysregulation is increasingly recognized in chronic inflammatory diseases, where uncleared apoptotic cells undergo secondary necrosis, perpetuating tissue damage. Moreover, defective efferocytosis impairs macrophage reprogramming and skews immune responses toward a pro-inflammatory phenotype (139). The efferocytosis capacity of *Lal* KO mice was shown to be significantly impaired, contributing to the observed immune dysfunction and failure to resolve inflammation (5).

1.12. Central Hypothesis

Previous studies have identified MMP-12 as one of the most dysregulated genes in the lungs of *Lal* KO mice. The overexpression of MMP-12 in myeloid cells was sufficient to induce several hallmark features of LAL-D, including a skewed hematopoietic progenitor profile, expansion of immunosuppressive CD11b+Gr-1+ cells, and impaired T-cell function. These striking similarities led to the hypothesis that MMP-12 may act as a key downstream effector contributing to the immune dysfunction and chronic inflammation of LAL-D.

To assess the functional relevance of MMP-12 in the context of LAL-D, we generated and characterized *Lal/Mmp12* double knockout (DKO) mice. This model allowed us to evaluate whether MMP-12 is merely a marker of inflammation or an active mediator of pathology. The present study aimed to determine whether MMP-12 deficiency ameliorates the immunological and inflammatory abnormalities of LAL-D, and to evaluate its potential as a therapeutic target.

2. Methods

2.1. Animals

Lal KO mice (56) were backcrossed onto the C57BL/6J background and crossed with *Mmp12* KO mice (C57BL/6J background) (JAX#004855; The Jackson Laboratory, Bar Harbor, ME, USA), generating *Lal/Mmp12* DKO mice. All animals were kept in a controlled environment under standard light-dark cycles (12-h/12-h) and provided with a standard chow diet or or challenged for 6 weeks on a high fat diet (HFD) [34% (w/w) crude fat, 1% (w/w) cholesterol; Ssniff®, Soest, Germany]. All animal experiments were conducted following EU Directive 2010/63/EU and approved by the Federal Ministry of Science, Research, and Economy, Vienna, Austria (BMBWF-66.010/0138-V/3b/2019).

2.2. Sample collection

Male mice at approximately 30 weeks of age were euthanized following a 6-h fasting period. Peripheral blood was collected through cheek puncture into EDTA-coated tubes. Whole blood was analyzed for a complete blood cell count using a V-sight device (Menarini Diagnostics, Florence, Italy), and Giemsa-stained blood smears (Merck, Darm stadt, Germany) were examined cytologically. Plasma was separated by centrifugation at 6,300 x g for 10 min at 4°C and stored at -20°C. Organs were excised after post-cervical dislocation, weighed, snap-frozen in liquid nitrogen, and preserved at -80°C. The femur, tibia, and spine were collected and kept in ice-cold 1x PBS for further analyses.

2.3. Hematoxylin and eosin (H&E) staining

Adipose tissue, spleen, thymus, and liver specimens were fixed in 10% formalin for 12 h and stored in PBS until paraffin embedding. Paraffin blocks were sectioned into 5-µm slices, deparaffinized, and subjected to H&E staining. The average adipocyte diameter in tissue sections was determined using Fiji Software (142) and the Adiposoft (143).

2.4. Immunofluorescence staining

Paraffin-embedded spleen tissue sections were deparaffinized and washed with 1x PBS-T (0.1% Tween-20). The sections were blocked with PBS-T + 10% goat serum for 30 min. Primary rabbit anti-Histone H3 (citrulline R2 + R8 + R17) antibody (1:1000; ab5103, abcam, Cambridge, UK) was diluted in PBS-T containing 10% goat serum and incubate on spleen sections over night at 4°C. The sections were washed with PBS-T, followed by incubation with donkey anti-rabbit Alexa Fuor 488 (1:500; A32790; Thermo Fisher Scientific, Waltham, MA,

USA) for 90 mins at RT. Then the sections were washed with PBS-T, stained with DAPI for 5 min, and mounted in Vectashield Antifade Mounting Medium (H-1000-10; Vector Laboratories, Newark, CA). The stained spleen sections were imaged with an Olympus BX63 microscope and analyzed using Qupath® (144).

2.5. Protein isolation and immunoblotting

Frozen spleen tissue (50 mg) was lysed in 100 µl RIPA buffer supplemented with protease and phosphatase inhibitors (1:1,000; Merck, Darmstadt, Germany). Lysates were centrifuged at 16,000 x g for 30 min at 4°C, and the protein concentration of the supernatant was measured using the DC Protein Assay (Bio-Rad Laboratories, Hercules, CA, USA). Proteins (100 µg) were resolved by SDS-PAGE and transferred onto a PVDF membrane. Membranes were incubated with a rabbit polyclonal anti-calnexin antibody (1:1,000, #2679T; Cell Signaling Technology, Danvers, MA, USA) and a rabbit monoclonal anti-CD3e antibody (1:1,000, #78588; Cell Signaling Technology). A secondary HRP-conjugated goat anti-rabbit antibody (1:2,500, #31460; Thermo Fisher Scientific, Waltham, MA, USA) was used before chemiluminescent detection with a ChemiDoc MP imaging system (Bio-Rad Laboratories). CD3e expression was quantified via densitometry (Fiji Software [34]) and normalized to calnexin as a loading control.

2.6. RNA isolation, reverse transcription, and real-time PCR

RNA from liver and spleen tissue was extracted using TriFast reagent (Peqlab, Erlangen, Germany) according to the manufacturer's guidelines. Two micrograms of RNA were reverse transcribed using the High Capacity cDNA Reverse Transcription Kit (Applied Biosystems, Carlsbad, CA). Quantitative real-time PCR (qRT-PCR) was conducted on a Bio-Rad CFX96 system (Bio-Rad Laboratories, Hercules, CA, USA) with GoTaq® qPCR Mastermix (Promega, Madison, WI, USA). Samples were analyzed in duplicate and normalized to either cyclophilin A (Ppia) or hypoxanthine phosphoribosyltransferase (Hprt).

Table 2: List of primers used for real-time PCR:

Gene	Forward Sequence 5´-3´	Reverse Sequence 5`-3`
Acat	GTGAAGGACAGGCCCCTA	ACACATAAGACTTTGAGAGGCCA
Acta1	TACCACCGGCATCGTGTTG	GCGCACAATCTCACGTTCAG
Acta2	GGACGTACAACTGGTATTGTGC	TCGGCAGTAGTCACGAAGGA
B220	CCAGTGATGGTGTGTTATCCAC	GGGGGTATCAACAGGAAAGGC

Ccl2	TTAAAAACCTGGATCGGAACCAA	GCATTAGCTTCAGATTTACGGGT
Ccl5	GCTGCTTTGCCTACCTCTCC	TCGAGTGACAAACACGACTGC
Cd3	GGTGCTCCAGGATTTCTCGG	GCCTTGGCCTTCCTATTCTTG
Cd36	GCAGGTCTATCTACGCTGTG	GGTTGTCTGGATTCTGGAGG
Cd68	AACAGGACCTACATCAGAGC	TCAAGGTGAACAGCTGGAGA
Col1a1	TAAGGGTCCCCAATGGTGAGA	GGGTCCCTCGACTCCTACAT
Col1a2	TCGTGCCTAGCAACATGCC	TTTGTCAGAATACTGAGCAGCAA
Cox2	TGAGCAACTATTCCAAACCAGC	TTCAACACACTCTATCACTGGC
Cxcl1	CTGGGATTCACCTCAAGAACATC	CAGGGTCAAGGCAAGCCTC
Cxcl2	AGTGAACTGCGCTGTCAATG	GCCCTTGAGAGTGGCTATGA
Cxcl5	AGCGGTTCCATCTCGCCATTC	CTCCGTTGCGGCTATGACTG
Cxcr1	TCTGGACTAATCCTGAGGGTG	GCCTGTTGGTTATTGGAACTCTC
Cxcr2	ATGCCCTCTATTCTGCCAGAT	GTGCTCCGGTTGTATAAGATGAC
Cxcr4	GACTGGCATAGTCGGCAATG	AGAAGGGGAGTGTGATGACAAA
Elane	CAGGAACTTCGTCATGTCAGC	AGCAGTTGTGATGGGTCAAAG
Eln	TGTCCCACTGGGTTATCCCAT	CAGCTACTCCATAGGGCAATTTC
Emr1	CTTTGGCTATGGGCTTCCAGTC	GCAAGGAGGACAGAGTTTATCGTG
Fasn	GAAGCCGAACACCTCTGTGCAGT	GCTCCTTGCTGCCATCTGTATTG
Hprt	GTTGGGCTTACCTCACTGCT	TAATCACGACGCTGGGACTG
Ifng	CTCAAGTGGCATAGATGTGG	GCTGTTGCTGAAGAAGGTAG
Il10	GCTGGACAACATACTGCTAACC	ATTTCCGATAAGGCTTGGCAA
Il1b	GAAATGCCACCTTTTGACAGTG	TGGATGCTCTCATCAGGACAG
Il6	CCAGAGATACAAAGAAATGATGG	ACTCCAGAAGACCAGAGGAAAT
Irf1	ATGCCAATCACTCGAATGCG	TTGTATCGGCCTGTGTGAATG
Junb	TCACGACGACTCTTACGCAG	CCTTGAGACCCCGATAGGGA
Ly6g	TGCCCCTTCTCTGATGGATT	TGCTCTTGACTTTGCTTCTGTGA
Mmp1a	CCTTGATGAGACGTGGACCAA	ATGTGGTGTTGTTGCACCTGT
Mmp2	ACCTGAACACTTTCTATGGCTG	CTTCCGCATGGTCTCGATG
Mmp3	ACATGGAGACTTTGTCCCTTTTG	TTGGCTGAGTGGTAGAGTCCC
Mmp7	CTTACCTCGGATCGTAGTGGA	CCCCAACTAACCCTCTTGAAGT
Mmp8	TGGTGATTTCTTGCTAACCCC	TACACTCCAGACGTGAAAAGC

Mmp9	GGACCCGAAGCGGACATTG	CGTCGTCGAAATGGGCATCT
Mmp10	CCCAGCTAACTTCCACCTTTC	AATTCAGGCTCGGGATTCCAA
Mmp11	CCACTCACTTTCACTGAGGTG	CGTCAAACGGCAAGTTGTCAC
Mmp12	CTGCTCCCATGAATGACAGTG	AGTTGCTTCTAGCCCAAAGAAC
Mmp12	CTGCTCCCATGAATGACAGTG	AGTTGCTTCTAGCCCAAAGAAC
Mmp13	CTTCTTCTTGTTGAGCTGGACTC	CTGTGGAGGTCACTGTAGACT
Mmp14	CAGTATGGCTACCTACCTCCAG	GCCTTGCCTGTCACTTGTAAA
Mmp15	ATGAAGAGACGAAAACGTGGATG	TGGAAGACCAATGGTGTGACC
Mmp16	TTACTCGCATTCAGCTCTGGA	CCGCAGACTGTAGCACATAAAA
Mmp17	ACTGTCCAAAGCGATTACTGC	GGGAGCATCGAGGGGTTTTC
Mmp19	CCTGGTCCCATGCCAAACC	CCCTTGAAAGCATAAGTCTTCCC
Mmp23	AGGGCAGCTCAGGGAAATGTA	GTATGTGAGGTTGAAGTGGTCC
Mmp24	GCATCTGCGTTGCATTCTGG	CACTCGATTGTTGTCTGATCCA
Mmp25	CTCCTGCCCGTCTCTACTACC	GACCTTCGCATCGGGATTCTG
Mmp27	AAGGTCACTCCACTGACGTTT	CACCACCTAGACCCAGACCA
Mmp28	AACCAGAGGTCCTAAATACTGCC	GGACGAGGCTCTACAGTGATG
Pgc1a	CCCTGCCATTGTTAAGACC	TGCTGCTGTTCCTGTTTTC
Ppara	TTCACAAGTGCCTGTCTGTC	GGCCTTGACCTTGTTCATGT
Ppia	GAGCTGTTTGCAGACAAAGTTC	CCCTGGCACATGAATCCTGG
Srebp	CACTCAGCAGCCACCATCTAGCCT	GCTGATGCCTGCAGTCTTCACG
Timp1	TCCTCTTGTTGCTATCACTGATAGCTT	CGCTGGTATAAGGTGGTCTCGTT
Timp2	CTCGCTGTCCCATGATCCC	GCCCATTGATGCTCTTCTCTGT
Timp3	CTTCTGCAACTCCGACATCGT	GGGGCATCTTACTGAAGCCTC

2.7. ALT, AST, and SAA measurements

Plasma alanine aminotransferase (ALT) and aspartate aminotransferase (AST) levels were assessed using GOT/AST-PIII Fuji Dri-Chem slides (#3150) and GPT/ALT-PIII Fuji Dri-Chem slides (#3250) with a Fuji Dri-chem NX500 analyzer (Fujifilm, Tokyo, Japan). Serum amyloid A (SAA) concentrations were measured using ELISA, following the manufacturer's protocol (DY2948-05; Bio-Techne, Minneapolis, MN, USA). Plasma sEDP concentration were quantified using the Mouse Soluble Elastin Fragments ELISA Kit (MBS3806004, MyBioSource, San Diego, CA, USA) according to the manufacturer’s protocol.

2.8. Platelet aggregation assay

Whole blood was collected from the retrobulbar plexus using a heparinized glass capillary and anticoagulated with 25 U/mL heparin/TBS. Aggregation was measured on a Multiplate® analyzer (Multiplate Services GmbH, Munich, Germany). Samples were transferred to measurement wells containing 0.9% NaCl, and aggregation was induced by the addition of collagen (final concentration 3.2 µg/mL, Hyphen Biomed, Neuville-sur-Oise, France).

2.9. Efferocytosis assay

Bone marrow-derived macrophages were generated as previously described (145). BMDMs were harvested using an enzyme-free cell dissociation buffer (Cat#13151014; Gibco™, ThermoFisher) and seeded at 80% confluency in 6-well cell culture plates and incubated at 37°C and 5% CO_2 overnight. Jurkat cells were collected via centrifugation and transfered into 1x PBS. Apoptosis was initiated by treating cells for 10 mins in a UV-cross linker [Amerscham Life Science; Amsterdam Netherlands]. pHrodo (iFL Red STP ester, amine reactive dye; P36010; Thermo Fisher Scientific) was diluted 1:100 in 1x PBS and added to cells. The Cells were incubated for 2 h at 37°C and 5% CO_2. Apoptotic Jurkat cells were added in a 1:1 ratio to BMDMs and incubate for 2 h at 37°C and 5% CO_2. Unattached apoptotic cells were gently washed away by 1x PBS. BMDMs were detached using an enzyme free cell dissociation buffer. Cells were stained with CD11b (Clone:M1/70; Cat#17-0112-82, Invitrogen, ThermoFisher) and F4/80 (Clone:BM8; Cat#11-4801-82; Invitrogen, ThermoFisher). Analysis was conducted on a Cytoflex LX using CytExpert (Beckman Coulter, Brea, CA, USA) and FlowJo software (Treestar Inc., San Carlos, CA, USA).

2.10. Tissue lipid extraction and quantification

Liver tissue (50 mg) was sonicated in 100 µl lysis buffer (100 mM potassium phosphate, 250 mM sucrose, 1 mM EDTA, pH 7) on ice (2 x 15 s). After centrifugation at 16,000 x g for 30 min at 4°C, protein concentrations were determined at 650 nm (DC Protein Assay, Bio-Rad Laboratories). Lipids were extracted using the Folch method from samples corresponding to 1 mg of protein. Free cholesterol (#1132300F, Greiner, Kremsmünster, Austria), total cholesterol (#113009910023; DiaSys Diagnostic Systems, Holzheim, Germany), triglycerides (#157600010023, DiaSys Diagnostic Systems), and free fatty acids (Wako Chemicals, Richmond, VA, USA) were measured spectrophotometrically at 490 nm. Cholesteryl ester levels were derived by subtracting free cholesterol from total cholesterol values.

2.11. Flow cytometry

Bone marrow was obtained by crushing femurs, tibiae, and spinal cords with a mortar and pestle and passing the material through a 70-µm cell strainer with 1x PBS containing 10% fetal calf serum. Fifty µl of peripheral blood was processed, ~30 mg of spleen tissue was dissociated through a 70-µm cell strainer, and bones were ground using a mortar and pestle. All samples were treated with ammonium-chloride-potassium buffer (150 mM NH_4Cl, 10 mM $KHCO_3$, 1 mM EDTA, pH 7.3) or red blood cell lysis and washed with HEPES-buffered saline containing 10% fetal calf serum. From bone marrow and spleen, 2 x 10^6 cells were aliquoted. Samples were stained with CD115-PE , CD11b-eF450, CD45-FITC, Ly6G-PE-Cy7, CD49b-APC-Cy7, B220-APC-Cy7, CD117-APC, and CD3e-APC-Cy7 (Table 3) for 45 min on ice in the dark. Dead cells were identified using a 1:200 dilution of 7-AAD (BD Biosciences). Analysis was conducted on a Cytoflex LX using CytExpert (Beckman Coulter, Brea, CA, USA) and FlowJo software (Treestar Inc., San Carlos, CA, USA).

Table 3: Antibody panel for the analysis of the immune cell compartment in the peripheral blood, bone marrow and spleen.

Antibody	Dilution	Source	Identifier
CD115 - PE	1:160	eBioscience	#12-1152-82
CD11b - eF450	1:160	eBioscience	#48-0112-82
GR-1 - PE-Cy7	1:160	eBioscience	#25-5931-82
CD117 (cKit) - APC	1:53	BD Pharmingen	#553356
B220 - APC-Cy7	1:160	BD Pharmingen	#552094
CD3e - APC-Cy7	1:20	BD Pharmingen	#557596
CD49b – APC-Cy7	1:20	Invitrogen	#47-5971-82

2.12. Characterization of bone marrow stem and progenitor cells

Lineage depletion (Mouse Hematopoietic Progenitor Cell Enrichment Set, #558451; BD Biosciences, Franklin Lakes, NJ, USA) was performed according to the manufacturer's protocol. In brief, bone marrow cells were stained with the Biotin Mouse Lineage Depletion Cocktail (#559971, BD Pharmingen), followed by magnetic labeling with Streptavidin Particles Plus. Lineage-positive cells were separated on a magnet with the negative fraction remaining in suspension. The lineage-negative cells were then stained with streptavidin-APC-Cy7 (BD Biosciences) for 15 min, split into two aliquots, and stained for hematopoietic stem cells (CD48-FITC, CD150-BV421, Sca1-PE-Cy7 and CD117-APC) or hematopoietic progenitor cells (CD16/32-eF450, Sca1-Pe-Cy7, CD34-PE and CD117-APC) (Table 4) for >45 min on ice.

Dead cells were stained with 1 µl 7-AAD (BD Biosciences) per 200 µl suspension. Samples were analyzed by flow cytometry as described above.

Table 4: Antibody panel for the analysis of bone marrow stem and progenitor cells

Antibody	Dilution	Source	Identifier
CD48 - FITC	1:40	BD Pharmingen	#103403
CD150 - BV421	1:10	BD Pharmingen	#115925
Ly6A/E (Sca1) - PE-Cy7	1:20	eBioscience	#25-5981-82
CD34 - PE	1:10	BD Pharmingen	#551387
CD117 (cKit) – APC	1:160	BD Pharmingen	#553356
CD16/32 - eF450	1:80	eBioscience	*#48-0161-82*

2.13. Statistical analysis

Data analysis was performed using GraphPad Prism 10 (GraphPad Software Inc., San Diego, CA, USA). Statistical significance was determined via two-tailed Student's t-tests for three independent comparisons: 1) WT vs *Mmp12* KO ($^{\dagger}p < 0.05$, $^{\dagger\dagger}p \leq 0.01$, $^{\dagger\dagger\dagger}p \leq 0.001$), 2) WT vs *Lal* KO ($^{*}p < 0.05$, $^{**}p \leq 0.01$, $^{***}p \leq 0.001$), and 3) *Lal* KO vs *Lal/Mmp12* DKO ($^{\#}p < 0.05$, $^{\#\#}p \leq 0.01$, $^{\#\#\#}p \leq 0.001$). Results are presented as mean + SD.

3. Results

3.1. Characterizing 15-week-old chow diet-fed *Lal/Mmp12* DKO mice

To investigate the extent to which MMP-12 contributes to the pathology of LAL-D, a new mouse model lacking both *Lal* and MMP-12 was generated. These *Lal/Mmp12* DKO mice were characterized to analyze possible reductions in the severity of LAL-D.

At 15 weeks of age, female *Lal* KO and *Lal/Mmp12* DKO mice were phenotypically indistinguishable. Both genotypes had similar brain (Figure 4A) and body weights (Figure 4A). LAL-D is known to cause hepatomegaly, whose extent was unchanged based on comparable liver weights between *Lal* KO and *Lal/Mmp12* DKO mice (Figure 4C). Similarly, the weights of subcutaneous white adipose tissue (sWAT), epididymal white adipose tissue (eWAT), and brown adipose tissue (BAT) were comparable in *Lal* KO and*Lal/Mmp12* DKO (Figure 4D), suggesting that the weight decline of adipose tissue was not affected by the deletion of *Mmp12*.

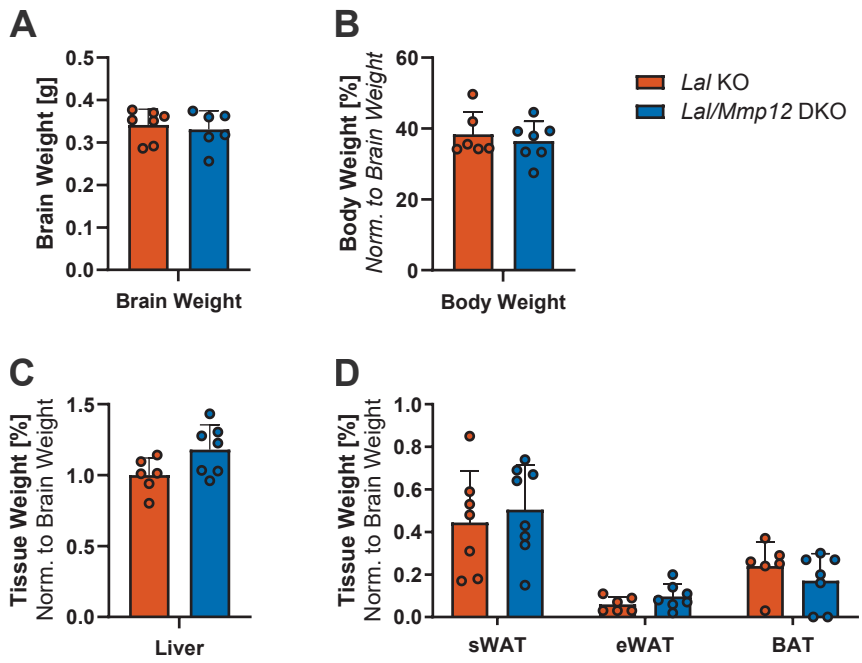

Figure 4: Unchanged body and tissue weights of Lal/Mmp12 DKO mice. 15-week-old mice were sacrificed after 6 h of fasting. **(A)** Brain weight, and **(B)** body weight, normalized to brain weight. **(C)** Liver weight normalized to brain weight. **(D)** Weight of subcutaneous white adipose tissue (sWAT), epididymal white adipose tissue (eWAT) and brown adipose tissue (BAT), normalized to brain weight. Data are shown as means (n = 6-7) + SD.

We proceeded to examine the plasma parameters of *Lal/Mmp12* DKO mice in greater detail. The plasma concentrations of alanine aminotransferase (ALT) and aspartate aminotransferase (AST), common clinical markers for hepatic injury, were not significantly changed following the deletion of *Mmp12* (Figure 5A). Similarly, plasma lipid parameters (Figure 5B) and hepatic lipid accumulation (Figure 5C) were identical in *Lal* KO and *Lal/Mmp12* DKO mice after 12 h of fasting, indicating that MMP-12 does unlikely contribute to hepatic lipid accumulation in *Lal* KO mice.

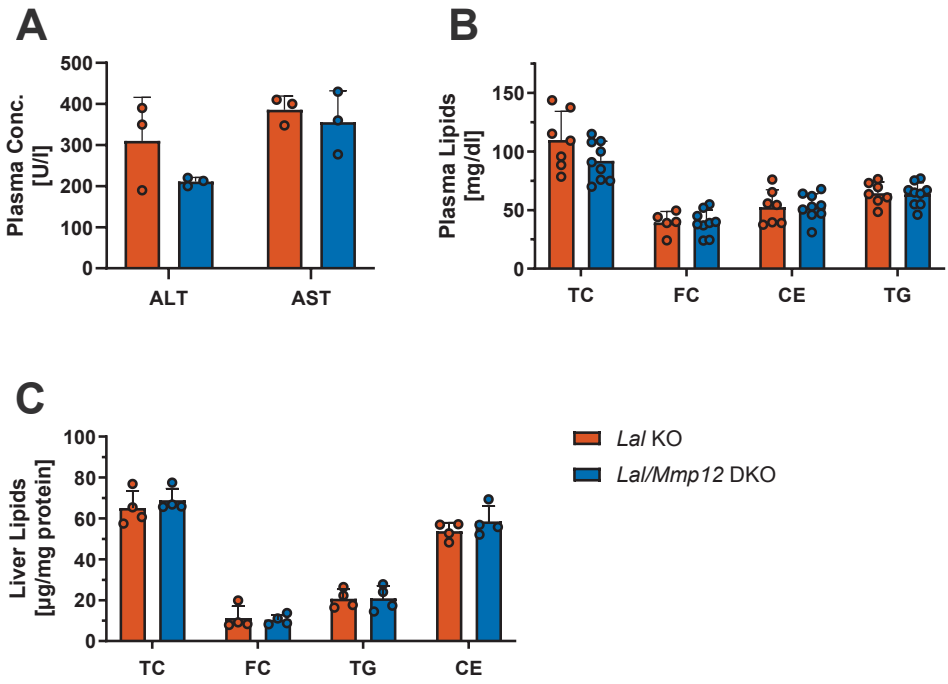

Figure 5: Unchanged plasma ALT, AST, and lipid parameters, and hepatic lipid accumulation in Lal/Mmp12 DKO mice. 15-week-old mice were sacrificed after 6 h of fasting. Plasma concentrations of **(A)** alanine aminotransferase (ALT) and aspartate aminotransferase (AST). **(B)** Plasma and **(C)** hepatic lipid parameters (Total cholesterol (TC), free cholesterol (FC), cholesteryl ester (CE) and triacylglycerol (TAG). Data are shown as means (n = 3-7) + SD.

In mice, LAL-D caused substantial adaptations in lipid metabolism, reflected by expression changes of key enzymes in cholesterol biosynthesis, fatty acid oxidation, triglyceride synthesis, and lipoprotein assembly (17). However, the deletion of *Mmp12* had no effect on the hepatic expression of *Fasn*, *Cd36*, *Acat*, *Srebp*, *Ppara* or *Pgc1a*. Similarly, the analysis of hepatic ECM-deposition, based on the expression of key ECM components such as collagen, actin, and elastin, revealed no detectable changes in *Lal/Mmp12* DKO mice (Figure 6B). The expression of pro-inflammatory markers, including *Cox2, Il6, Ifng,* and *Tnf*, as well as the TNF-target genes *Irf1* and *Junb*, and the anti-inflammatory marker *Il10*, were comparable between

Lal KO and *Lal/Mmp12* DKO mice, suggesting no significant amelioration to hepatic inflammation. The chemotaxis markers *Ccl2* and *Ccl5*, as well as the macrophage marker *Emr1* were similarly unaffected by the deletion of *Mmp12* (Figure 6C).

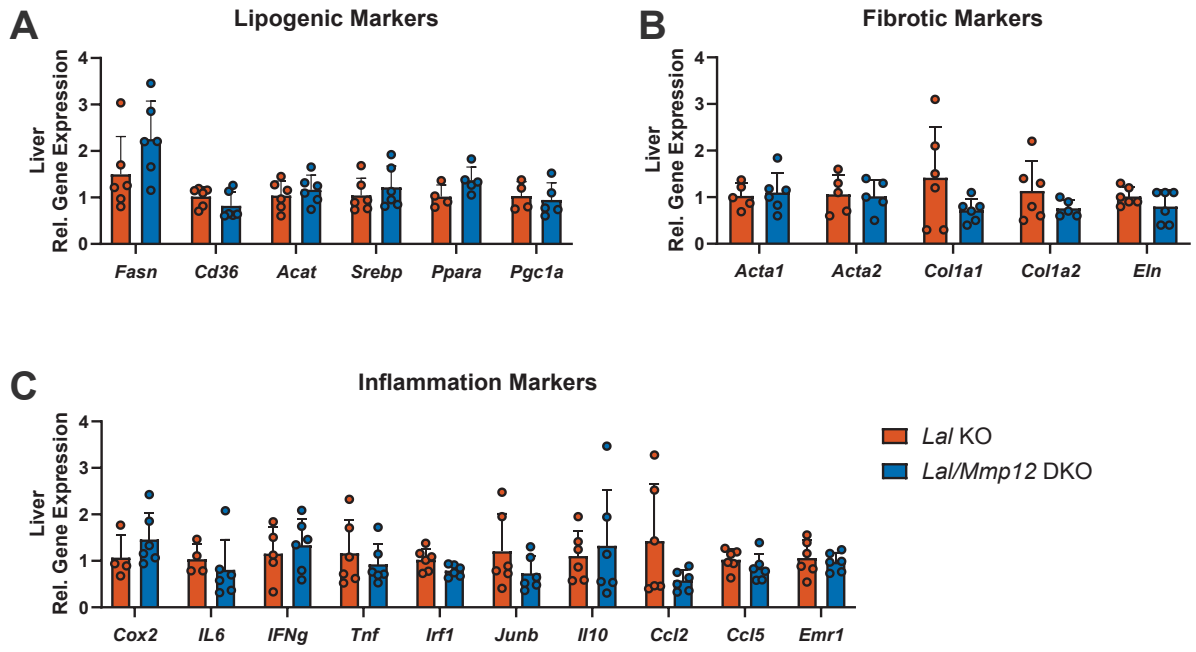

Figure 6: Gene expression markers for hepatic inflammation and fibrosis were unaffected in *Lal/Mmp12* DKO mice. 15-week-old mice were sacrificed after 6 h of fasting. Hepatic mRNA expression of **(A)** lipogenic markers (*Fasn, Cd36, Acat, Srebp, Ppara and Pgc1a*), **(B)** fibrotic markers (*Acta1*, *Acta2*, *Col1a1*, *Col1a2* and *Eln*), **(C)** pro-inflammatory markers (*Cox2, Il6, Ifng and Tnf),* TNF target genes *(Irf1 and Junb),* anti-inflammatory marker (*Il10*), chemotaxis markers (*Ccl2* and *Ccl5*), macrophage marker (*Emr1*). Data are shown as means (n = 3-7) + SD. $^{\#}p \leq 0.05$ and $^{\#\#\#}p \leq 0.001$ for the comparison between *Lal* KO and *Lal/ Mmp12* DKO mice.

Matrix metalloproteinases can be inhibited by tissue inhibitors of matrix metalloproteinases (TIMPs), and, thus, we analyzed possible changes in the expression of the four known *Timp* genes. We observed identical mRNA expression of *Timp1*, *Timp2*, *Timp3*, and *Timp4* in both genotypes (Figure 7B). Furthermore, we determined the hepatic expression of other members of the MMP family. First, we verified the deletion of *Mmp12* by the absence of its expression (Figure 7A). The liver of *Lal/Mmp12* DKO mice exhibited decreased expressions for *Mmp3*, *Mmp10*, and *Mmp13* (Figure 7B). In conclusion, targeting MMP-12 was ineffective in ameliorating any aspect of the hepatic pathology in 15-week-old *Lal* KO mice.

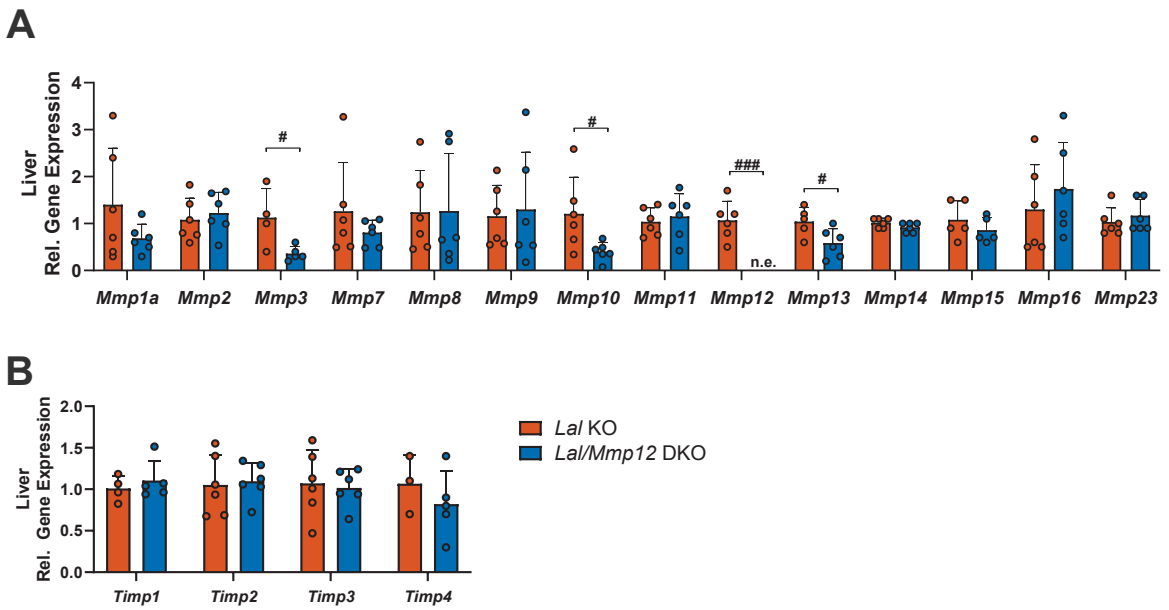

Figure 7: Reduced hepatic expression of *Mmp3*, *Mmp10,* and *Mmp13* in *Lal/Mmp12* DKO mice. 15-week-old mice were sacrificed after 6 h of fasting. **(A)** Tissue inhibitors of MMPs (TIMPs) (*Timp1 – 4*), and **(B)** mouse MMP family members (*Mmp1a, Mmp2, Mmp3, Mmp7, Mmp8, Mmp9, Mmp10, Mmp11, Mmp12, Mmp13, Mmp14, Mmp15 Mmp16* and *Mmp23).* Data are shown as means (n = 3-7) + SD. $^{\#}p \leq 0.05$ and $^{\#\#\#}p \leq 0.001$ for the comparison between *Lal* KO and *Lal/Mmp12* DKO mice.

The lungs of *Lal* KO mice display pronounced inflammation and fibrosis. The connection between LAL-D and *Mmp12* overexpression was first demonstrated in the lungs of *Lal* KO mice (146). Similarly, the expression of *Mmp12* was found to be significantly correlated with the severity of chronic inflammatory conditions of the lungs, such as smoking-induced COPD (147). However, targeting MMP-12 in *Lal* KO mice did not result in reduced expression of pro-inflammatory markers, TNF target genes, anti-inflammatory markers, chemotaxis or macrophage markers in *Lal/Mmp12* DKO mice (Figure 8). Moreover, the expression of extracellular matrix proteins, including *Acta1*, *Acta2*, *Col1a1*, and *Col1a2*, was identical between the two genotypes (Figure 8). Only the expression of elastin (*Eln*) was reduced by 30% in the lungs of *Lal/Mmp12* DKO mice, suggesting a correlation between *Mmp12* expression and elastin turnover.

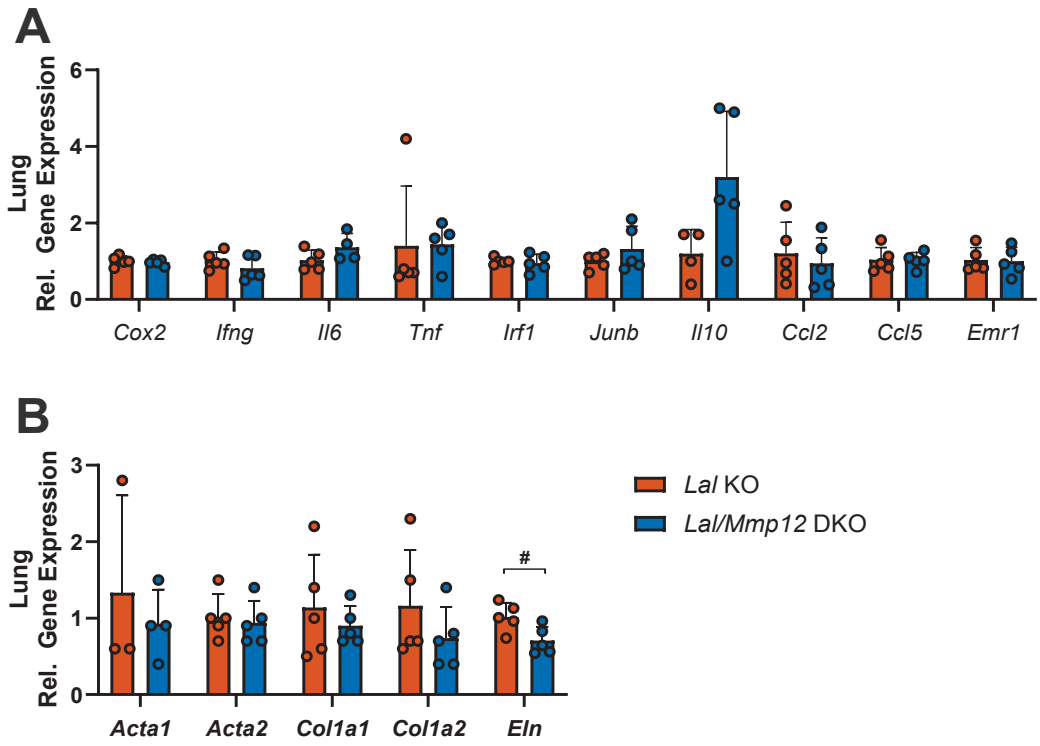

Figure 8: Only minor changes in pulmonary gene expression in *Lal/Mmp12* DKO mice. 15-week-old mice were sacrificed after 6 h of fasting. Hepatic mRNA expression of **(A)** pro-inflammation markers (*Cox2, Il6, Ifng, Tnf),* TNF target genes *(Irf1, Junb)*, anti-inflammatory marker (Il10), chemotaxis marker (*Ccl2* and *Ccl5*) and the macrophage marker (*Emr1*), **(B)** fibrotic markers (*Acta1*, *Acta2*, *Col1a1*, *Col1a2* and *Eln*)**.** *Data are* shown as means (n = 3-6) + SD. $^{\#}p \leq 0.05$, and $^{\#\#\#}p \leq 0.001$ for the comparison between *Lal* KO and *Lal/Mmp12* DKO mice.

Similar to the hepatic expression of TIMPs, the lungs of *Lal/Mmp12* DKO mice showed no changes in the expression of *Timp1*, *Timp2*, *Timp3* or *Timp4* (Figure 9A). Of the 18 MMP family members expressed in the lung of *Lal* KO mice, only *Mmp3* showed a marked reduction in *Lal/Mmp12* DKO mice (Figure 9B-C), indicating that MMP-12 may regulate the expression of *Mmp3* in both the liver and lung.

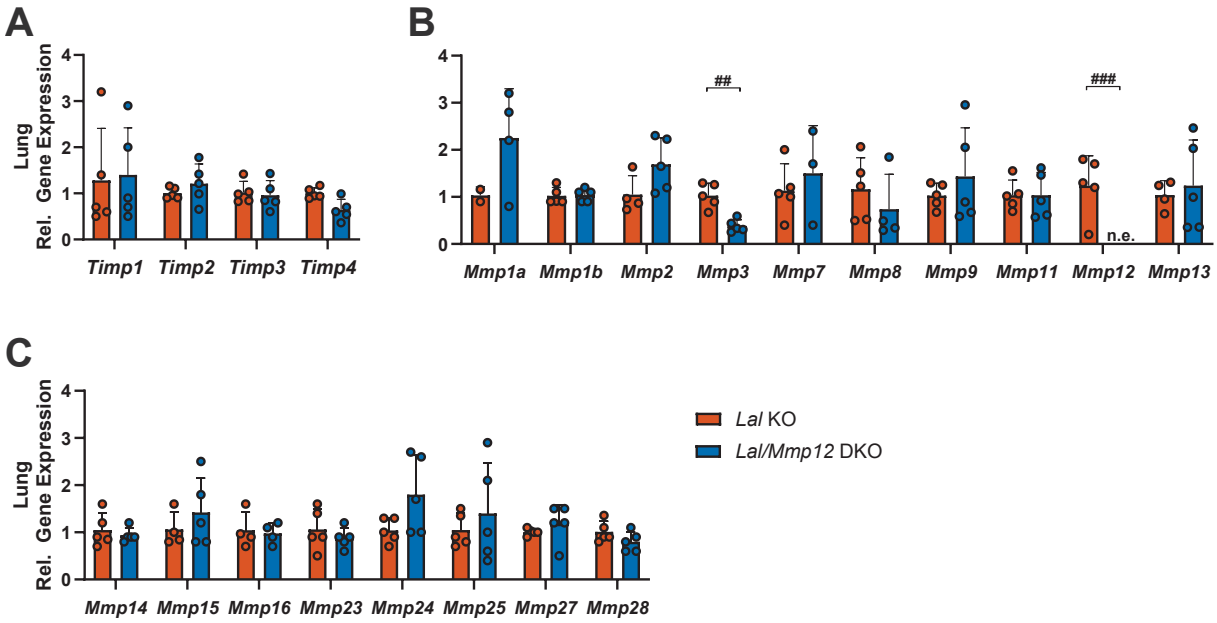

Figure 9: Only *Mmp3* exhibited a reduced pulmonary expression in *Lal/Mmp12* DKO mice. 15-week-old mice were sacrificed after 6 h of fasting. Hepatic mRNA expression of **(A)** *t*issue inhibitors of MMPs (TIMPs) (*Timp1 - 4*). ***(B-C)*** mouse MMP family members (*Mmp1a, Mmp1b, Mmp2, Mmp3, Mmp7, Mmp8, Mmp9, Mmp11, Mmp12, Mmp13, Mmp14, Mmp15 Mmp16, Mmp23, Mmp24, Mmp25, Mmp27,* and *Mmp28) and*, *Data are* shown as means (n = 3-6) + SD. $^{\#}p \leq 0.05$, and $^{\#\#\#}p \leq 0.001$ for the comparison between *Lal* KO and *Lal/Mmp12* DKO mice.

In summary, the deletion of *Mmp12* in 15-week-old mice did not ameliorate the emphysema-like lung phenotype associated with LAL-D. Neither reduced body and tissue weights, nor hepatomegaly, hepatic macrophage accumulation, or pulmonary inflammation were affected in *Lal/Mmp12* DKO mice. We propose that with chow diet feeding or at this relatively early disease stage, *Mmp12* expression may be insufficient to significantly contribute to the pathology of LAL-D.

3.2. Characterizing 15-week-old high-fat diet-fed *Lal/Mmp12* DKO mice

To test whether challenging mice might magnify the contribution of MMP-12 to the pathology of LAL-D, we fed mice from the age of 9 to 15 weeks with a high-fat, high-cholesterol diet (HFD). Furthermore, wild type (WT) mice were included to better contextualize the pathology of *Lal* KO and potential ameliorations in *Lal/Mmp12* DKO mice.

After challenging mice with a high fat diet for 6 weeks, *Lal* KO and *Lal/Mmp12* DKO mice still displayed comparable reductions in body weights (Figure 10A). All three genotypes exhibited

a similar body weight increase (Figure 10B) and total weight gains (Figure 10C). Similar to chow diet feeding, 6 weeks of HFD did not alter liver, spleen, sWAT or BAT weights between *Lal* KO and *Lal/Mmp12* DKO mice compared to WT mice.

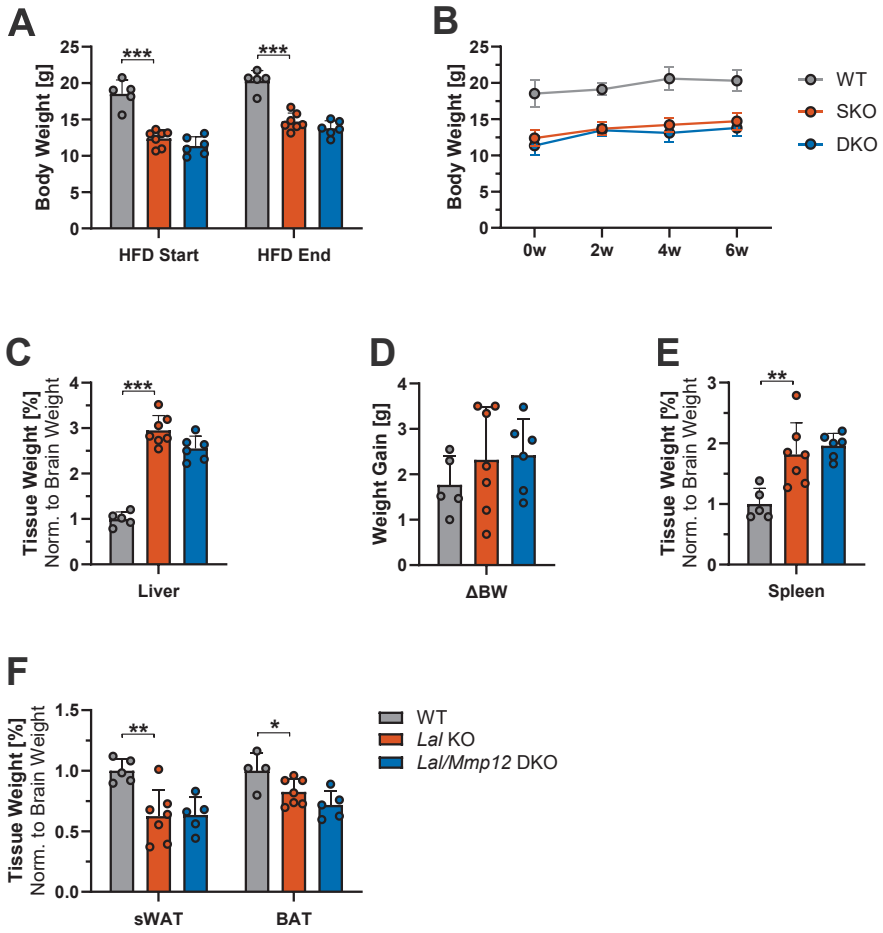

Figure 10: Six weeks of HFD feeding did not alter body or tissue weights of *Lal/Mmp12* DKO mice. 15-week-old female mice were fed a high fat diet (HFD) for 6 weeks, fasted for 6 h, and sacrificed. **(A)** Body weights at 9 weeks (Start) and 15 weeks (End) of age, **(B)** body weight, and **(C)** body weight gain. Tissue weight of the **(D)** liver, **(E)** spleen, **(F)** subcutaneous white adipose tissue (sWAT), and brown adipose tissue (BAT). All tissue weights were normalized to brain weight; WT mice were arbitrarily set to 1. Data are shown as means (n = 5-7) + SD. ***p ≤ 0.001 for the comparison between *Lal* KO and *Lal/Mmp12* DKO mice.

Next, we assessed whether HFD feeding modified the effect of *Mmp12* deletion on plasma and hepatic lipid parameters. At 9 weeks of age, chow-fed *Lal* KO mice displayed significantly elevated TC levels, primarily driven by an increase in the FC fraction, while CE and TAG levels remained comparable to WT controls (Figure 11A). After 6 weeks of HFD feeding, the increase in TC and FC was further exacerbated in *Lal* KO mice and accompanied by elevated CE levels. Across all measured lipids, no differences were observed between *Lal* KO and *Lal/Mmp12* DKO mice, indicating that *Mmp12* deletion did not affect plasma lipid composition under these conditions (Figure 11A). Consistent with the plasma, hepatic cholesterol levels were markedly increased in *Lal* KO mice, resulting from elevated FC and CE accumulation (Figure 11B). In contrast, hepatic TG content was comparable across all three genotypes (Figure 11B).

To evaluate hepatocyte injury, plasma AST and ALT concentrations were measured. While chow-fed WT and *Lal* KO mice exhibited only modest differences in transaminase levels, HFD feeding induced a pronounced increase in both AST and ALT concentrations specifically in *Lal/Mmp12* DKO mice. These findings suggest that *Mmp12* deletion may sensitize the liver to HFD-induced stress or injury, potentially through a mechanism independent of lipid accumulation.

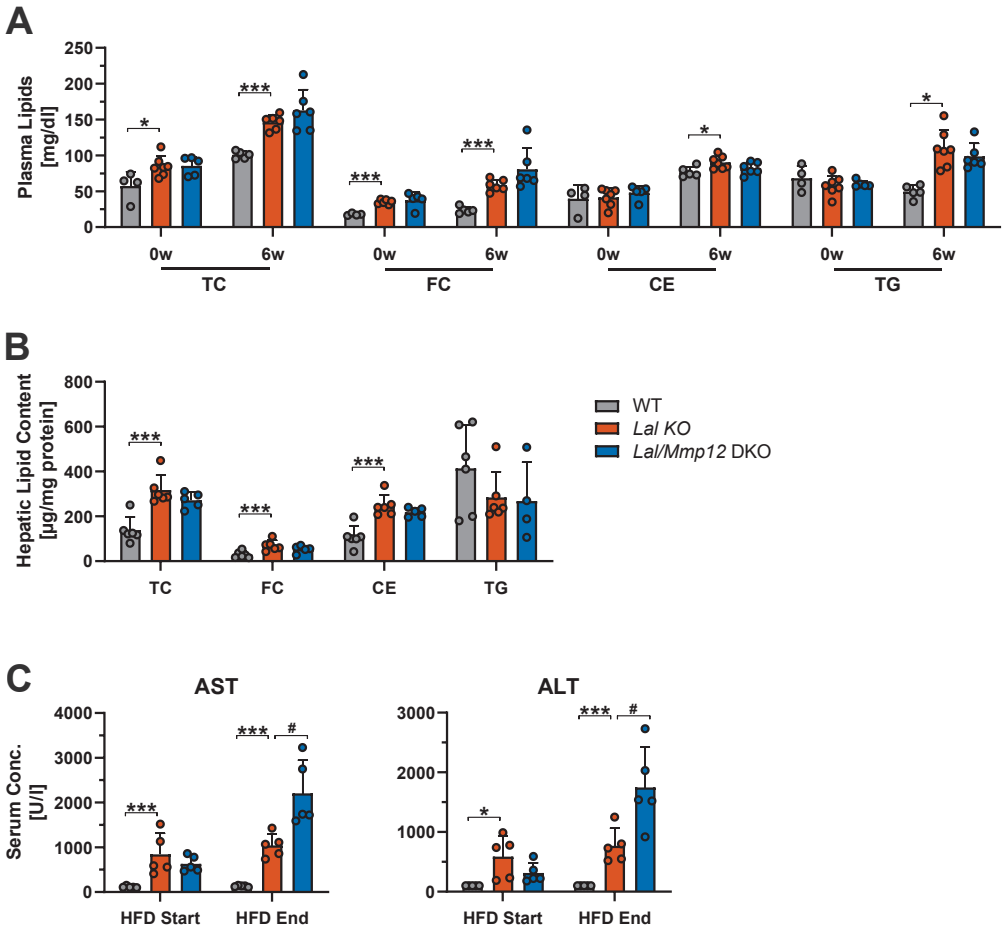

Figure 11: No changes in lipid paramters and plasma AST & ALT concentrations following the deletion of *Mmp12*. 15-week-old female mice were fed a high-fat diet (HFD) for 6 weeks, fasted for 6 h, and sacrificed. **(A)** Plasma lipid parameters at the start and end of HFD-feeding, **(B)** hepatic lipid content, and **(C)** plasma concentrations of aspartate aminotransferase (AST) and alanine aminotransferase (ALT) at the start and end of HFD-feeding. Data are shown as means (n = 4-7) + SD. *p ≤ 0.05 and ***p ≤ 0.001 for the comparison between WT and *Lal* KO mice; #p ≤ 0.05 for the comparison between *Lal* KO and *Lal/Mmp12* DKO mice.

The objective of challenging mice for 6 weeks on a HFD was to enhance the expression of *Mmp12*, thereby potentially amplifying the hypothesized contribution of MMP-12 to the hepatic pathology. An ~750-fold elevated *Mmp12* expression was observed in *Lal* KO mice (Figure 12A). However, the Ct value for *Lal* KO mice remained approximately at 23, regardless of dietary regimen (data not shown), indicating that HFD feeding was insufficient to further upregulate the expression of *Mmp12*. Notably, in *Lal/Mmp12* DKO mice, the expression of the anti-inflammatory marker *Il10* was restored to levels comparable to those observed in WT mice

(Figure 12B). However, the pro-inflammatory markers *Tnf* and *Il1b* remained unchanged by the deletion of *Mmp12* (Figure 12B). Similarly, mRNA expression of *Emr1* and *Cd68* was equivalent in *Lal* KO and *Lal/Mmp12* DKO mice (Figure 12C), indicating that, similar to mice fed a chow diet, HFD feeding did not result in altered hepatic accumulation of lipid-laden macrophages in *Lal/Mmp12* DKO mice. Instead, the expression of *Ly6G* and *Elane*, two neutrophil markers, was found to be 516- and 520-fold elevated in *Lal* KO mice, but only 216- and 175-fold in *Lal/Mmp12* DKO mice (Figure 12D). Immunofluorescence staining for the neutrophil marker Ly6G demonstrated the presence and localization of neutrophils surrounding some individual lipid-loaded macrophage aggregates (Figure 12E). In agreement with the expression of *Ly6g*, these neutrophil accumulations appeared less dense on *Lal/Mmp12* DKO section than for *Lal* KOs. Taken together, these findings suggest that the deletion of *Mmp12* had a modest impact on neutrophil accumulation and that a more comprehensive characterization of immune cell populations in *Lal/Mmp12* DKO is warranted.

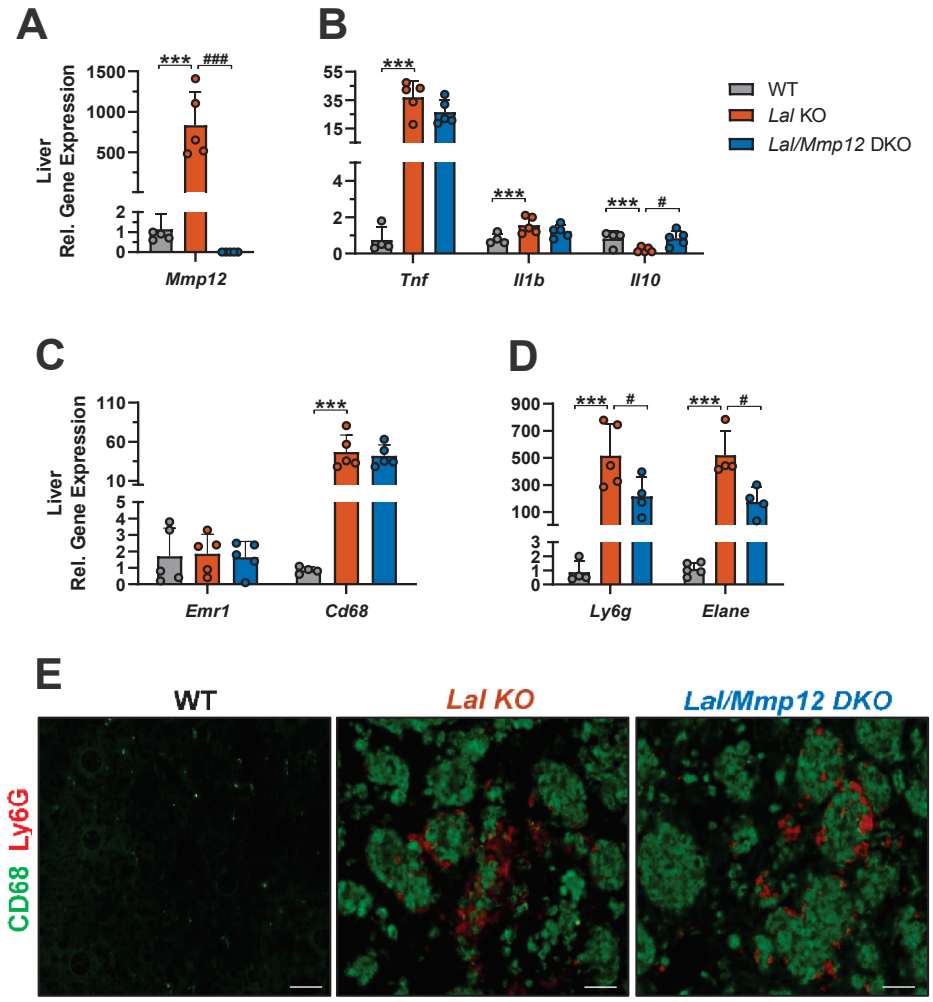

Figure 12: Reduced expression of the neutrophil markers Ly6G and Elane in the liver of *Lal/Mmp12* DKO mice. 15-week-old female mice were fed a high fat diet (HFD) for 6 weeks, fasted for 6 h, and sacrificed. Hepatic mRNA expresion of **(A)** *Mmp12,* **(B)** pro-inflammatory (*Tnf* and *Il1b)* and anti-inflammatory (*IL10)* markers, **(C)** macrophage markers (*Emr1* and *Cd68*), and **(D)** neutrophil markers (*Ly6G* and *Elane*). **(E)** Paraffin sections stained by immunofluorescence targeting of CD68 (green) and Ly6G (red). Data are shown as means (n = 4-7) + SD. ***p ≤ 0.001 for the comparison between WT and *Lal* KO mice; #p ≤ 0.05 and ###p ≤ 0.001 for the comparison between *Lal* KO and *Lal/Mmp12* DKO mice.

3.3. Characterizing 30-week-old chow diet-fed *Lal/Mmp12* DKO mice

In the next cohort, we increased the age of mice to 30 weeks to both improve comparability to previously published data on *Lal* KO mice and to characterize mice in a more advanced stage of LAL-D. At 30 weeks of age, male *Lal* KO and *Lal/Mmp12* DKO mice displayed comparable reductions in body weight compared to WT littermates (Figure 13A). Similarly, the extent of hepatomegaly was identical in *Lal* KO and *Lal/Mmp12* DKO mice (Figure 13B). Next, we verified the hepatic expression of *Mmp12* and observed a significant 275-fold increase in *Lal* KO mice and a complete lack of expression in *Lal/Mmp12* DKO mice (Figure 13C). The mRNA expression levels of pro-inflammatory markers (*Tnf, Il1b*) and the macrophage chemotaxis marker *(Ccl2*) were comparable between the livers of *Lal* KO and *Lal/Mmp12* DKO mice (Figure 13D).

The enlargement of the liver (hepatomegaly) seen in *Lal* KO mice is primarily mediated by the progressive buildup of CE-loaded macrophages (29). Elevated liver weights are complemented by 25.8- and 194-fold increased hepatic expression of the macrophage markers *Emr1* and *Cd68* (Figure 13E), as well as increased CE accumulation in the liver of *Lal* KO mice (Figure 13G). However, both the expression of macrophage markers, and hepatic lipid accumulation remained comparable in *Lal/Mmp12* DKO mice. This is further substantiated by the absence of discernible differences in hepatic histology between *Lal* KO and *Lal/Mmp12* DKO sections. Both genotypes displayed identical macrophage aggregates, forming granuloma-like structures (Figure 13F), indicating that MMP-12 does not contribute to hepatomegaly or hepatic macrophage accumulation.
In conclusion, our data suggest that MMP-12 is unlikely to modulate macrophage accumulation or their associated dysfunction in the context of LAL-D.

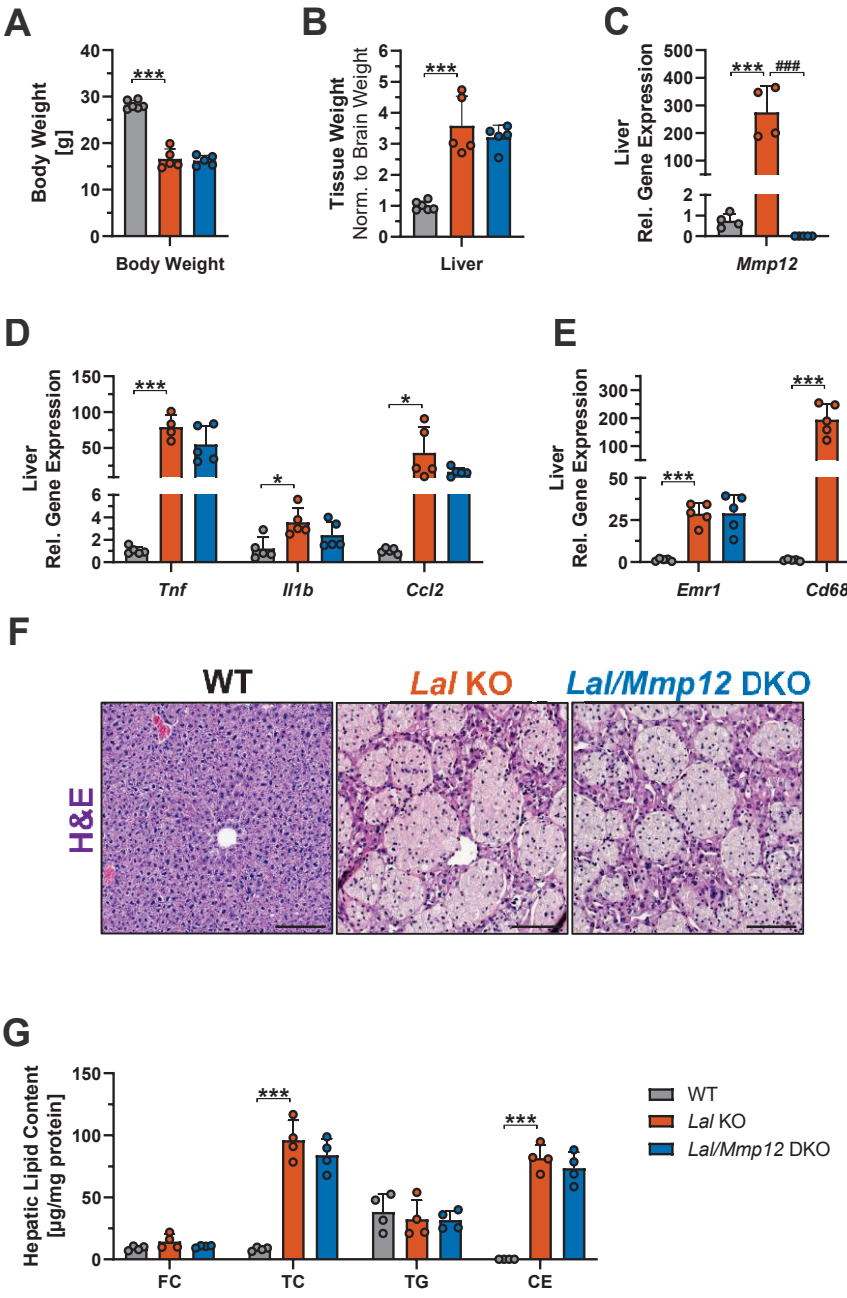

Figure 13: Unchanged liver weight, macrophage accumulation, and inflammation in *Lal/Mmp12* DKO mice. 30-week-old male chow diet-fed mice were sacrificed after 6 h of fasting. **(A)** Body and **(B)** liver weight normalized to brain weight; WT mice were arbitrarily set to 1. Hepatic mRNA expresion of **(C)** *Mmp12,* **(D)** pro-inflammatory markers (*Tnf*, *Il1b* and *Ccl2*) and **(E)** macrophage markers (*Emr1* and *Cd68*). **(F)** Representative images of liver sections stained with H&E. **(G)** Hepatic lipid paramters. Data are shown as means (n = 4-7) + SD. *p ≤ 0.05 and ***p ≤ 0.001 for the comparison between WT and *Lal* KO mice; ###p ≤ 0.05 for the comparison between *Lal* KO and *Lal/Mmp12* DKO mice. The use of this figure obtained from (148) is allowed under the terms described in the appendix.

LAL-D has been shown to cause a depletion of white and brown AT in *Lal* KO mice (56). Since MMP-12 secreted by AT macrophages, was shown to promote insulin resistance while also reducing HFD-induced AT expansion (149), we examined whether dysregulated MMP-12 expression might contribute to the AT pathology in *Lal* KO mice. The loss of AT in the *Lal* KO mice was evidenced by a strong reduction of sWAT weight and to a lesser extent in BAT (Figure 14A) and was not ameliorated in *Lal/Mmp12* DKO mice. In agreement, the mean area of sWAT adipocytes were 2.8-fold and 2.6-fold reduced in *Lal* KO and *Lal/Mmp12* DKO mice, respectively (Figure 14B). Similarly, the count of adipocytes below 10 µm in diameter was markedly elevated, while diameters between 20 - 30 µm were greatly diminished in both *Lal* KO and *Lal/Mmp12* DKO mice (Figure 14C). Based on our data, we conclude that MMP-12 does not contribute to adipocyte loss in *Lal* KO mice.

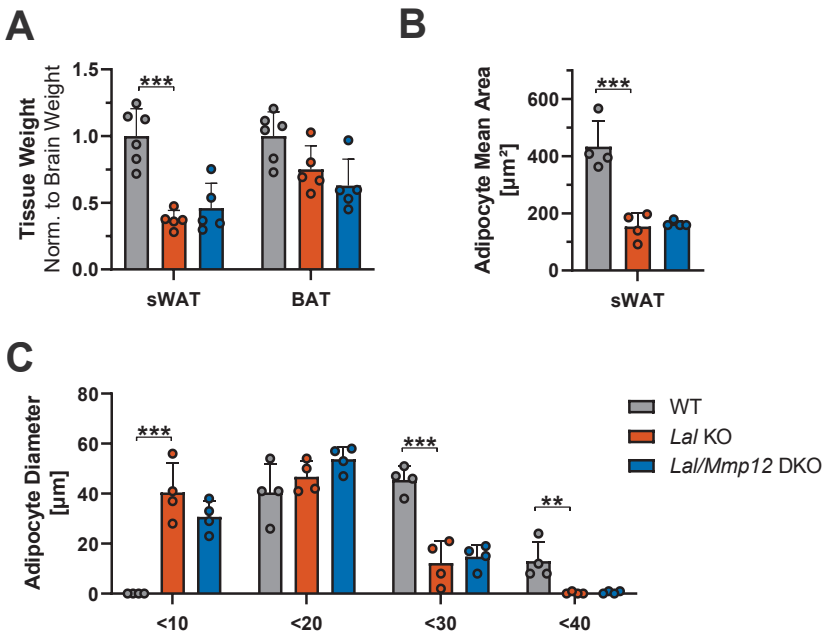

Figure 14: Comparable reduction of adipose tissue weights in 30-week old *Lal* KO and *Lal/Mmp12* DKO mice. 30-week old chow diet-fed mice were sacrificed after 6 h of fasting. **(A)** The weight of subcutaneous white adipose tissue (sWAT) and brown adipose tissue (BAT) normalized to brain weight; WT mice were arbitrarily set to 1. **(B)** Mean area and **(C)** diameter of adipocytes from sWAT paraffin sections. Data are shown as means (n = 4-6) + SD. **p ≤ 0.01 and ***p ≤ 0.001 for the comparison between WT and *Lal* KO mice. The use of this figure obtained from (148) is allowed under the terms described in the appendix.

Next, we assess the effect of MMP-12 loss on different plasma parameters. The plasma concentrations of AST and ALT are commonly used as a clinical biomarker for liver health. In *Lal* KO mice, we observed a 7.3-fold increase in AST and a 5.1-fold increase of ALT (Figure 15A), further emphasizing the severity of the hepatic pathology in LAL-D. However, AST and ALT levels in *Lal/Mmp12* DKO mice were comparable to those in *Lal* KO mice. Similarly, serum amyloid A concentrations (Figure 15B), a hepatocyte-derived acute phase protein, were comparable across both genotypes, suggesting that the deletion of *Mmp12* does not affect markers of hepatocyte injury or systemic inflammation.

After 6 h of fasting, blood glucose levels were significantly reduced in both *Lal* KO and *Lal/Mmp12* DKO mice (Figure 15C). However, plasma lipid parameters after 6 h of fasting did not differ significantly between WT, *Lal* KO, and *Lal/Mmp12* DKO mice (Figure 15D), suggesting that MMP-12 does not contribute to the metabolic phenotype of LAL-D.

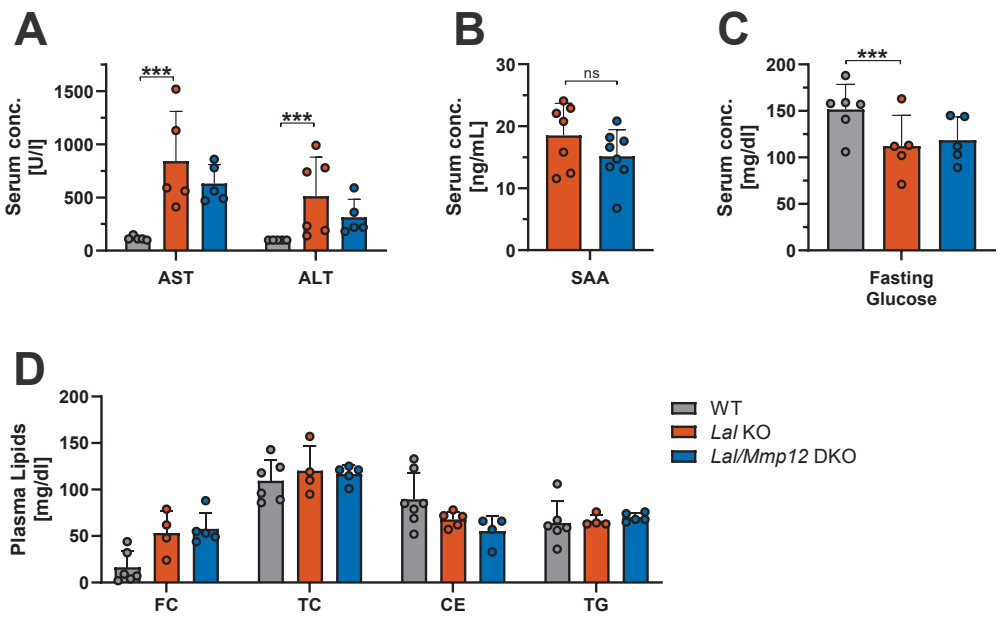

Figure 15: No changes in plasma parameters in *Lal/Mmp12* DKO mice. Blood was collected from 30-week-old chow diet-fed mice after 6 h of fasting. **(A)** Plasma concentrations of aspartate aminotransferase (AST), alanine aminotransferase (ALT), and **(B)** serum amyloid A (SAA). **(C)** Fasting glucose and **(D)** plasma lipid parameters after 6 h of fasting. Data are shown as means (n = 4-8) + SD. *p ≤ 0.05 and ***p ≤ 0.001 for the comparison between WT and *Lal* KO mice. The use of this figure obtained from (148) is allowed under the terms described in the appendix.

Before examining possible effects deleting *Mmp12* has on the pathology of immune cells, we performed a preliminary evaluation of whether *Mmp12* KO mice display alterations in their complete blood counts and whether sex specific differences must be accounted for.

To this end, we performed complete blood counts of 15-week-old male and female WT and *Mmp12* KO mice. Interestingly, we observed a 33.7% reduction in total leukocyte counts (Figure 16A), 40.1% reduction in lymphocytes (Figure 16B), and a 32% reduction of granulocytes in *Mmp12* KO mice (Figure 16C), indicating a cell type-independent effect of *Mmp12* deletion on cell counts.

Taken together, this suggests a physiological role of MMP-12 in the absence of chronic inflammation and that this effect is sex-independent. We conclude that a proper characterization of the immune system of *Mmp12* KO and *Lal/Mmp12* DKO mice is required and that either sex may be used.

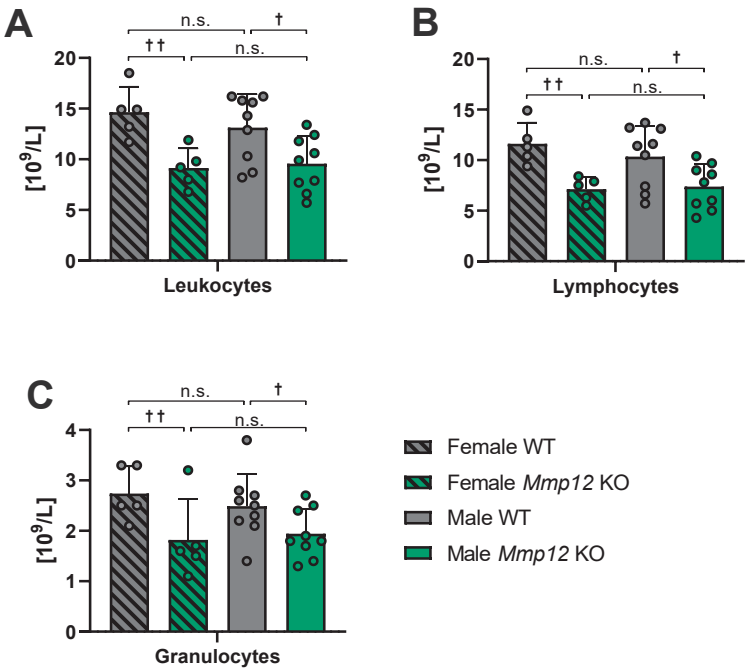

Figure 16: No sex specific differences in blood cell counts in *Mmp12* KO mice. Peripheral blood was collected from the submandibular vein of 15-week-old chow diet-fed mice. Cell counts for **(A)** total leukocytes, **(B)** lymphocytes, and **(C)** granulocytes. Data are shown as means (n = 6-12) + SD. $^{\dagger}p < 0.05$ and $^{\dagger\dagger}p < 0.01$ for the comparison between WT and *Mmp12* KO mice.

3.4. Characterizing the immune system of *Lal/Mmp12* DKO mice

The peripheral blood of *Lal* KO mice has been shown to be heavily skewed towards the myeloid lineage. To analyze whether the deletion of *Mmp12* affects the lymphoid-to-myeloid shift in *Lal* KO mice, we measured the complete blood counts of 30-week-old chow diet-fed male mice. We observed a nearly identical reduction in leukocyte, lymphocyte, and granulocyte counts (26.4%, 26.3%, and 27.1%, respectively) between WT and *Mmp12* KO mice (Figure 17A-B). Accordingly, lymphocytes accounted for ~77% and granulocytes for ~20% of circulating cells in both WT and *Mmp12* KO mice (Figure 17C), indicating that in the absence of an inflammatory stimulus and under physiological conditions, the deletion of *Mmp12* has no effect on the lymphoid-to-myeloid ratio of peripheral blood immune cells. Consistent with this, cytological examination of Giemsa-stained blood smears showed that 82.8% and 79.3% of immune cells were of the myelomonocytic lineage in WT and *Mmp12* KO mice, respectively (Figure 17D). Platelet counts were equally elevated in both *Lal* KO and *Lal/Mmp12* DKO mice (Figure 17E). These results indicate that the deletion of *Mmp12* has a cell type-independent effect on peripheral blood immune cell counts. Total leukocyte counts in *Lal* KO mice increased by 14%, originating from a 43.9% decrease in lymphocytes but a 3.39-fold increase in granulocyte counts (Figure 17A-B). This shift was reflected by a reduction in lymphocytes to 36.9% and an increase in granulocytes to 58.6% of total circulating immune cells (Figure 17C). This was further corroborated by cytological examination, with only 41.1% of cells exhibiting a lymphoid appearance. Regarding other parameters of the complete blood count, *Lal* KO mice displayed a 77.6% increase in platelet counts (Figure 17E) and pronounced reductions of the mean corpuscular volume, hematocrit, hemoglobin, and mean corpuscular hemoglobin (Table 3), indicating that the wide-ranging pathology of LAL-D also significantly affects thrombocytes and erythrocytes. Compared to WT mice, *Mmp12* KO and *Lal* KO mice, *Lal/Mmp12* DKO mice displayed greater variability in their blood counts. Nevertheless, total leukocyte counts appeared on average comparable between *Lal* KO and *Lal/Mmp12* DKO mice (Figure 17A). The highest lymphocyte counts of *Lal/Mmp12* DKO mice were comparable to that of an average WT mouse, while the lowest counts were equal to an average count of a *Lal* KO mice (Figure 17B). However, in *Lal/Mmp12* DKO mice with the highest lymphocyte counts, we also observed proportionally elevated granulocyte counts (Figure 17B), resulting in an unchanged ratio of lymphocytes to granulocytes compared to *Lal* KO mice. To complement automated complete blood counts, we performed cytological examination and manually counted the ratio of myeloid to lymphoid cells, leading to a marginally non-significant increase ($p=0.056$) in the lymphoid cells (Figure 17D). Of note, the number of thrombocytes was not affected and remained elevated in *Lal/Mmp12* DKO mice (Figure 17E). However, hemoglobin (HGB) levels

were markedly reduced from 13.9 g/dl in WT mice to 9 g/dl in *Lal* KO mice and were partially ameliorated to 10.4 g/dl in *Lal/Mmp12* DKO mice (Figure 17F). This increase in HGB may be attributed to a complementary rise in erythrocyte (RBC) counts that were comparable in WT, *Mmp12* KO and *Lal* KO, but increased 17% (p=0.022) in *Lal/Mmp12* DKO mice (Table 3). Since RBC counts were unchanged in *Lal* KO mice but increased in the DKO mice, they are the most probable source of the observed rise in HGB levels.

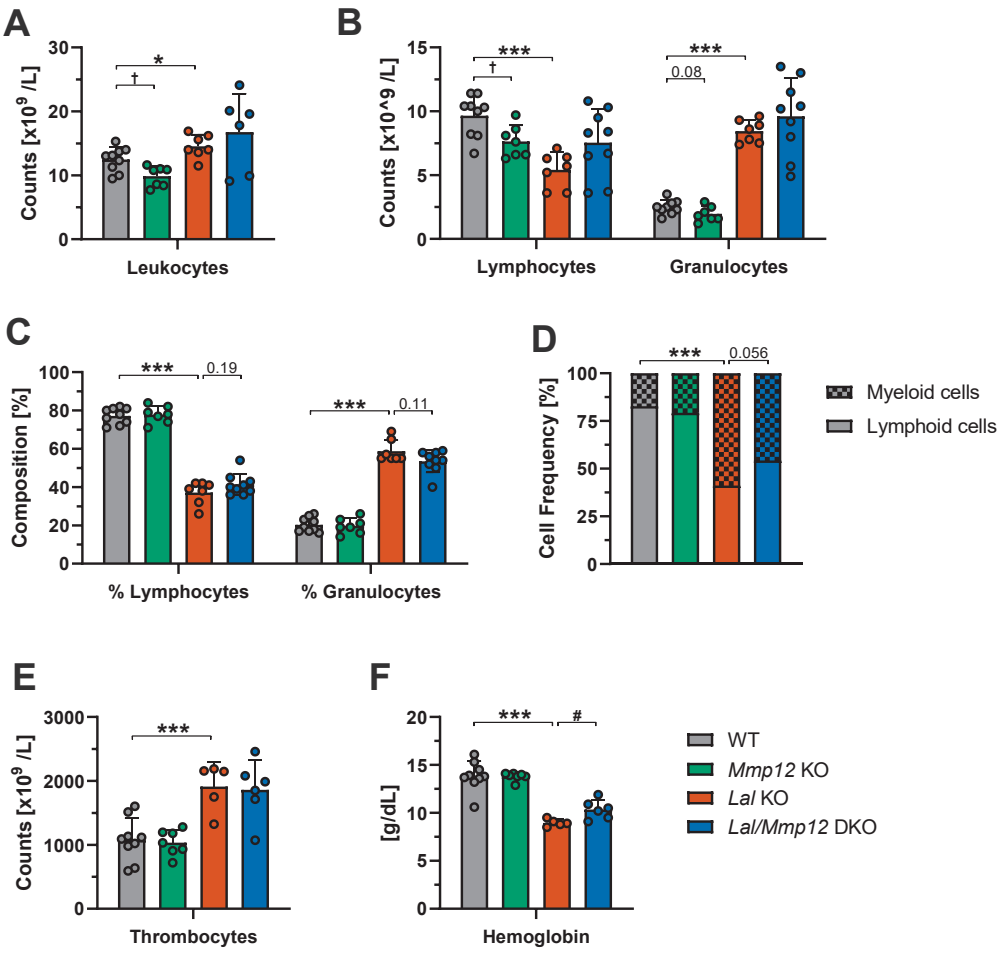

Figure 17: First indications of ameliorate lymphocyte and granulocyte counts in *Lal/Mmp12* DKO mice. Peripheral blood was collected from the submandibular vein of 30-week-old chow diet-fed mice. Cell counts for **(A)** total leukocytes, **(B)** lymphocytes, and granulocytes. **(C)** The percentages of lymphocytes or granulocytes. **(D)** The freqency of lymphoid and myeliod cells determined by cytological examinaton of Giemsa-stained blood smears. **(E)** Total thrombocyte counts and **(F)** hemoglobin levels. Data are shown as means (n = 6-12) + SD. $^{\dagger}p < 0.05$ for the comparison between WT and *Mmp12* KO mice. *p ≤ 0.05 and ***p ≤ 0.001 for the comparison between WT and *Lal* KO mice; $^{\#}p \leq 0.05$ for the comparison between *Lal* KO and *Lal/Mmp12* DKO mice. The use of this figure obtained from (148) is allowed under the terms described in the appendix.

Table 3: Complete blood count (CBC) analysis: Peripheral blood was collected from the submandibular vein of 30-week-old chow diet-fed male mice. Values are presented as mean ± SD. Statistical comparisons were performed between Lal KO and Lal/Mmp12 DKO mice.

	Wild Type	***Mmp12* KO**	***Lal KO***	***Lal/Mmp12* DKO**	**t-test** (*Lal* KO vs *Lal/Mmp12* DKO)
PLT	1077 +/- 337	1035 +/- 196	1913 +/- 375	1861 +/- 460	0.84
MPV	4.4 +/- 0.58	4.4 +/- 0.16	4.2 +/- 0.16	4.6 +/- 0.30	0.039
PCT	0.4 +/- 0.11	0.5 +/- 0.09			
PDW	16.3 +/- 0.55	16.2 +/- 0.11	15.9 +/- 0.19	16.1 +/- 0.28	0.15
RBC	9.9 +/- 0.68	9.6 +/- 0.78	9.3 +/- 1.06	11.0 +/- 0.94	0.022
MCV	45.0 +/- 1.66	44.1 +/- 1.02	30.9 +/- 3.05	29.4 +/- 1.64	0.35
HCT	0.4 +/- 0.03	0.4 +/- 0.03	0.3 +/- 0.01	0.3 +/- 0.02	0.0094
HGB	13.9 +/- 1.53	13.8 +/- 0.42	9.0 +/- 0.37	10.4 +/- 1.00	0.017
MCH	14.0 +/- 1.42	14.5 +/- 1.10	9.6 +/- 0.79	9.4 +/- 0.62	0.62
MCHC	32.6 +/- 1.51	32.9 +/- 2.17	31.5 +/- 1.24	32.3 +/- 1.12	0.29
% RDW	15.9 +/- 0.82	15.5 +/- 0.31	21.6 +/- 2.25	22.4 +/- 1.42	0.50
WBC	12.5 +/- 1.90	9.9 +/- 1.56	14.5 +/- 1.83	16.8 +/- 5.52	0.37
LYM	9.7 +/- 1.62	7.6 +/- 1.25	5.4 +/- 1.37	7.1 +/- 2.63	0.21
GRA	2.5 +/- 0.55	2.0 +/- 0.59	8.4 +/- 0.88	8.7 +/- 2.99	0.84
MON	0.3 +/- 0.07	0.3 +/- 0.08	0.6 +/- 0.21	1.0 +/- 0.39	0.11
% LYN	0.77 +/- 0.04	0.77 +/- 0.04	0.37 +/- 0.06	0.42 +/- 0.05	0.19
% GRA	0.20 +/- 0.04	0.20 +/- 0.04	0.59 +/- 0.06	0.53 +/- 0.06	0.11
% MON	0.03 +/- 0.01	0.03 +/- 0.01	0.05 +/- 0.01	0.06 +/- 0.01	0.085
% EOS	0.0 +/- 0	0.0 +/- 0	0.0 +/- 0	0.0 +/- 0	

Abbreviations: PLT - platelet count; MPV - mean platelet volume; PCT - procalcitonin; PDW - platelet distribution width; RBC - red blood cell count; MCV - mean corpuscular volume; HCT - hematocrit; HGB - hemoglobin; MCH - mean corpuscular hemoglobin; MCHC - mean corpuscular hemoglobin concentration; RDW - red blood cell distribution width; WBC - white blood cell count; LYM - lymphocytes; GRA - granulocytes; MON - monocytes; % LYN - relative lymphocyte frequency; % GRA - relative granulocyte frequency; % MON - relative monocyte frequency; % EOS - relative eosinophil frequency. The use of this table obtained from (148) is allowed under the terms described in the appendix.

The spleen is an important secondary lymphoid organ responsible for filtering of senescent blood cells, serving as a reservoir for lymphocytes, and functioning as a central hub of the mononuclear phagocyte (150). In *Lal* KO mice, splenomegaly manifests as a 2.3-fold increase in spleen weight (Figure 18A). Following the deletion of *Mmp12*, splenomegaly was mildly ameliorated and only increased by 1.78-fold (p=0.062) compared to WT mice (Figure 18A). In addition, we observed a distinct amelioration of thymus weights, which were on average 68.6% reduced in *Lal* KO mice, but only 43.5% smaller in *Lal/Mmp12* DKO mice compared to WT mice. Histological examination of H&E-stained thymus sections revealed a complete loss of the medulla, leaving only the darker-staining cortical region intact in the thymus of *Lal* KO mice. In contrast, thymus sections of *Lal/Mmp12* DKO mice displayed a distinctive improvement in morphology, showing reduced disorganization and a clearer delineation between medullary and cortical regions (Figure 18B). Nevertheless, we still observed the accumulation of lipid-laden macrophages in both *Lal* KO mice and *Lal/Mmp12* DKO mice (Figure 18C).

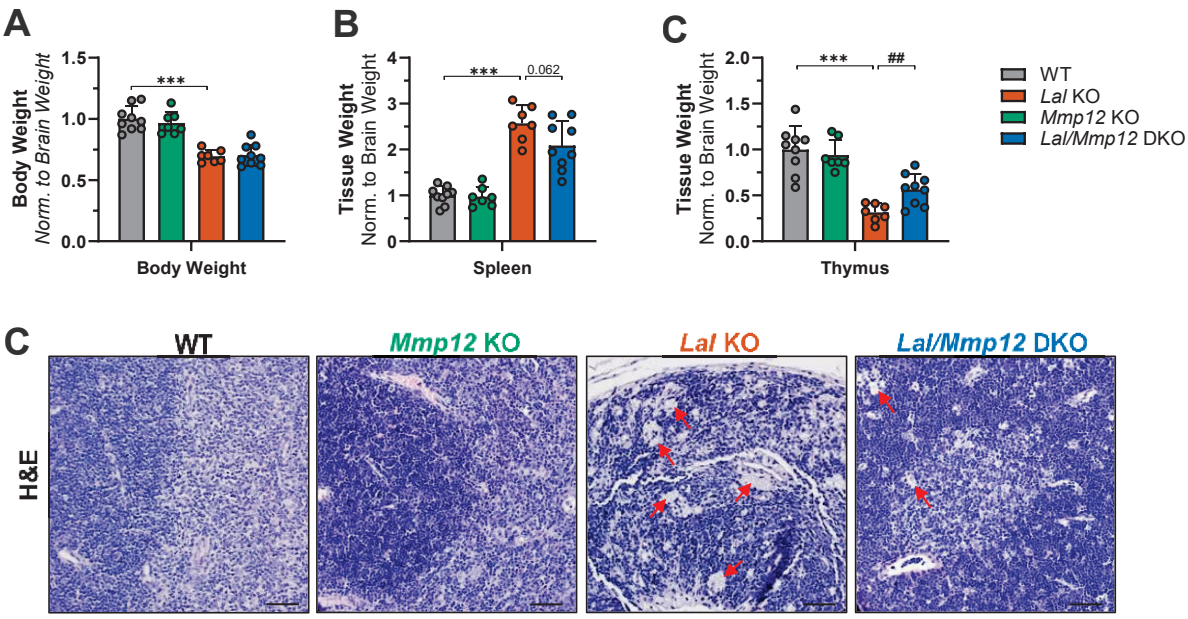

Figure 18: Markedly inproved thymus weight and morphology of *Lal/Mmp12* DKO mice. Tissues were collected from 30-week-old male mice fed a chow diet at libidum. **(A)** Body weight and the tissue weights of the **(B)** spleen and **(C)** thymus; WT mice were arbitrarily set to 1. **(D)** Representative images of H&E-stained thymus paraffin sections of WT, *Lal* KO, and *Lal/Mmp12* DKO mice. Scale bars = 100 µm. Red arrows indicate lipid-laden macrophage aggregates. Data are shown as means (n = 6-10) + SD. ***p ≤ 0.001 for the comparison between WT and *Lal* KO mice; ##p ≤ 0.01 for the comparison between *Lal* KO and *Lal/Mmp12* DKO mice. The use of this figure obtained from (148) is allowed under the terms described in the appendix.

Automated hematology analysis has clear limitations and is generally used only as an initial step to gain a broad overview. To obtain more detailed insights into the consequences of targeting MMP-12 on the composition of immune cells, we analyzed the immune cell compartments of the peripheral blood, bone marrow and spleen via multi-color flow cytometry. The lymphoid-to-myeloid expansion of *Lal* KO mice was distinctly visible across all three tissues (Figure 19A). Represented as the % of CD45+ cells, the CD11b+ Ly6G+ fraction accounted for 87.6% in the peripheral blood, 87.6% in the bone marrow, and 33% in the spleen of *Lal* KO mice (Figure 19A). The deletion of *Mmp12* had no effect on *Mmp12* KO mice, as the CD11b+ Ly6G+ fractions were identical to WT mice across all three immune cell compartments. On the other hand, *Lal/Mmp12* DKO mice displayed a distinct reduction of the CD11b+ Ly6G+ fraction from 60.6% to 39.3% in the peripheral blood, from 87.6% to 78.6% in the bone marrow, and from 33% to 16.9% in the spleen (Figure 19A). This suggests that indeed the lymphoid-to-myeloid shift of *Lal* KO mice was partially ameliorated by the deletion of *Mmp12*, indicating a contribution of MMP-12 to the immune cell pathology of LAL-D.

The expansion of myeloid cells in *Lal* KO mice has already been thoroughly characterized (59). It was shown that the hematopoietic bone marrow progenitor compartment was heavily skewed towards the myeloid lineage and lead to a systemic expansion of CD11b+ Gr-1+ cells. In addition, the characterization of a mouse model with a myeloid linage specific overexpressing of MMP-12 displayed a similar expansion of myeloid cells across the peripheral blood, bone marrow and spleen, as well as major alterations in the hematopoietic bone marrow progenitor compartment.

To evaluate whether deleting *Mmp12* in *Lal* KO mice reverses pathological alterations to hematopoiesis, we characterized the hematopoietic progenitor cell compartment in *Lal/Mmp12* DKO mice. We observed only marginal changes to the hematopoietic stem cell compartment (Lin- Sca-1+ c-Kit+) across all four genotypes (Figure 19B), but a significant increase in the progenitor cell compartment (Lin- c-Kit+) from 38.5% in WT mice to 51.5% in *Lal* KO mice (Figure 19B). This increase was partially ameliorated by a reduction from 51.5% to 44.0% in *Lal/Mmp12* DKO mice, albeit insignificant with a p-value of 0.07. The composition of the Lin- c-Kit+ fraction was further separated into individual progenitor fractions, where common myeloid progenitor cell (CMPs) content appeared comparable across all four genotypes (Figure 19C). In line with previous reports, the granulocyte macrophage progenitor cell fraction was 2.59-fold elevated in *Lal* KO mice and 2.1-fold (p=0.29) in *Lal/Mmp12* DKO mice (Figure 19C). Notably, the megakaryocyte erythrocyte progenitors (MEPs) fraction displayed greater variations in *Mmp12* KO mice yielding to two distinct populations within this group. Considering

that thrombocyte and erythrocyte counts were equal in WT and *Mmp12* KO mice, this variation is most likely a measurement error without biological relevance.

Although a myeloid-specific overexpression of MMP-12 caused hematopoietic changes similar to those seen in *Lal* KO mice, the absence of improvement in the hematopoietic progenitor cell compartment of *Lal/Mmp12* DKO mice suggests that in the context of LAL deficiency, MMP-12 does not significantly contribute to pathological alterations in hematopoiesis. In conclusion, reduced CD11b+ Ly6G+ fractions across the bone marrow, peripheral blood and the spleen were not complemented by alterations in the bone marrow hematopoietic progenitor cell compartment of *Lal/Mmp12* DKO mice. Thus, it is unlikely that changes in the production of immune cells can account for the observed reduction in CD11b+ Ly6G+ cells.

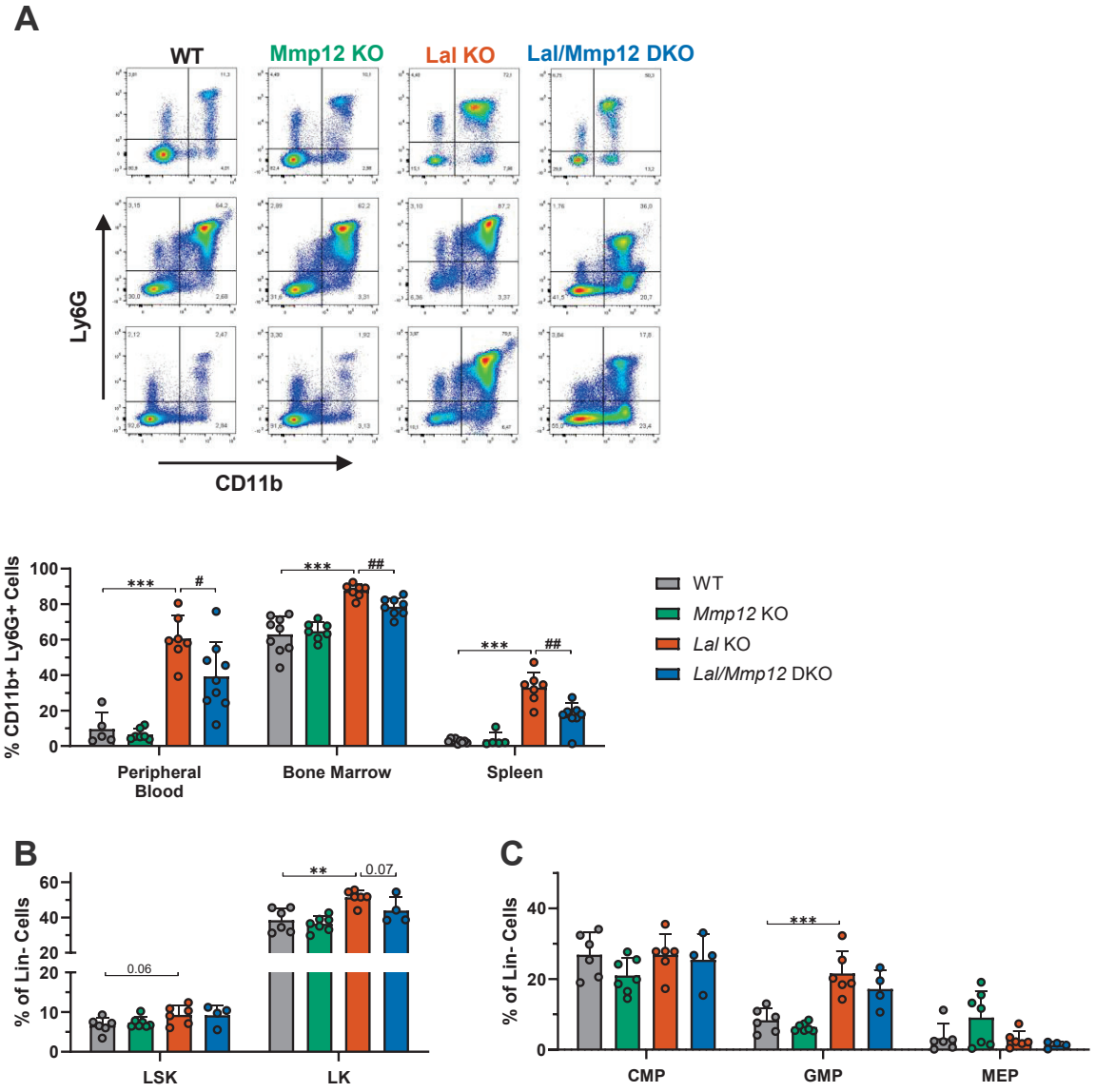

Figure 19: Reduced CD11b+Ly6G+ counts across the immune cell compartment of peripheral blood, bone marrow, and spleen of *Lal/Mmp12* DKO mice. Samples were collected from 30-week-old mice fed a chow diet at libidum. **(A)** Representative flow cytometry plots depicting the CD11b+Ly6G+ fraction in the immune cell compartment of the peripheral blood, bone marrow, and spleen. The size of **(B)** Lin- Sca1+ c-Kit+ (LSK) and Lin- c-Kit+ (LK) fractions, **(C)** hematopoietic progenitor cells [common myeloid progenitors (CMPs), granulocyte macrophage progenitors (GMPs), and megakaryocyte erythrocyte progenitor cells (MEPs)] depicted as % of 7-AAD lineage-negative bone marrow cells. Data are shown as means (n = 5 - 9) + SD. **p ≤ 0.01 and ***p ≤ 0.001 for the comparison between WT and *Lal* KO mice; $^{\#}$p ≤ 0.05 $^{\#\#}$p ≤ 0.01 for the comparison between *Lal* KO and *Lal/Mmp12* DKO mice. The use of this figure obtained from (148) is allowed under the terms described in the appendix.

The immune cell compartment of the spleen displayed the strongest reduction of CD11b+ Ly6G+ cells. To assess whether this reduction had beneficial effects on the spleen pathology of LAL-D, we characterized the spleen of *Lal/Mmp12* DKO mice.

A histological examination of spleen paraffin sections demonstrated the two functionally and anatomically distinct regions in WT mice (Figure 20A). The darker, more nuclei dense white pulp, indicated by green arrows, serves as a reservoir of T-lymphocytes and macrophages, whereas the red pulp, indicated by red arrows, comprises a dense network of venous tissue that facilitates the phagocytosis of old, damaged, and dead blood cells and antigens (Figure 20A). This separation of morphological features was absent from *Lal* KO and *Lal/Mmp12* DKO sections, which displayed markedly disorganized and heterogeneous red and white pulp fragments, interspersed by granuloma-like lipid-laden macrophage aggregates (Figure 20A). Notably, both the morphological disorganization of the spleen and macrophage aggregates appeared identical in *Lal* KO and *Lal/Mmp12* DKO spleens (Figure 20A). In agreement, the mRNA expression of the macrophage marker *Cd68* was equally elevated in *Lal* KO and *Lal/Mmp12* DKO mice (Figure 20B). Surprisingly, the expression of the two neutrophil markers *Ly6g* and *Elane* were not reduced in *Lal/Mmp12* DKO compared to *Lal* KO mice, which was the case in the liver of *Lal/Mmp12* DKO mice (Figure 20C-D). The expression of *Mmp12* was only 12.5-fold elevated in *Lal* KO mice, whereas at a similar age, the liver exhibited a 275-fold increase (Figure 20E). We confirmed that *Mmp12* expression was absent in *Lal/Mmp12* DKO mice (Figure 20E).

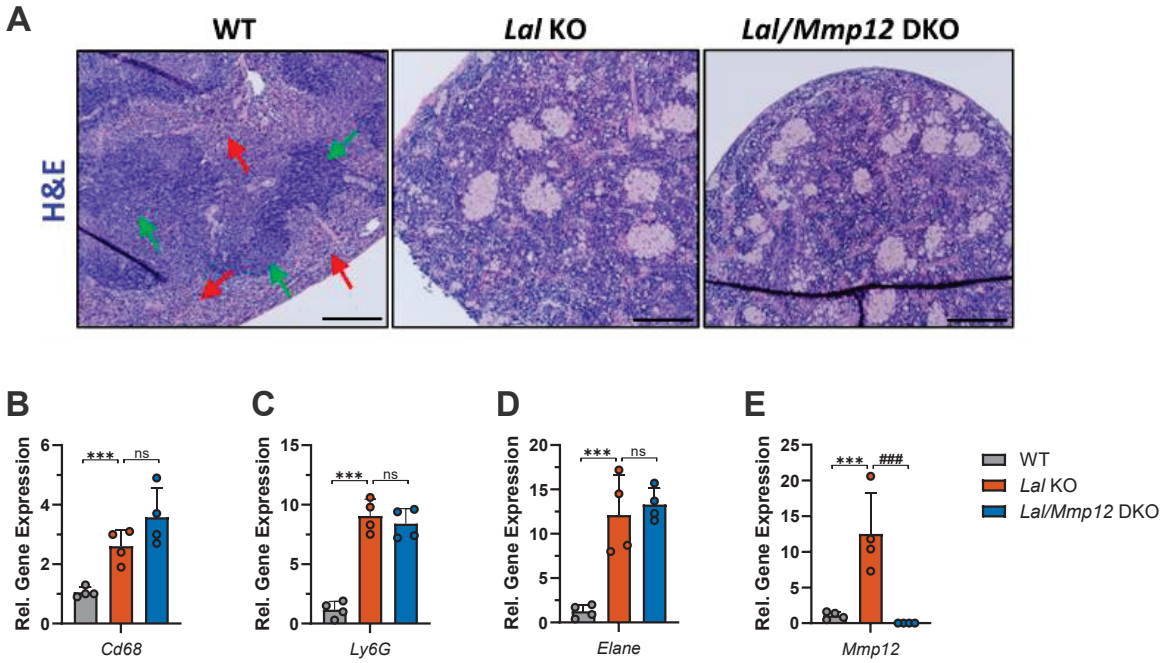

Figure 20: Unchanged accumulation of lipid-laden macrophages in *spleens of Lal/Mmp12* DKO mice. Samples were collected from 30-week-old mice fed a chow diet at libidum. **(A)** Representative images of H&E-stained spleen paraffin sections from WT, *Lal* KO, and *Lal/Mmp12* DKO spleens. Red arrows indicate red pulps, green arrows indicate white pulps. Scale bars, 100 µm. Gene expression of **(B)** the macrophage marker *Cd68*, the neutrophil markers **(C)** *Ly6G* and **(D)** *Elane, and* **(E)** *Mmp12*. Data are shown as means (n = 4) + SD. ***p ≤ 0.001 for the comparison between WT and *Lal* KO mice; ###p ≤ 0.001 for the comparison between *Lal* KO and *Lal/Mmp12* DKO mice. The use of this figure obtained from (148) is allowed under the terms described in the appendix.

The spleen is an important secondary lymphoid organ acting as a reservoir of lymphocytes and facilitates antigen presentation and lymphocyte activation (150). Previous studies have shown that CD11b+Ly6G+ neutrophils in *Lal* KO mice display expression signatures of myeloid-derived suppressor cells (MDSCs) exerting immunosuppressive properties on lymphocyte proliferation and function (69). Based on the observation that neutrophil counts were reduced following the deletion of *Mmp12*, we hypothesized that this could alleviate the impaired lymphocyte function associated with LAL-D. To test this, we analyzed lymphocyte markers in spleens of *Lal/Mmp12* DKO mice. However, the mRNA expression levels of the lymphocyte markers B220 and Cd3e were identical in *Lal* KO and *Lal/Mmp12* DKO mice (Figure 21A). Similarly, the protein expression of Cd3e was comparable between the two genotypes (Figure 21B), suggesting that the reduction of neutrophil-derived immunosuppression alone is insufficient to restore lymphocyte populations and activation in the context of LAL-D.

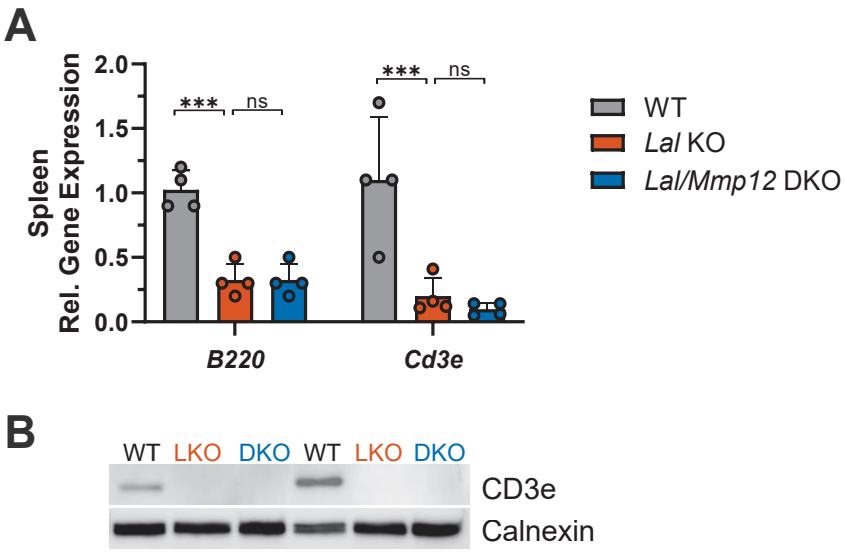

Figure 21: Markers for lymphocyte pathology were equally diminished in *Lal* KO and *Lal/Mmp12* DKO spleens. Spleen tissue was collected from 30-week-old mice fed a chow diet at libidum. **(A)** Gene expression of lymphocyte markers (*B220*, *Cd3e*) in the spleen of WT, *Lal* KO, and *Lal/Mmp12* DKO mice. **(B)** Immunoblot analysis of CD3e. Data are shown as means (n = 4 - 5) + SD. **p ≤ 0.01 and ***p ≤ 0.001 for the comparison between WT and *Lal* KO mice. The use of this figure obtained from (148) is allowed under the terms described in the appendix.

The MMP family shares several functional similarities, most notably in their capacity to degrade ECM proteins. Among these, at least eight MMPs exhibit specificity for collagen degradation, and four MMPs are primarily categorized as elastases. Additionally, many MMP family members display overlapping specificity for cytokines such as IL-1β and TNF. We therefore considered the possibility that although the pathological contribution of MMP-12 to LAL-D was successfully targeted, the upregulation of one or more other MMPs might mask the absence of MMP-12. Consequently, we explored whether the absence of significant improvements to lymphocyte population and the broader spleen pathology of LAL-D in *Lal/Mmp12* DKO mice could result from a spleen-specific compensatory upregulation of another MMP family member.

Of the 23 known mouse MMPs, only 16 displayed relevant expression levels in the spleen of WT, *Lal* KO, and *Lal/Mmp12* DKO mice. The expression of *Mmp12* was most dysregulated in *Lal* KO samples with a 10.8-fold increase (Figure 22). Nevertheless, several other MMPs (*Mmp8, Mmp9, Mmp14, Mmp25,* and *Mmp27*) also exhibited elevated expressions in *Lal* KO spleens, whereas the expressions of *Mmp15* and *Mmp17 were* reduced by 50% and 40% respectively (Figure 22). Importantly, not a single analyzed MMP displayed a compensatory

upregulation in *Lal/Mmp12* DKO spleens compared to *Lal* KO samples. Instead, the deletion of *Mmp12* resulted in significantly decreased expressions of *Mmp3* and *Mmp13* by 77% and 64%, respectively (Figure 22). Together, these results suggest that compensatory upregulation by other MMP family members is unlikely to occur and therefore does not explain the mild phenotype observed in *Lal/Mmp12* DKO mice.

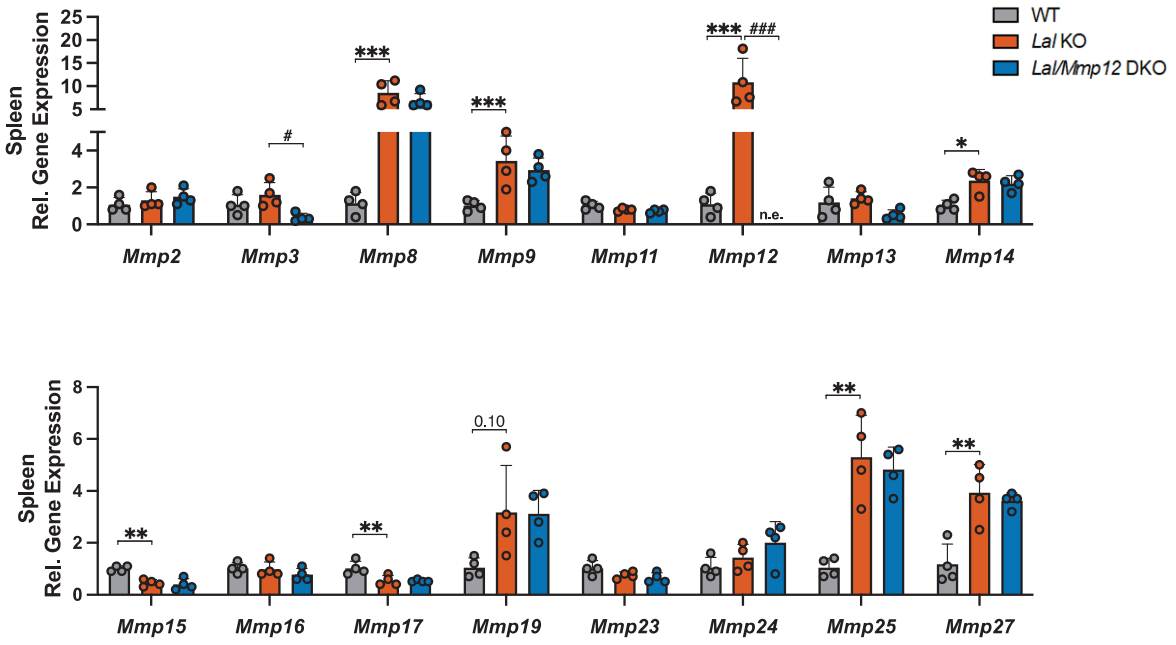

Figure 22: No compensatory upregulation of other matrix metalloproteinases in spleens of *Lal/Mmp12* DKO mice. Gene expression of matrix metalloproteinase (MMP) family members in the spleen of 30-week-old chow diet-fed male mice. Data are shown as means (n = 4) +SD. *p ≤ 0.05, **p ≤ 0.01 and ***p ≤ 0.001 for the comparison between WT and *Lal* KO mice; #p < 0.05 and ###p ≤ 0.001 for the comparison between *Lal* KO and *Lal/Mmp12* DKO mice. The use of this figure obtained from (148) is allowed under the terms described in the appendix.

3.5. Investigating possible mechanisms of action of MMP-12

The deletion of *Mmp12* resulted in limited alleviations of specific pathologies in *Lal* KO mice. The phenotype of *Lal/Mmp12* DKO mice demonstrated a direct, albeit modest, contribution of MMP-12 to the pathology of LAL-D. However, the mechanism by which MMP-12 exerts this contribution remains unknown. Based on the literature of MMP-12 in the context of other chronic inflammatory conditions, we evaluated several potential mechanisms.

In vitro, MMP-12 was shown to cleave all three major chemokines (mCXCL1, mCXCL2, and mCXCL3) involved in the chemotaxis of neutrophils (89). In line, *Mmp12* KO mice exhibited reduced neutrophil infiltration following LPS injection (89). Based on these observations, we considered the possibility that the deletion of *Mmp12* could affect the chemotaxis of neutrophils. We observed a significantly elevated mRNA expression of *Cxcr1* and *Cxcr2*, two major receptors for neutrophil activation and chemotaxis in both *Lal* KO and *Lal/Mmp12* DKO mice (Figure 23 A-B). In contrast, the expression of *Cxcr4*, a chemokine receptor known to regulate tissue exfiltration and bone marrow homing in aged neutrophils (151), was unchanged across all three genotypes (Figure 23C). In mice, CXCR1 and CXCR2 share three ligands mCXCL1, mCXCL2, mCXCL3*)*, and neither exhibited a significantly altered expression across WT, *Lal* KO, and *Lal/Mmp12* DKO mice (Figure 23 D-F). Taken together, we suggest that altered neutrophil chemotaxis is unlikely to account for the observed phenotype of *Lal/Mmp12* DKO mice.

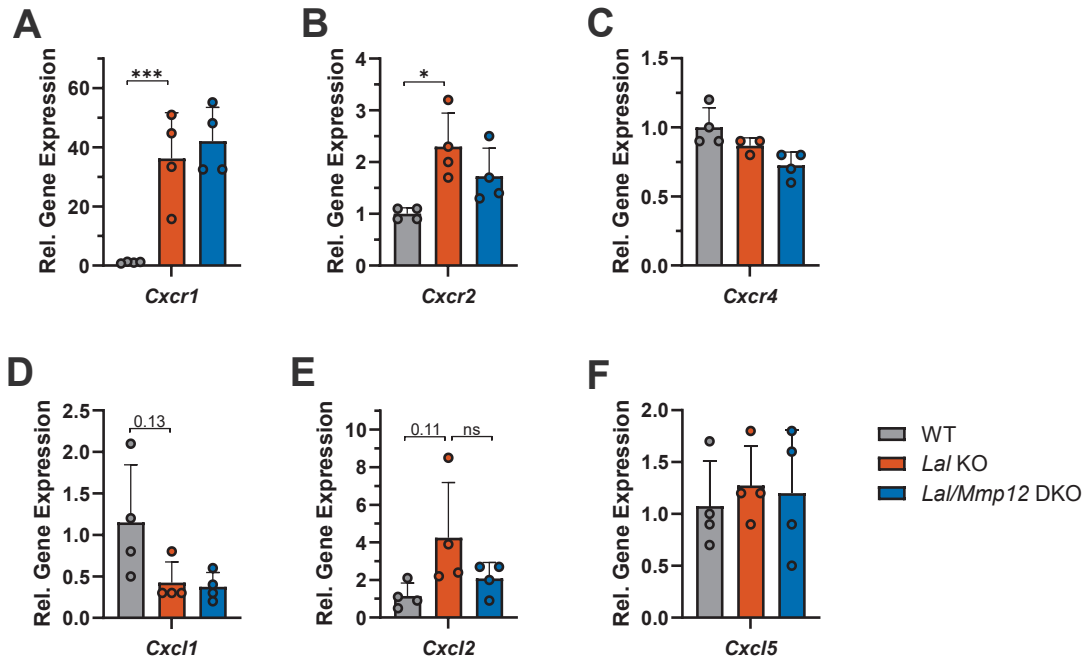

Figure 23: Markers of neutrophil chemotaxis appeared unaffected by the deletion of *Mmp12*. Spleen gene expression of **(A-C)** chemokine receptors (*Cxcr1, Cxcr2, Cxcr4*) and **(D-F)** chemokine ligands (*Cxcl1, Cxcl2, Cxcl5*). Data are shown as means (n = 3 - 5) + SD. *p ≤ 0.05 and ***p ≤ 0.001 for the comparison between WT and *Lal* KO mice. The use of this figure obtained from (148) is allowed under the terms described in the appendix.

As an alternative mechanism to classical chemotaxis of neutrophils, we considered the effect of chemotactic elastin derived peptides (EDPs), which are known to be liberated by elastases like MMP-12. The major receptor of EDPs, the Elastin binding protein (EBP) is expressed on the surface of neutrophils (152). The stimulation of EBP by sEDP treatment was shown to induce an oxidative burst in neutrophils (153) and to act as a chemoattractant (154). Thus, we hypothesized that changes in plasma soluble EDP (sEDP) concentrations may explain the observed reductions of CD11b+ Ly6G+ counts in *Lal/Mmp12* DKO mice.

At 15 weeks of age, serum concentrations of elastin fragments were comparable across all genotypes (Figure 24), suggesting that in early stages of LAL-D, sEDP has at best a negligible contribution. With a more progressed pathology at 30 weeks of age, sEDP levels increased by 17% (p=0.0059) in *Lal* KO mice compared to WT (Figure 24). Following the deletion of *Mmp12*, we observed an 8% reduction (p=0.0037) (Figure 24), suggesting a small contribution of MMP-12 to the production of sEDPs. Nevertheless, we suggest that the absence of more pronounced changes in sEDP concentration between WT and *Lal* KO mice, as well as following the deletion of *Mmp12*, indicates a negligible contribution of elastin fragments to the pathology of LAL-D. Therefore, alterations in sEDP concentrations are unlikely capable of explaining the phenotype of *Lal/Mmp12* DKO mice.

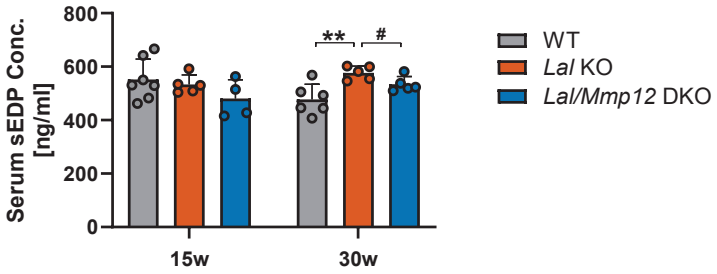

Figure 24: Only minor differences in soluble elastin-derived peptide concentrations between *Lal* KO and *Lal/Mmp12* DKO mice. Quantification of soluble elastin-derived peptide (sEPD) concentrations by ELISA. Data are shown as means (n = 4 - 7) + SD. **p ≤ 0.01 for the comparison between WT and *Lal* KO mice; #p ≤ 0.05 for the comparison between *Lal* KO and *Lal/Mmp12* DKO mice.

MMP-12 has been shown to alter platelet function by cleaving CEACAM1, resulting in significantly increased collagen-induced platelet aggregation (104). In addition, the formation of platelet leukocyte aggregates (PLAs) has recently gained considerable attention for their role in modulating both the functions and survival of different immune cells (98). Therefore, we used *Mmp12* KO mice to assess whether changes in platelet function or PLA formation might explain the observed reductions in CD11b+Ly6G+ counts in DKO mice.

Complete blood counts of *Mmp12* KO mice displayed a small increase in platelet counts (Figure 25A), suggesting potential changes to hemostatic function. To investigate possible changes in platelet function, we performed a standard collagen-induced platelet aggregation assay with WT and *Mmp12* KO blood but observed no significant differences (Figure 25B). This indicated that deletion of *Mmp12* had no unintended side effects on hemostatic function. An evaluation of PLA formation via flow cytometry of peripheral blood samples revealed that 70.9% of CD115+ cells were positively stained by the platelet-specific marker CD41 in WT, but only 38.3% in *Mmp12* KO mice (Figure 25C). Similarly, of all Ly6G+ cells, 91.1% of cells stained positive for CD41 in WT, but only 40.3% in *Mmp12* KO mice. Our data suggest that MMP-12 is involved in the formation of PLAs and may provide a link to the observed reduction in CD11b+Ly6G+ counts following the deletion of *Mmp12*. Nevertheless, we decided against further pursuing PLAs in the context of LAL-D and instead focused on characterizing neutrophils.

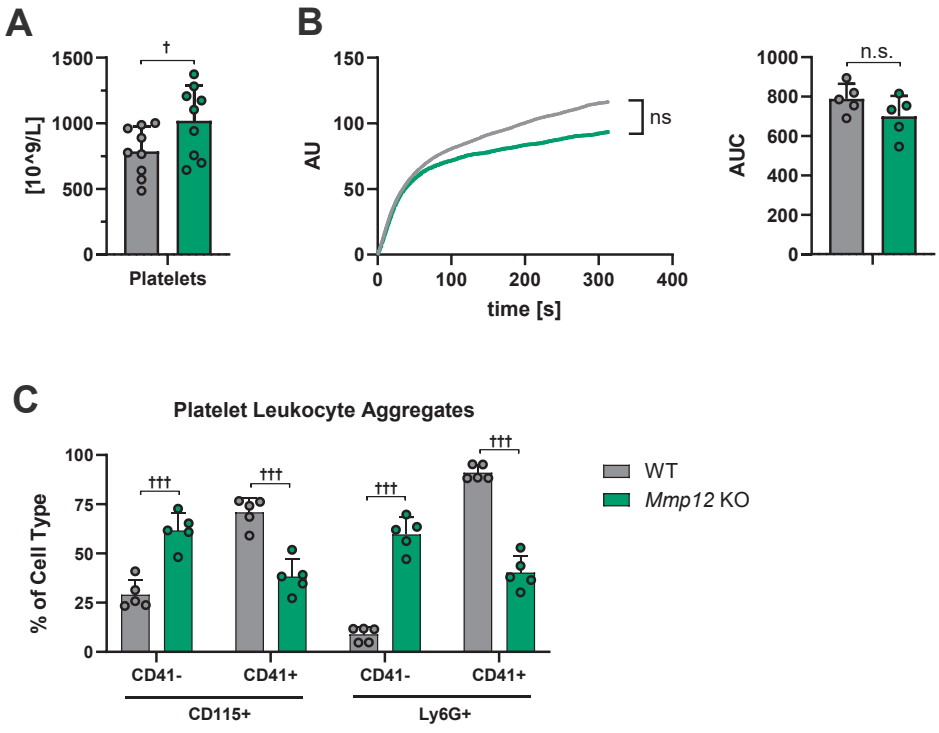

Figure 25: Reduced formation of platelet-leukocyte aggregates, but unchanged collagen-induced platelet aggregation of *Mmp12* KO blood. (A) Total platelet counts in the peripheral blood. **(B)** Averaged collagen-induced platelet aggregation plot and calculated area under the curve. **(C)** Platelet leukocyte aggregate formation determined by CD41 staining of monocytes (CD115+) and neutrophils (Ly6G+). Data are shown as means (n = 5 - 10) + SD. $^{\dagger}p < 0.05$ and $^{\dagger\dagger\dagger}p < 0.05$ for the comparison between WT and *Mmp12* KO mice.

Next, we explored the possibility that the phenotype of *Lal/Mmp12* DKO mice might be explained by an altered tendency of neutrophils to undergo a specific form of cell death resulting in the formation of neutrophil extracellular traps (NETs or NETosis). To this end, we stained spleen paraffin sections with both DAPI and an antibody against citrullinated histone 3 (H3Cit), to identify H3Cit & DAPI double-positive areas. We observed only residual H3Cit+ staining in the WT control section, which did not co-localize with DAPI staining (Figure 26B). The absence of H3Cit+/DAPI+ staining indicates that NET formation did not occur in WT tissues. In contrast, 16.3% of *Lal* KO spleen sections stained positive for H3Cit, of which the majority overlapped with DAPI staining, yielding 13.0% of the tissue area as H3Cit+DAPI+ (Figure 26B). This observation marks the first demonstration of unwarranted NET formation in the spleen of *Lal* KO mice. Following deletion of *Mmp12*, the percentage of tissue area stained for H3Cit decreased to 8.8% and resulted in a complementary decrease in the H3Cit+DAPI+ area (Figure 26B). Despite this 43.1% reduction in the H3Cit+DAPI+ area in *Lal/Mmp12* DKO mice, pro-inflammatory NET-compounds (such as myeloperoxidase, neutrophil elastase, and cathepsin G) are still likely to significantly contribute to the pathology of LAL-D. We conclude that the deletion of *Mmp12* ameliorated the extent of NET formation in LAL-D. However, based on the absence of differences in the spleen pathology between *Lal* KO and *Lal/Mmp12* DKO mice, we question the functional relevance of reduced NET formation in the broader context of LAL-D pathology. Unfortunately, it remains unknown whether this reduction in NETs is a direct consequence of reduced CD11b+Ly6G+ counts or reflects a reduced intrinsic tendency of neutrophils to undergo NETosis. Thus, a specific exploration of neutrophil NETosis in *Lal/Mmp12* DKO mice remains unexplored.

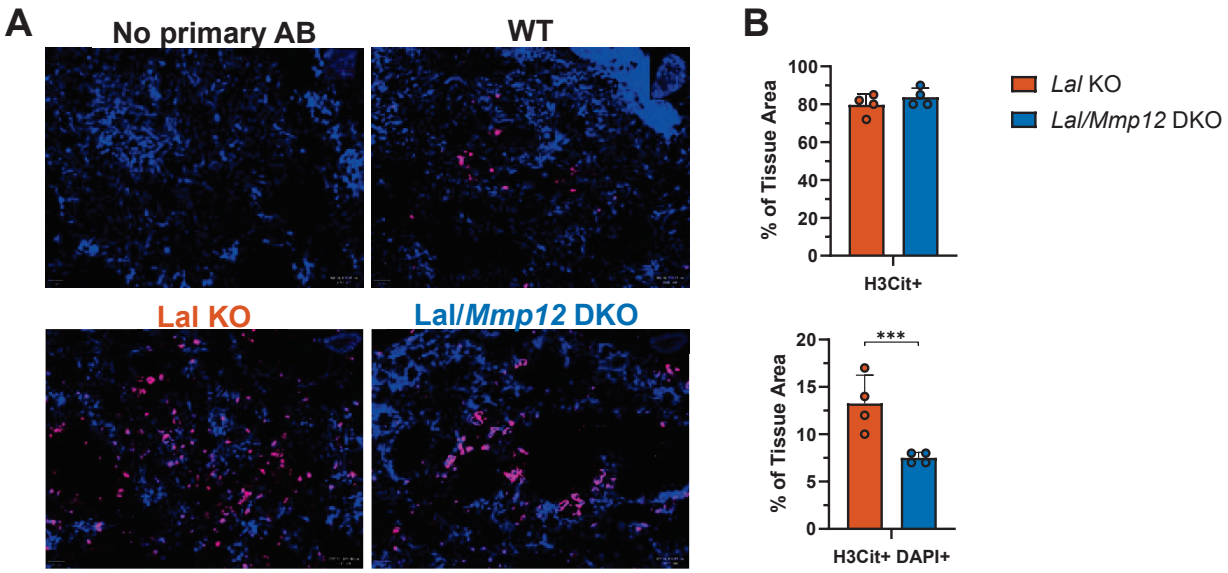

Figure 26: Identification and quantification of neutrophil extracellular traps in spleens of *Lal* KO and *Lal/Mmp12* DKO mice. (**A**) Representative immunofluorescence images depicting the negative control without a primary antibody, WT, *Lal* KO, and *Lal/Mmp12* DKO sections. (**B**) Quantification of the tissue area positively stained for H3Cit+ and H3Cit+DAPI+. Data are shown as means (n = 4) + SD.

Under physiological conditions, phagocytes such as macrophages and dendritic cells clear NETs to prevent excess tissue damage (127). Bone marrow-derived macrophages from *Lal* KO mice have been shown to exhibit significantly reduced efferocytosis capacity (5). Thus, we hypothesized that improvements in the efferocytosis capacity of macrophages could explain the observed reductions of NETs in the spleens of *Lal/Mmp12* DKO mice. After incubating BMDMs for 2 h with pHrodo-stained apoptotic cells, we observed that 53.9% and 49.9% of *Lal* KO and *Lal/Mmp12* DKO F4/80+ cells, respectively, were positively stained for pHrodo (Figure 27). Consistent with the absence of changes in macrophage accumulation, macrophage dysfunction, and efferocytosis capacity, we suggest that the reduction in NETs is most likely a direct consequence of decreased neutrophil counts. Taken together, our data suggests that deletion of *Mmp12* had no effect on efferocytosis and hence cannot account for the phenotype of *Lal/Mmp12* DKO mice.

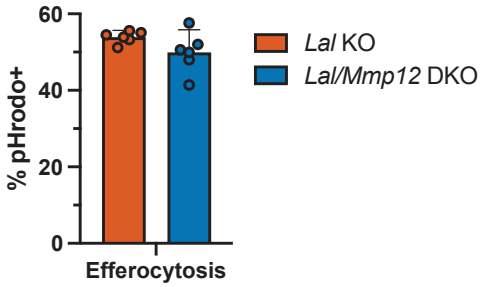

Figure 27: Unchanged efferocytosis capacity of *Lal/Mmp12* DKO BMDMs. Quantification of the % of BMDMs exhibiting a fluorescence signal originating from pHrodo-stained and apoptotic Jurkat cells. Data are shown as means (n = 6) + SD.

Considering that neutrophils are the most short-lived immune cell type, with an average half-life of only several h in the circulation of a healthy mouse, even small alterations in neutrophil survival can greatly affect neutrophil number. This is especially the case in the context of LAL-D, with a progressive myeloid expansion and systemic chronic inflammation. To investigate possible alterations in neutrophil survival or apoptosis following the deletion of *Mmp12*, we stained bone marrow with Ly6G, 7-AAD and Annexin-V to analyzed the viability of neutrophils via flow cytometry.

First, we evaluated whether neutrophil-derived MMP-12 may affect the survival of neutrophils. To this end, we compared the viability of Ly6G+ cells of WT and *Mmp12* KO bone marrow after 24, 36, and 72 h. We observed an identical cell viability for both WT and *Mmp12* KO neutrophils (Figure 28), suggesting that the genotype of neutrophils does not affect their survival or life span. For this reason, we grouped WT and *Mmp12* KO bone marrow samples together to increase the sample size and reduce the number of variables.

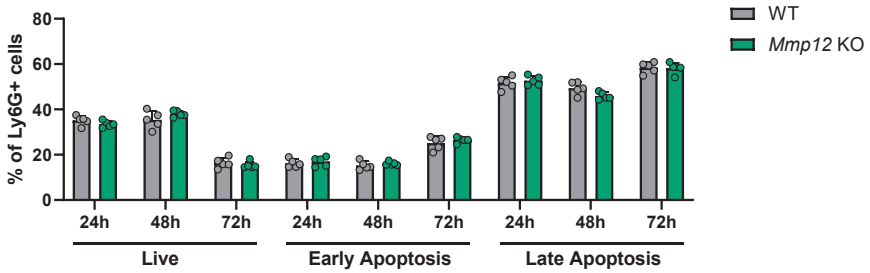

Figure 28: Comparable viability decline of WT and *Mmp12* KO neutrophils. Flow cytometry analysis of cultured bone marrow neutrophils (Ly6G+) by Annexin-V & 7-AAD staining. Decline in viability of Ly6G+ cells in WT and *Mmp12* KO bone marrow cultures after 24, 48, and 72 h. Data are shown as means (n = 5 - 9) + SD.

Next, we treated bone marrow samples with either empty growth media or conditioned media derived from the supernatant of WT or *Mmp12* KO BMDMs. After 24 h of incubation, we observed a comparable Annexin-V- 7-AAD- fraction across all three culture conditions (Figure 29A). However, after 48 h, the viability of neutrophils cultured in empty growth medium declined to 1.7%, whereas cultures treated with condition media derived from WT or *Mmp12* KO BMDMs maintained viability at 30.0% and 36.7%, respectively (Figure 29A). This 6.7% ($p = 0.001$) difference in cell viability increased to 10.4% after 72 h (Figure 29A), demonstrating a clear increase of neutrophil viability in the absence of *Mmp12*. In contrast, the Annexin-V+ 7-AAD- fraction, representing early apoptotic neutrophils, progressively decreased in cultures treated with *Mmp12* KO conditioned media compared to WT conditioned media (Figure 29B). The difference in the Annexin-V+ 7-AAD- fraction was 1.7% ($p=0.012$) after 24 h, 3.8% (0.001) after 48 h, and 8.29% ($p=0.000$) after 72 h of incubation (Figure 29B). Interestingly, Annexin-V+ 7-AAD+ cells were only markedly elevated in empty growth media-treated cultures yet remained identical between cultures treated with conditioned media derived from WT and *Mmp12* KO BMDMs (Figure 29C). Taken together, this finding suggests that the absence of MMP-12 has the potential to reduce the survival of neutrophils and thus provides a plausible explanation for the observed phenotype of *Lal/Mmp12* DKO mice.

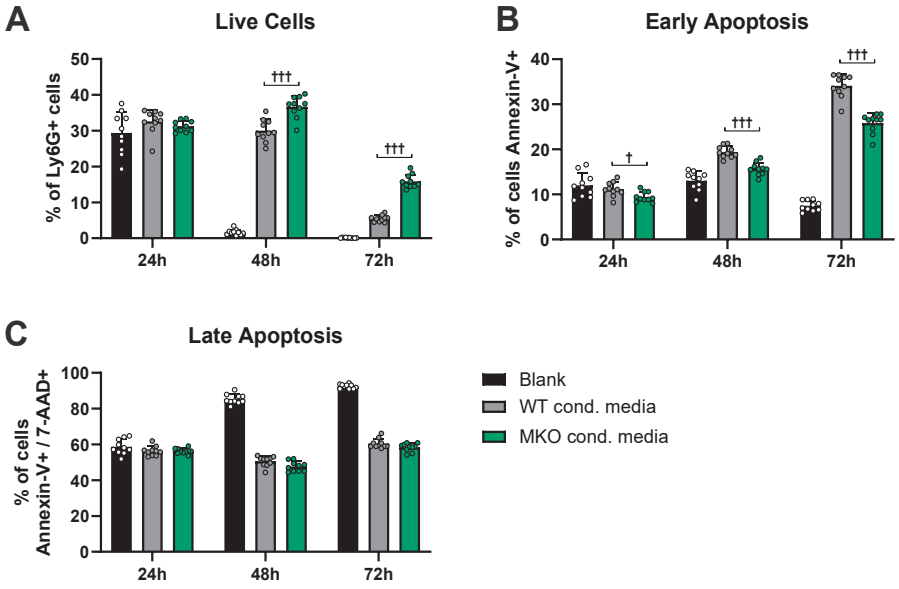

Figure 29: Delayed apoptosis in neutrophils treated with *Mmp12* KO condition media. Flow cytometry analysis of bone marrow neutrophils (Ly6G+) by Annexin-V & 7-AAD staining. Comparing the effects of empty growth media to conditioned media derived from WT and *Mmp12* KO BMDMs on the viability of Ly6G+ bone marrow cells. **(A)** Annexin-V- & 7-AAD- (Live cells), **(B)** Annexin-V+ & 7-AAD- (Early Apoptosis), and **(C)** Annexin-V+ & 7-AAD+ (Late Apoptosis). Data are shown as means (n = 5 - 9) + SD. $^{\dagger}p \leq 0.05$, $^{\dagger\dagger}p \leq 0.01$ and $^{\dagger\dagger\dagger}p \leq 0.001$ for the comparison between *Lal* KO and *Lal/Mmp12* DKO mice.

4. Discussion

LAL-D has been shown to cause a massive increase in the expression of MMP-12 in the lungs and in myeloid lineage cells of *Lal* KO mice (74, 155). Consistent with a pathogenic contribution of MMP-12, a myeloid lineage-specific overexpression of MMP-12 established a causal relationship between increased MMP-12 expression and the occurrence of progressive lymphocyte dysfunction accompanied by an expansion of CD11b+Ly6G+ cells (155). The pathology of this transgenic mouse model closely mirrors several key aspects of the clinical setting of LAL-D (59). The authors concluded that the overexpression of MMP-12 causes an abnormal development of hematopoietic progenitor cells, favoring the myeloid lineage (155). However, their investigation did not include experiments designed to rescue or ameliorate the pathology of *Lal* KO mice. Thus, it has remained unclear whether or to what extent the pathology of LAL-D can be ameliorated by targeting MMP-12. Therefore, we generated *Lal/Mmp12* DKO mice to directly assess the actual contribution of MMP-12 to the immune cell dysfunction in LAL-D and to determine whether MMP-12 represents a viable therapeutic target for the treatment of this disease.

At 15 weeks of age, *Lal/Mmp12* DKO mice were visually indistinguishable from their *Lal* KO littermates. Both genotypes exhibited comparable brain and body weights, extent of hepatomegaly and loss of adipose tissue, suggesting that the deletion of *Mmp12* had little to no effect on the LAL-D phenotype. Similarly, neither plasma and hepatic lipid parameters nor the pulmonary or hepatic gene expression of lipogenic, fibrotic, and inflammatory markers were ameliorated in *Lal/Mmp12* DKO mice. Following greatly overlapping substrate specificities among many MMP family members, we explored the possibility that the deletion of MMP-12 was actively compensated for by an upregulation of other MMP family members. To exclude this possibility, we analyzed both the pulmonary and hepatic expression of all known mouse MMPs. Among the 24 known MMPs, we detected the expression of 12, 18, and 16 different MMPs in the lung, liver, and spleen, respectively. Notably, the deletion of *Mmp12* did not lead to a compensatory increase in the expression of any other MMP, suggesting that no other MMP family member masks the phenotype of KO mice. Instead, we observed a downregulation of several MMPs in *Lal/Mmp12* DKO mice, pointing to a broader regulatory role of MMP-12. Most strikingly, *Mmp3* expression was markedly reduced across all examined tissues, suggesting that MMP-12 might play a non-tissue-specific role in regulating *Mmp3*. However, the precise relationship between MMP-3 and MMP-12 remains unexplored. Given that *Mmp3* expression is known to depend on various growth factors and pro-inflammatory cytokines (156), we speculate that MMP-12 may cleave or liberate such a factor to indirectly modulate *Mmp3*

expression. Additionally, the expression of *Mmp10* and *Mmp13* were significantly reduced in the liver of *Lal/Mmp12* DKO mice. The MMP family is known for its complexity and interrelated proteolytic processing (e.g. activation of a zymogen) (157). Importantly, our findings are based solely on gene expression data, leaving open the possibility that compensatory mechanisms occured at the post-translational level. Our results indicate that the deletion of MMP-12 leads to a reduction, rather than compensation, in the expression of several MMPs, substantiating its potential role as an upstream regulator of multiple other MMPs. Given the limited literature on the precise interactions between MMP family members, further studies are needed to unravel the precise molecular mechanisms governing MMP-12-dependent regulation of other MMPs.

Since LAL-D displays a complex phenotype, manifesting in multiple systemic pathologies, it is possible that *MMP12* contributes to the systemic inflammation of LAL-D but, because it is not the only mediator, its contribution might be insignificant compared to the broader pathology.
The hypothesized beneficial effects of deleting MMP-12 are most likely directly dependent on its initial expression level. The more MMP-12 is produced, the greater the effect of its deletion should be. Therefore, we attempted to amplify the expression of MMP-12 by challenging mice for 6 weeks with a HFD. However, HFD feeding did not have the intended effect of increasing *Mmp12* expression, with an average Ct value of 23 in HFD-fed *Lal* KO mice, as compared to 22.6 on age-matched chow diet-fed *Lal* KO mice. It is therefore not surprising that body weight gains and tissue weights were not affected by the deletion of *Mmp12*. In line, the expression of two pro-inflammatory markers, *Tnf* and *Il1b*, remained comparable in *Lal* KO and *Lal/Mmp12* DKO mice.

MMP-12 is highly expressed in patients with metabolic dysfunction-associated steatotic liver disease (MASLD) (158) and targeting of MMP-12 by siRNA ameliorated steatosis in HFD-fed mice (88). Similarly, MMP-12 generated EDPs were shown to contribute to the development of metabolic dysfunction-associated steatohepatitis (85). Therefore, we assessed whether the deletion of *Mmp12* ameliorated HFD-induced metabolic adaptations. Despite these reports, hepatic lipid accumulation remained unaffected in *Lal* KO and *Lal/Mmp12* DKO mice after 6-weeks of HFD feeding. This suggests that MMP-12 is unlikely involved in HFD-induced metabolic adaptations. More importantly, MASLD and LAL-D are two fundamentally distinct pathologies. MASLD is characterized by an ectopic accumulation of TAG in hepatocytes (159), whereas in LAL-D, macrophages are the main cell type accumulating both CE and TAG (63).

Consequently, it is not surprising that these differences limit the translation of the beneficial effects of deleting *Mmp12* on hepatic lipid accumulation.

The relative expression of *Mmp12* in the liver of 30-week-old *Lal* KO mice increased approximately 275-fold, compared to an 880-fold increase in 15-week-old *Lal* KO mice. This difference should be interpreted in the context of a known age-associated rise in *Mmp12* expression in WT mice (160). In WT controls, *Mmp12* expression increased from a Ct value of 31.6 at 15 weeks to 29.4 at 30 weeks of age. In contrast, the housekeeping gene *Hprt* remained stable, with Ct values of 25.8 and 25.5, respectively. Consequently, the elevated baseline expression of *Mmp12* in older WT mice reduces the calculated fold change, despite a markedly higher absolute expression of *Mmp12* in 30-week-old *Lal* KO mice.

Even at a more advanced stage of LAL-D, the deletion of *Mmp12* was not able to alleviate diminished body size or weight nor alter tissue weights (e.g., hepatosplenomegaly) of *Lal* KO mice. Similarly, gene expression markers for hepatic inflammation (*Tnf*, *Il1b*, and *Ccl2*) and serum levels of AST, ALT, and SAA were comparable between *Lal* KO and *Lal/Mmp12* DKO mice, suggesting that an abundant hepatic expression of *Mmp12* does not significantly contribute to hepatomegaly, hepatocyte injury, or systemic inflammation in *Lal* KO mice. The hepatic pathology of *Lal* KO mice is primarily driven by the progressive accumulation of lipid-laden macrophages (63). The liver weight of a *Lal* KO mouse can increase by more than 3-fold and may account for over 20% of total body weight. The deletion of *Mmp12* has been shown to alter monocyte recruitment into the liver following LPS treatment (161), diminish macrophage infiltration in colitis and irritable bowel syndrome models (162), and reduce macrophage recruitment during atherosclerotic plaque formation (163). Similarly, the administration of recombinant human MMP-12 induced alveolar macrophage recruitment (164). MMP-12 was even shown to cleave and inactivate several monocyte chemotactic proteins (CCL2, CCL7, CCL8, and CCL13) (89). Therefore, we investigated potential reductions in macrophage accumulation in the liver of *Lal/Mmp12* DKO mice. However, given the comparable extent of hepatomegaly, hepatic expression of macrophage markers (*Emr1* and *Cd68*), and similar hepatic accumulation of TC and CE in *Lal* KO and *Lal/Mmp12* DKO mice, we suggest that MMP-12 is unlikely to significantly contribute to hepatic pathology. Taken together, our data strongly suggest that deletion of *Mmp12* was unable to ameliorate hepatic macrophage accumulation or the overall hepatic pathology of *Lal* KO mice.

Macrophages are not the only immune cells greatly expanded in *Lal* KO mice. Rather, the entire CD11b+Gr-1+ myeloid cell fraction is systemically expanded across the bone marrow, spleen, and peripheral blood (59). To test whether neutrophil numbers might be altered in *Lal/Mmp12* DKO mice, we analyzed gene expression of the neutrophil-specific marker *Ly6g* and the neutrophil granule enzyme *Elane*. A significantly decreased hepatic expression of both *Ly6g* and *Elane* indicated that although macrophages secrete the majority of MMP-12, other immune cells such as neutrophils might be of even greater relevance. We observed several indicators for reduced immune system pathology in *Lal/Mmp12* DKO mice. Most notably, the size and morphology of the thymus, a primary lymphoid organ essential for the maturation of T-cells, were markedly improved compared to *Lal* KO mice. However, unchanged circulating lymphocytes numbers and unchanged expression of the T- and B-cell markers (*Cd3e* and *B220*) in the spleen suggested that an improved thymic pathology did not influence lymphocyte numbers in *Lal/Mmp12* DKO mice.

It has been well established that persistent, unresolved inflammation causes the development of CD11b+ Ly6G+ MDSCs (165), and *Lal* KO mice are no exception (69, 166). MDSCs are immature neutrophils and monocytes in a pathologically active state, suppressing the immune response and preventing the elimination of a threat (65, 165). The immune-suppressive properties of MDSCs were shown to inhibit the proliferation and function of T-cells (60, 62, 66, 155), and MDSCs have been implicated in cancer, infectious diseases, autoimmune disorders and obesity (65). To date, no unique surface marker signatures have been identified to discriminate MDSCs from neutrophils and monocytes. Therefore, the investigation of MDSCs has exclusively relied on more complex functional assays and more costly analysis of gene expression signatures (167), rendering their investigations and characterization rather complex. Our data provided no indications that MDSC function was altered in *Lal/Mmp12* DKO mice, however, a reduction in CD11b+ Ly6G+ MDSCs may explain improvements in thymus weight and morphology in *Lal/Mmp12* DKO mice.

In addition to lymphocyte dysfunction, the expansion of myeloid cells significantly contributes to the lymphoid-to-myeloid shift observed in *Lal* KO mice (59, 62). A combination of blood counts, cytological examination of blood smears, and immunophenotyping by flow cytometry indicated a partial reversal of the systemic lymphoid-to-myeloid shift in *Lal/Mmp12* DKO mice. Observations of reduced myeloid expansion in *Lal/Mmp12* DKO mice, contrasted with increased myeloid expansion following the overexpression of *Mmp12*, provide evidence for a direct contribution of MMP-12 to the myeloid expansion in LAL-D. Nevertheless, the modest

phenotype of *Lal/Mmp12* DKO mice indicates that in relation to the complex inflammatory phenotype of *Lal* KO mice, MMP-12 can at best be considered one driving factor among many.

Remarkably, immune system alterations observed in *Lal* KO and *Mmp12*-overexpressing mice share underlying changes in hematopoietic bone marrow progenitor cells (59, 155). However, comparable progenitor cell populations in *Lal* KO and *Lal/Mmp12* DKO mice suggest that MMP-12 itself does not directly influence bone marrow hematopoiesis in LAL-D. In agreement, *Mmp12* mRNA exhibits only a very low expression (Ct value > 33) in the bone marrow of both WT and *Lal* KO mice (data not shown), suggesting that the bone marrow is less likely affected compared to other tissues displaying a very high expression of *Mmp12* (e.g. hepatic expression of Ct<20). Furthermore, the absence of a myeloid cell expansion in lung epithelial cell-specific *Mmp12*-overexpressing mice (91) indicates that peripherally secreted MMP-12 does not directly impact bone marrow hematopoiesis. In contrast, the overexpression of *Mmp12* in myeloid lineage cells results in the production of MMP-12 by myeloid cells located in the bone marrow.

The degradation of ECM-matrix proteins by MMPs is known to generate bioactive peptide fragments with chemotactic properties. In the case of MMP-12, its degradation of elastin leads to the liberation of EDPs containing VGVAPG hexapeptide repeats (80). VGVAPG fragments are recognized by the elastin receptor complex located on the surface of many different cell types, including monocytes, neutrophils, lymphocytes, and fibroblasts (168), leading to their recruitment to the site of EDP generation. However, their functions extend beyond chemotaxis, including inducing monocytes to secrete proteases and generate free radicals, thereby increasing oxidized LDL formation (169). Neutrophils respond to EDP stimulation by elevated cytokine and chemokine secretion, promoting further immune cell infiltration (168). We therefore hypothesized that the deletion of *Mmp12* might result in a significant reduction in circulating sEDP, providing a plausible explanation of the phenotype of *Lal/Mmp12* DKO mice. In plasma samples from 15-week-old mice, sEDP concentrations were comparable between all three genotypes. Upon an increased age of 30 weeks, we observed a significant increase of sEDPs levels in *Lal* KO samples, and a partial reduction in *Lal/Mmp12* DKO mice. Although the changes in plasma EDP concentrations followed the expected trajectory, several concerns must be noted. First and foremost, sEDP levels slightly decreased between 15 and 30 weeks of age, directly contradicting a well-documented age-dependent increase in elastase activity and EDP release (83, 170, 171). Moreover, a modest 17% increase in *Lal* KO samples, followed by an 8% decrease in *Lal/Mmp12* DKO mice, represent only minor deviations from

the WT baseline levels. Chronic and unregulated expression of MMP-12 should result in substantially larger alterations in circulating sEDP concentrations. In comparison, the serum sEDP concentrations were increased over 2-fold in patients affected by atherosclerosis (172) and chronic kidney disease (171), two comparatively less severe conditions exhibiting lower increases in MMP-12 expression. We therefore question the biological relevance of such small differences in sEDP concentrations and doubt their capacity to explain the observed reductions in CD11b+Ly6G+ counts in *Lal/Mmp12* DKO mice. Unfortunately, circulating EDP concentrations vary significantly depending on the method of quantification (86). Only a few reliable quantifications of elastin fragments in mice have been published. Several studies have used commercially available VGVAPG hexapeptides for *in vitro* experiments (173-175). One publication using a colorimetric assay (85) reported plasma EDP concentrations of approximately 4 µg/ml in mice. Our attempt to reproduce this assay yielded concentrations for WT mice in the g/dl range, exceeding even the concentration of albumin, the most abundant plasma protein. As a result, we chose to utilize a commercially available ELISA kit designed for quantifying murine sEDPs. However, this ELISA kit has not been independently validated, leaving open the possibility of unreliable or inaccurate results. Taken together, we conclude that our obtained changes in sEDP concentrations are unlikely to explain the phenotype of DKO mice.

MMP-12 has been well established as a modulator of neutrophil chemotaxis (89, 147, 164, 176). Injection of recombinant human MMP-12 led to neutrophil infiltration (164), while inhibition of MMP-12 attenuated neutrophil recruitment into the lungs following smoke exposure (147). Similarly, the deletion of *Mmp12* in a mouse model of myocardial infarction prolonged inflammation and exacerbated neutrophil influx (176). Despite this well-documented role of MMP-12 in neutrophil chemotaxis, we did not observe significant differences in the expression of prominent chemokine receptors or their ligands (106, 108), suggesting that neutrophil chemotaxis was unlikely affected by the deletion of *Mmp12*. Consistently, CD11b+Ly6G+ counts were reduced across multiple immune cell compartments. If alterations in neutrophil chemotaxis alone were responsible for this phenotype, an opposing increase in another immune cell compartment would be expected. Therefore, we suggest that other mechanisms are more likely responsible for the phenotype of *Lal/Mmp12* DKO mice. In support of this notion, the gene expressions of the neutrophil markers *Ly6g* and *Elane* remained unchanged in the *Lal/Mmp12* DKO spleen, whereas flow cytometry yielded reductions in CD11b+ Ly6G+ neutrophil counts across several immune cell compartments. These two observations are not mutually exclusive, as qPCR quantifies the total abundance of mRNA in

a tissue sample, whereas flow cytometry only provides a semi-quantification measure of viable cells expressing a specific surface marker. We speculate that the deletion of *Mmp12* may have altered neutrophil maturation, activation, or viability (177), resulting in disproportional changes between viable CD11b+Ly6G+ cells and total *Ly6g* expression.

Platelets have been shown to form PLAs, resulting in the activation of both platelets and leukocytes and triggers platelets to release cytokines (94, 98, 178). These platelet-derived cytokines modulate leukocyte function, altering their response to inflammation, injury, and infections (98). Additionally, interactions between platelets and neutrophils can boost their oxidative burst and the formation of NETs (98). Therefore, the alterations in NET formation could constitute a possible link between changes in platelet function and the reduction of neutrophil counts in *Lal/Mmp12* DKO mice. The incubation of platelets with recombinant MMP-12 was shown to increase and accelerate collagen-induced platelet activation through cleavage of the surface receptor CEACAM1 (104). The authors observed changes in platelet aggregation, adhesion, and α-granule secretion (104), indicating that altered MMP-12 expression could influence platelet function. Compared to WT mice, the deletion of *Mmp12* caused a massive drop in the percentage of monocytes (CD115+) and neutrophils (Ly6G+) positively stained with the platelet-specific marker CD41. This indicated that even physiological expression levels of MMP-12 significantly influenced PLA formation. However, unchanged collagen-induced platelet aggregation in *Mmp12* KO mice suggests that hemostatic functions remained unaffected by the deletion of *Mmp12*. It should be noted that circulating MMP-12 levels in WT mice are very low, which may explain the discrepancies with previous in vitro studies using recombinant MMP-12 (104). We conclude that PLAs are a plausible mechanism by which the deletion of *Mmp12* might affect neutrophil counts.

Notably, CEACAM1 expression is not limited to platelets and has been shown to extensively regulate various immune cell types (179). It inhibits natural killer cell cytotoxicity(180), activates monocytes during fibrosis (181), and modulates T-cell tolerance (182). Consistent with these roles, CEACAM1 is abundantly expressed on the surface of naïve lymphocytes (183, 184) and regulates human T-cell function (185). Additionally, CEACAM1 promotes monocyte survival and differentiation (186) and regulates apoptosis in Jurkat cells by acting as a tumor suppressor (187), indicating a direct role in immune cell survival. In resting neutrophils, CEACAM1 is stored in granules (188) and is rapidly transported to the plasma membrane upon neutrophil activation (189). Deletion of *Ceacam1* results in defective granulopoiesis and subsequent neutrophilia (190), and CEACAM1 has also been implicated in modulating neutrophil susceptibility to NETosis (191). Thus, CEACAM1 provides a plausible mechanistic

link between MMP-12 and alterations in neutrophil numbers, independent of platelet-derived factors. Notably, CEACAM1 has 11 isoforms, each containing different numbers of extracellular immunoglobulin-like domains (192). Whether MMP-12 can process all isoforms remains unknown and could limit the extent of its regulatory effect.

Alterations in the tendency of neutrophils to form NETs could explain the observed reductions in CD11b+Ly6G+ counts in *Lal/Mmp12* DKO mice. However, NET formation had not previously been characterized in the context of LAL-D. The gold standard for NETs detection involves a co-localized DAPI staining with citrullinated Histone 3 (H3Cit) staining in tissue sections (193). *Lal* KO spleen sections exhibited an average of 13% of the tissue area as H3Cit+ DAPI+, demonstrating NET formation in the context of LAL-D. Given the established role of NETs in exacerbating inflammation and contributing to disease pathology, their presence in *Lal* KO mice suggests a potential mechanism through which neutrophils drive inflammation and tissue damage (128, 194). Notably, deletion of *Mmp12* resulted in a significant reduction in NET formation. However, this reduction was not accompanied by any notable improvements in overall spleen pathology of *Lal/Mmp12* mice, indicating that although abundant, NETs may not significantly contribute to the pathology of LAL-D. We propose that the observed reduction in NET formation is most likely a direct consequence of the reduced neutrophil numbers following the deletion *of Mmp12*.

Under physiological conditions, apoptotic neutrophils are efficiently cleared via efferocytosis by phagocytes like macrophages and dendritic cells (141). Given previous reports of significantly impaired efferocytosis in macrophages from *Lal* KO mice (5), we hypothesized that improvements in efferocytosis function associated with *Mmp12* loss could explain the observed reduction in CD11b+Ly6G+ cells and NETs in *Lal/Mmp12* DKO spleens. However, we observed no improvements in efferocytosis capacity in *Lal/Mmp12* DKO macrophages. This finding suggests that reduced neutrophil numbers and diminished NET formation are not due to an ameliorated clearance by macrophages. Considering that we observed no changes in the hematopoietic stem and progenitor cell compartment, we exclude an increased production of neutrophils. Similarly, altered neutrophil chemotaxis, NET formation, or efferocytosis cannot explain the observed phenotype. Therefore, altered neutrophil survival or apoptosis is arguable, the most plausible mechanism by which the deletion of *Mmp12* reduced the number of neutrophils.

Preliminary experiments comparing the effects of conditioned media derived from *Mmp12* KO BMDMs demonstrated a reproducible increase in the viability of cultured neutrophils after 48 and 72 h of incubation compared to WT conditioned media. This observation, however, contrasts with previous reports, suggesting that MMP-12 polarizes neutrophils towards an apoptotic signature (47). Based on existing literature, we hypothesize that this effect may be partially mediated through altered NF-κB signaling. Notably, MMP-12 has been reported to bind the promoter and induce the expression of inhibitor of NF-κB alpha (IκBα) (195). Given that the removal of NF-κB inhibition has been associated with prolonged neutrophil survival through sustained activation of the p38-MAPK pathway (48), one might predict that MMP-12 deletion would result in decreased IκBα expression, increased NF-κB activity, and, consequently, reduced neutrophil viability. However, the NF-κB signaling pathway is not a simple linear cascade but rather a highly intricate network, comprising five transcription factors that form both homo- and heterodimers, along with seven IκB inhibitors (196). With over 150 physiological and pathological functions attributed to NF-κB (87), its regulation and derived consequences are inherently complex.

To fully elucidate the role of MMP-12 in neutrophil apoptosis and NF-κB signaling, a comprehensive, context-specific analysis of its molecular interactions is warranted. Future studies should aim to dissect the precise mechanisms by which MMP-12 integrates into this broader signaling landscape, potentially revealing the mechanism by which MMP-12 alters neutrophil lifespan in LAL-D.

Conclusion

Previous studies have identified MMP-12 as one of the most dysregulated genes in the lungs of *Lal* KO mice. Striking similarities between MMP-12 overexpression and the pathophysiology of LAL-D led to the hypothesis that MMP-12 may act as a key downstream effector contributing to immune dysfunction and chronic inflammation in LAL-D. Our investigation revealed significantly improved thymus size and morphology, reduced CD11b+Ly6G+ neutrophil counts across multiple immune compartments, and a marked reduction of NETs in the spleen of *Lal/Mmp12* DKO mice. However, the deletion of *Mmp12* did not ameliorate the overall severity of LAL-D, suggesting that while MMP-12 is clearly involved in and contributes to the disease phenotype, it does not play a central role. Therefore, targeting MMP-12 does not constitute a viable therapeutic strategy for LAL-D in mice.

5. References

1. Sheriff S, Du H, Grabowski GA. Characterization of lysosomal acid lipase by site-directed mutagenesis and heterologous expression. J Biol Chem. 1995;270(46):27766-72.
2. Warner TG, Dambach LM, Shin JH, O'Brien JS. Purification of the lysosomal acid lipase from human liver and its role in lysosomal lipid hydrolysis. J Biol Chem. 1981;256(6):2952-7.
3. Grumet L, Eichmann TO, Taschler U, Zierler KA, Leopold C, Moustafa T, et al. Lysosomal Acid Lipase Hydrolyzes Retinyl Ester and Affects Retinoid Turnover. J Biol Chem. 2016;291(34):17977-87.
4. Zechner R, Madeo F, Kratky D. Cytosolic lipolysis and lipophagy: two sides of the same coin. Nat Rev Mol Cell Biol. 2017;18(11):671-84.
5. Viaud M, Ivanov S, Vujic N, Duta-Mare M, Aira LE, Barouillet T, et al. Lysosomal Cholesterol Hydrolysis Couples Efferocytosis to Anti-Inflammatory Oxysterol Production. Circ Res. 2018;122(10):1369-84.
6. Anderson RA, Rao N, Byrum RS, Rothschild CB, Bowden DW, Hayworth R, et al. In situ localization of the genetic locus encoding the lysosomal acid lipase/cholesteryl esterase (LIPA) deficient in Wolman disease to chromosome 10q23.2-q23.3. Genomics. 1993;15(1):245-7.
7. Ameis D, Merkel M, Eckerskorn C, Greten H. Purification, characterization and molecular cloning of human hepatic lysosomal acid lipase. Eur J Biochem. 1994;219(3):905-14.
8. Zschenker O, Oezden D, Ameis D. Lysosomal acid lipase as a preproprotein. J Biochem. 2004;136(1):65-72.
9. Rajamohan F, Reyes AR, Tu M, Nedoma NL, Hoth LR, Schwaid AG, et al. Crystal structure of human lysosomal acid lipase and its implications in cholesteryl ester storage disease. J Lipid Res. 2020;61(8):1192-202.
10. Lohse P, Lohse P, Chahrokh-Zadeh S, Seidel D. The acid lipase gene family: three enzymes, one highly conserved gene structure. J Lipid Res. 1997;38(5):880-91.
11. Du H, Witte DP, Grabowski GA. Tissue and cellular specific expression of murine lysosomal acid lipase mRNA and protein. J Lipid Res. 1996;37(5):937-49.
12. Emanuel R, Sergin I, Bhattacharya S, Turner J, Epelman S, Settembre C, et al. Induction of lysosomal biogenesis in atherosclerotic macrophages can rescue lipid-induced lysosomal dysfunction and downstream sequelae. Arterioscler Thromb Vasc Biol. 2014;34(9):1942-52.
13. Settembre C, De Cegli R, Mansueto G, Saha PK, Vetrini F, Visvikis O, et al. TFEB controls cellular lipid metabolism through a starvation-induced autoregulatory loop. Nat Cell Biol. 2013;15(6):647-58.
14. Lettieri Barbato D, Tatulli G, Aquilano K, Ciriolo MR. FoxO1 controls lysosomal acid lipase in adipocytes: implication of lipophagy during nutrient restriction and metformin treatment. Cell Death Dis. 2013;4(10):e861.
15. Heltianu C, Robciuc A, Botez G, Musina C, Stancu C, Sima AV, et al. Modified low density lipoproteins decrease the activity and expression of lysosomal acid lipase in human endothelial and smooth muscle cells. Cell Biochem Biophys. 2011;61(1):209-16.
16. Lipinski P, Cielecka-Kuszyk J, Bozkiewicz-Kasperczyk A, Perkowska B, Jurkiewicz E, Tylki-Szymanska A. Role of Myeloperoxidase Oxidants in the Modulation of Cellular Lysosomal Enzyme Function: A Contributing Factor to Macrophage Dysfunction in Atherosclerosis. Mol Genet Metab Rep. 2020;23:100594.
17. Radović B, Vujić N, Leopold C, Schlager S, Goeritzer M, Patankar JV, et al. Lysosomal acid lipase regulates VLDL synthesis and insulin sensitivity in mice. Diabetologia. 2016;59(8):1743-52.

18. Tan HWS, Anjum B, Shen HM, Ghosh S, Yen PM, Sinha RA. Lysosomal inhibition attenuates peroxisomal gene transcription via suppression of PPARA and PPARGC1A levels. Autophagy. 2019;15(8):1455-9.
19. Montaigne D, Butruille L, Staels B. PPAR control of metabolism and cardiovascular functions. Nat Rev Cardiol. 2021;18(12):809-23.
20. Bowden KL, Dubland JA, Chan T, Xu YH, Grabowski GA, Du H, et al. LAL (Lysosomal Acid Lipase) Promotes Reverse Cholesterol Transport In Vitro and In Vivo. Arterioscler Thromb Vasc Biol. 2018;38(5):1191-201.
21. Martin H. Role of PPAR-gamma in inflammation. Prospects for therapeutic intervention by food components. Mutat Res. 2010;690(1-2):57-63.
22. Wu L, Yan C, Czader M, Foreman O, Blum JS, Kapur R, et al. Inhibition of PPARgamma in myeloid-lineage cells induces systemic inflammation, immunosuppression, and tumorigenesis. Blood. 2012;119(1):115-26.
23. Schlager S, Vujic N, Korbelius M, Duta-Mare M, Dorow J, Leopold C, et al. Lysosomal lipid hydrolysis provides substrates for lipid mediator synthesis in murine macrophages. Oncotarget. 2017;8(25):40037-51.
24. Li F, Zhang H. Lysosomal Acid Lipase in Lipid Metabolism and Beyond. Arterioscler Thromb Vasc Biol. 2019;39(5):850-6.
25. Farooqui AA, Farooqui T. Phospholipids, Sphingolipids, and Cholesterol-Derived Lipid Mediators and Their Role in Neurological Disorders. International Journal of Molecular Sciences [Internet]. 2024; 25(19).
26. Korbelius M, Kuentzel KB, Bradic I, Vujic N, Kratky D. Recent insights into lysosomal acid lipase deficiency. Trends Mol Med. 2023;29(6):425-38.
27. Hoffman EP, Barr ML, Giovanni MA, Murray MF. Lysosomal Acid Lipase Deficiency. In: Adam MP, Feldman J, Mirzaa GM, Pagon RA, Wallace SE, Bean LJH, et al., editors. GeneReviews(®). Seattle (WA): University of Washington, Seattle
Copyright © 1993-2024, University of Washington, Seattle. GeneReviews is a registered trademark of the University of Washington, Seattle. All rights reserved.; 1993.
28. Bernstein DL, Hülkova H, Bialer MG, Desnick RJ. Cholesteryl ester storage disease: Review of the findings in 135 reported patients with an underdiagnosed disease. Journal of Hepatology. 2013;58(6):1230-43.
29. Burton BK, Balwani M, Feillet F, Barić I, Burrow TA, Camarena Grande C, et al. A Phase 3 Trial of Sebelipase Alfa in Lysosomal Acid Lipase Deficiency. N Engl J Med. 2015;373(11):1010-20.
30. Carter A, Brackley SM, Gao J, Mann JP. The global prevalence and genetic spectrum of lysosomal acid lipase deficiency: A rare condition that mimics NAFLD. J Hepatol. 2019;70(1):142-50.
31. Reiner Ž, Guardamagna O, Nair D, Soran H, Hovingh K, Bertolini S, et al. Lysosomal acid lipase deficiency--an under-recognized cause of dyslipidaemia and liver dysfunction. Atherosclerosis. 2014;235(1):21-30.
32. Fouchier SW, Defesche JC. Lysosomal acid lipase A and the hypercholesterolaemic phenotype. Curr Opin Lipidol. 2013;24(4):332-8.
33. Gaddi A, Cicero AF, Odoo FO, Poli AA, Paoletti R. Practical guidelines for familial combined hyperlipidemia diagnosis: an up-date. Vasc Health Risk Manag. 2007;3(6):877-86.
34. Reiner Z, Catapano AL, De Backer G, Graham I, Taskinen MR, Wiklund O, et al. ESC/EAS Guidelines for the management of dyslipidaemias: the Task Force for the management of dyslipidaemias of the European Society of Cardiology (ESC) and the European Atherosclerosis Society (EAS). Eur Heart J. 2011;32(14):1769-818.
35. Hamilton J, Jones I, Srivastava R, Galloway P. A new method for the measurement of lysosomal acid lipase in dried blood spots using the inhibitor Lalistat 2. Clinica Chimica Acta. 2012;413(15):1207-10.

36. Lukacs Z, Barr M, Hamilton J. Best practice in the measurement and interpretation of lysosomal acid lipase in dried blood spots using the inhibitor Lalistat 2. Clin Chim Acta. 2017;471:201-5.
37. Desai PK, Astrin KH, Thung SN, Gordon RE, Short MP, Coates PM, et al. Cholesteryl ester storage disease: pathologic changes in an affected fetus. Am J Med Genet. 1987;26(3):689-98.
38. Yokoyama S, McCoy E. Long-term treatment of a homozygous cholesteryl ester storage disease with combined cholestyramine and lovastatin. J Inherit Metab Dis. 1992;15(2):291-2.
39. Ginsberg HN, Le NA, Short MP, Ramakrishnan R, Desnick RJ. Suppression of apolipoprotein B production during treatment of cholesteryl ester storage disease with lovastatin. Implications for regulation of apolipoprotein B synthesis. J Clin Invest. 1987;80(6):1692-7.
40. Levy R, Ostlund RE, Jr., Schonfeld G, Wong P, Semenkovich CF. Cholesteryl ester storage disease: complex molecular effects of chronic lovastatin therapy. J Lipid Res. 1992;33(7):1005-15.
41. Krivit W, Peters C, Dusenbery K, Ben-Yoseph Y, Ramsay NKC, Wagner JE, et al. Wolman disease successfully treated by bone marrow transplantation. Bone Marrow Transplantation. 2000;26(5):567-70.
42. Tolar J, Petryk A, Khan K, Bjoraker KJ, Jessurun J, Dolan M, et al. Long-term metabolic, endocrine, and neuropsychological outcome of hematopoietic cell transplantation for Wolman disease. Bone Marrow Transplant. 2009;43(1):21-7.
43. Sreekantam S, Nicklaus-Wollenteit I, Orr J, Sharif K, Vijay S, McKiernan PJ, et al. Successful long-term outcome of liver transplantation in late-onset lysosomal acid lipase deficiency. Pediatr Transplant. 2016;20(6):851-4.
44. Bernstein DL, Lobritto S, Iuga A, Remotti H, Schiano T, Fiel MI, et al. Lysosomal acid lipase deficiency allograft recurrence and liver failure- clinical outcomes of 18 liver transplantation patients. Mol Genet Metab. 2018;124(1):11-9.
45. Balwani M, Breen C, Enns GM, Deegan PB, Honzík T, Jones S, et al. Clinical effect and safety profile of recombinant human lysosomal acid lipase in patients with cholesteryl ester storage disease. Hepatology. 2013;58(3):950-7.
46. Valayannopoulos V, Malinova V, Honzík T, Balwani M, Breen C, Deegan PB, et al. Sebelipase alfa over 52 weeks reduces serum transaminases, liver volume and improves serum lipids in patients with lysosomal acid lipase deficiency. J Hepatol. 2014;61(5):1135-42.
47. Burton BK, Feillet F, Furuya KN, Marulkar S, Balwani M. Sebelipase alfa in children and adults with lysosomal acid lipase deficiency: Final results of the ARISE study. J Hepatol. 2022;76(3):577-87.
48. Burton BK, Sanchez AC, Kostyleva M, Martins AM, Marulkar S, Abel F, et al. Long-Term Sebelipase Alfa Treatment in Children and Adults With Lysosomal Acid Lipase Deficiency. J Pediatr Gastroenterol Nutr. 2022;74(6):757-64.
49. Demaret T, Lacaille F, Wicker C, Arnoux JB, Bouchereau J, Belloche C, et al. Sebelipase alfa enzyme replacement therapy in Wolman disease: a nationwide cohort with up to ten years of follow-up. Orphanet J Rare Dis. 2021;16(1):507.
50. Vijay S, Brassier A, Ghosh A, Fecarotta S, Abel F, Marulkar S, et al. Long-term survival with sebelipase alfa enzyme replacement therapy in infants with rapidly progressive lysosomal acid lipase deficiency: final results from 2 open-label studies. Orphanet J Rare Dis. 2021;16(1):13.
51. Lam P, Ashbrook A, Zygmunt DA, Yan C, Du H, Martin PT. Therapeutic efficacy of rscAAVrh74.miniCMV.LIPA gene therapy in a mouse model of lysosomal acid lipase deficiency. Mol Ther Methods Clin Dev. 2022;26:413-26.
52. Rosenbaum AI, Rujoi M, Huang AY, Du H, Grabowski GA, Maxfield FR. Chemical screen to reduce sterol accumulation in Niemann–Pick C disease cells identifies novel

lysosomal acid lipase inhibitors. Biochimica et Biophysica Acta (BBA) - Molecular and Cell Biology of Lipids. 2009;1791(12):1155-65.
53. Rosenbaum AI, Cosner CC, Mariani CJ, Maxfield FR, Wiest O, Helquist P. Thiadiazole carbamates: potent inhibitors of lysosomal acid lipase and potential Niemann-Pick type C disease therapeutics. J Med Chem. 2010;53(14):5281-9.
54. Bradić I, Kuentzel KB, Honeder S, Grabner GF, Vujić N, Zimmermann R, et al. Off-target effects of the lysosomal acid lipase inhibitors Lalistat-1 and Lalistat-2 on neutral lipid hydrolases. Mol Metab. 2022;61:101510.
55. Du H, Duanmu M, Witte D, Grabowski GA. Targeted disruption of the mouse lysosomal acid lipase gene: long-term survival with massive cholesteryl ester and triglyceride storage. Hum Mol Genet. 1998;7(9):1347-54.
56. Du H, Heur M, Duanmu M, Grabowski GA, Hui DY, Witte DP, et al. Lysosomal acid lipase-deficient mice: depletion of white and brown fat, severe hepatosplenomegaly, and shortened life span. J Lipid Res. 2001;42(4):489-500.
57. Du H. Lysosomal Acid Lipase Deficiency: Correction of Lipid Storage by Adenovirus-Mediated Gene Transfer in Mice. 2002.
58. Bianco V, Korbelius M, Vujic N, Akhmetshina A, Amor M, Kolb D, et al. Impact of (intestinal) LAL deficiency on lipid metabolism and macrophage infiltration. Mol Metab. 2023;73:101737.
59. Qu P, Shelley WC, Yoder MC, Wu L, Du H, Yan C. Critical roles of lysosomal acid lipase in myelopoiesis. Am J Pathol. 2010;176(5):2394-404.
60. Yan C, Du H. Lysosomal acid lipase is critical for myeloid-derived suppressive cell differentiation, development, and homeostasis. World J Immunol. 2014;4(2):42.
61. Zlotoff DA, Bhandoola A. Hematopoietic progenitor migration to the adult thymus. Ann N Y Acad Sci. 2011;1217:122-38.
62. Qu P, Du H, Wilkes DS, Yan C. Critical roles of lysosomal acid lipase in T cell development and function. Am J Pathol. 2009;174(3):944-56.
63. Yan C, Lian X, Li Y, Dai Y, White A, Qin Y, et al. Macrophage-specific expression of human lysosomal acid lipase corrects inflammation and pathogenic phenotypes in lal-/- mice. Am J Pathol. 2006;169(3):916-26.
64. Qu P, Yan C, Blum JS, Kapur R, Du H. Myeloid-specific expression of human lysosomal acid lipase corrects malformation and malfunction of myeloid-derived suppressor cells in lal-/- mice. J Immunol. 2011;187(7):3854-66.
65. Veglia F, Perego M, Gabrilovich D. Myeloid-derived suppressor cells coming of age. Nat Immunol. 2018;19(2):108-19.
66. Veglia F, Sanseviero E, Gabrilovich DI. Myeloid-derived suppressor cells in the era of increasing myeloid cell diversity. Nat Rev Immunol. 2021;21(8):485-98.
67. Park M-J, Lee S-H, Kim E-K, Lee E-J, Baek J-A, Park S-H, et al. Interleukin-10 produced by myeloid-derived suppressor cells is critical for the induction of Tregs and attenuation of rheumatoid inflammation in mice. Scientific Reports. 2018;8(1):3753.
68. Ge Y, Cheng D, Jia Q, Xiong H, Zhang J. Mechanisms Underlying the Role of Myeloid-Derived Suppressor Cells in Clinical Diseases: Good or Bad. Immune Netw. 2021;21(3).
69. Yan C, Ding X, Dasgupta N, Wu L, Du H. Gene Profile of Myeloid-Derived Suppressive Cells from the Bone Marrow of Lysosomal Acid Lipase Knock-Out Mice. PLoS ONE. 2012;7(2):e30701.
70. Ding X, Du H, Yoder MC, Yan C. Critical role of the mTOR pathway in development and function of myeloid-derived suppressor cells in lal-/- mice. Am J Pathol. 2014;184(2):397-408.
71. Liu GY, Sabatini DM. mTOR at the nexus of nutrition, growth, ageing and disease. Nat Rev Mol Cell Biol. 2020;21(4):183-203.

72. Vaupel P, Schmidberger H, Mayer A. The Warburg effect: essential part of metabolic reprogramming and central contributor to cancer progression. Int J Radiat Biol. 2019;95(7):912-9.
73. Du H. Lysosomal acid lipase deficiency causes respiratory inflammation and destruction in the lung. 2003.
74. Lian X, Yan C, Qin Y, Knox L, Li T, Du H. Neutral lipids and peroxisome proliferator-activated receptor-{gamma} control pulmonary gene expression and inflammation-triggered pathogenesis in lysosomal acid lipase knockout mice. Am J Pathol. 2005;167(3):813-21.
75. Hofmann HS, Hansen G, Richter G, Taege C, Simm A, Silber RE, et al. Matrix metalloproteinase-12 expression correlates with local recurrence and metastatic disease in non-small cell lung cancer patients. Clin Cancer Res. 2005;11(3):1086-92.
76. Verma RP, Hansch C. Matrix metalloproteinases (MMPs): chemical-biological functions and (Q)SARs. Bioorg Med Chem. 2007;15(6):2223-68.
77. Morrison CJ, Butler GS, Rodríguez D, Overall CM. Matrix metalloproteinase proteomics: substrates, targets, and therapy. Current Opinion in Cell Biology. 2009;21(5):645-53.
78. Brew K, Dinakarpandian D, Nagase H. Tissue inhibitors of metalloproteinases: evolution, structure and function11Dedicated to Professor H. Neurath on the occasion of his 90th birthday. Biochimica et Biophysica Acta (BBA) - Protein Structure and Molecular Enzymology. 2000;1477(1):267-83.
79. Shipley JM, Wesselschmidt RL, Kobayashi DK, Ley TJ, Shapiro SD. Metalloelastase is required for macrophage-mediated proteolysis and matrix invasion in mice. Proc Natl Acad Sci U S A. 1996;93(9):3942-6.
80. Taddese S, Weiss AS, Jahreis G, Neubert RH, Schmelzer CE. In vitro degradation of human tropoelastin by MMP-12 and the generation of matrikines from domain 24. Matrix Biol. 2009;28(2):84-91.
81. Maquart FX, Pasco S, Ramont L, Hornebeck W, Monboisse JC. An introduction to matrikines: extracellular matrix-derived peptides which regulate cell activity. Implication in tumor invasion. Crit Rev Oncol Hematol. 2004;49(3):199-202.
82. Blanchevoye C, Floquet N, Scandolera A, Baud S, Maurice P, Bocquet O, et al. Interaction between the elastin peptide VGVAPG and human elastin binding protein. J Biol Chem. 2013;288(2):1317-28.
83. Szychowski KA, Skora B, Wojtowicz AK. Elastin-Derived Peptides in the Central Nervous System: Friend or Foe. Cell Mol Neurobiol. 2021.
84. Senior RM, Griffin GL, Mecham RP. Chemotactic activity of elastin-derived peptides. J Clin Invest. 1980;66(4):859-62.
85. Romier B, Ivaldi C, Sartelet H, Heinz A, Schmelzer CEH, Garnotel R, et al. Production of Elastin-Derived Peptides Contributes to the Development of Nonalcoholic Steatohepatitis. Diabetes. 2018;67(8):1604-15.
86. Blaise S, Romier B, Kawecki C, Ghirardi M, Rabenoelina F, Baud S, et al. Elastin-derived peptides are new regulators of insulin resistance development in mice. Diabetes. 2013;62(11):3807-16.
87. Liu T, Zhang L, Joo D, Sun SC. NF-κB signaling in inflammation. Signal Transduct Target Ther. 2017;2:17023-.
88. Song M, Zhang S, Tao Z, Li J, Shi Y, Xiong Y, et al. MMP-12 siRNA improves the homeostasis of the small intestine and metabolic dysfunction in high-fat diet feeding-induced obese mice. Biomaterials. 2021;278:121183.
89. Dean RA, Cox JH, Bellac CL, Doucet A, Starr AE, Overall CM. Macrophage-specific metalloelastase (MMP-12) truncates and inactivates ELR+ CXC chemokines and generates CCL2, -7, -8, and -13 antagonists: potential role of the macrophage in terminating polymorphonuclear leukocyte influx. Blood. 2008;112(8):3455-64.

90. Di Gregoli K, Somerville M, Bianco R, Thomas AC, Frankow A, Newby AC, et al. Galectin-3 Identifies a Subset of Macrophages With a Potential Beneficial Role in Atherosclerosis. Arterioscler Thromb Vasc Biol. 2020;40(6):1491-509.
91. Qu P, Du H, Wang X, Yan C. Matrix metalloproteinase 12 overexpression in lung epithelial cells plays a key role in emphysema to lung bronchioalveolar adenocarcinoma transition. Cancer Res. 2009;69(18):7252-61.
92. Hautamaki RD, Kobayashi DK, Senior RM, Shapiro SD. Requirement for macrophage elastase for cigarette smoke-induced emphysema in mice. Science. 1997;277(5334):2002-4.
93. Holinstat M. Normal platelet function. Cancer Metastasis Rev. 2017;36(2):195-8.
94. Schrottmaier WC, Mussbacher M, Salzmann M, Assinger A. Platelet-leukocyte interplay during vascular disease. Atherosclerosis. 2020;307:109-20.
95. Bhatnagar N, Hall GW. Major bleeding disorders: diagnosis, classification, management and recent developments in haemophilia. Arch Dis Child. 2018;103(5):509-13.
96. Hartz S, Menart B, Tschoepe D. Leukocyte apoptosis in whole blood involves platelet-dependent coaggregation. Cytometry A. 2003;52(2):117-21.
97. Dib PRB, Quirino-Teixeira AC, Merij LB, Pinheiro MBM, Rozini SV, Andrade FB, et al. Innate immune receptors in platelets and platelet-leukocyte interactions. J Leukoc Biol. 2020;108(4):1157-82.
98. Kral JB, Schrottmaier WC, Salzmann M, Assinger A. Platelet Interaction with Innate Immune Cells. Transfus Med Hemother. 2016;43(2):78-88.
99. Clark SR, Ma AC, Tavener SA, McDonald B, Goodarzi Z, Kelly MM, et al. Platelet TLR4 activates neutrophil extracellular traps to ensnare bacteria in septic blood. Nature Medicine. 2007;13(4):463-9.
100. Rayes J, Jenne CN. Platelets: bridging thrombosis and inflammation. Platelets. 2021;32(3):293-4.
101. Wang X, Qin W, Sun B. New strategy for sepsis: Targeting a key role of platelet-neutrophil interaction. Burns Trauma. 2014;2(3):114-20.
102. Austin KM, Covic L, Kuliopulos A. Matrix metalloproteases and PAR1 activation. Blood. 2013;121(3):431-9.
103. Jaffré F, Friedman AE, Hu Z, Mackman N, Blaxall BC. β-adrenergic receptor stimulation transactivates protease-activated receptor 1 via matrix metalloproteinase 13 in cardiac cells. Circulation. 2012;125(24):2993-3003.
104. Wang J, Ye Y, Wei G, Hu W, Li L, Lu S, et al. Matrix metalloproteinase12 facilitated platelet activation by shedding carcinoembryonic antigen related cell adhesion molecule1. Biochem Biophys Res Commun. 2017;486(4):1103-9.
105. Hidalgo A, Chilvers ER, Summers C, Koenderman L. The Neutrophil Life Cycle. Trends Immunol. 2019;40(7):584-97.
106. Metzemaekers M, Gouwy M, Proost P. Neutrophil chemoattractant receptors in health and disease: double-edged swords. Cell Mol Immunol. 2020;17(5):433-50.
107. Palmblad J, Malmsten CL, Udén AM, Rådmark O, Engstedt L, Samuelsson B. Leukotriene B4 is a potent and stereospecific stimulator of neutrophil chemotaxis and adherence. Blood. 1981;58(3):658-61.
108. Rajarathnam K, Schnoor M, Richardson RM, Rajagopal S. How do chemokines navigate neutrophils to the target site: Dissecting the structural mechanisms and signaling pathways. Cell Signal. 2019;54:69-80.
109. Nakagawa H, Komorita N. Complement component C3-derived neutrophil chemotactic factors purified from exudate of rat carrageenin-induced inflammation. Biochem Biophys Res Commun. 1993;194(3):1181-7.
110. Schiffmann E, Corcoran BA, Wahl SM. N-formylmethionyl peptides as chemoattractants for leucocytes. Proc Natl Acad Sci U S A. 1975;72(3):1059-62.
111. Sadik CD, Luster AD. Lipid-cytokine-chemokine cascades orchestrate leukocyte recruitment in inflammation. J Leukoc Biol. 2012;91(2):207-15.

112. Basu S, Hodgson G, Katz M, Dunn AR. Evaluation of role of G-CSF in the production, survival, and release of neutrophils from bone marrow into circulation. Blood. 2002;100(3):854-61.
113. Bargatze RF, Kurk S, Butcher EC, Jutila MA. Neutrophils roll on adherent neutrophils bound to cytokine-induced endothelial cells via L-selectin on the rolling cells. J Exp Med. 1994;180(5):1785-92.
114. Diacovo TG, Roth SJ, Buccola JM, Bainton DF, Springer TA. Neutrophil rolling, arrest, and transmigration across activated, surface-adherent platelets via sequential action of P-selectin and the beta 2-integrin CD11b/CD18. Blood. 1996;88(1):146-57.
115. Ligeti E, Mócsai A. Exocytosis of neutrophil granulocytes. Biochem Pharmacol. 1999;57(11):1209-14.
116. Cotzomi-Ortega I, Rosowski EE, Wang X, Sanchez-Zamora YI, Lopez-Torres JM, Sanchez-Orellana G, et al. Neutrophil NADPH oxidase promotes bacterial eradication and regulates NF-κB-Mediated inflammation via NRF2 signaling during urinary tract infections. Mucosal Immunology. 2024.
117. Herant M, Heinrich V, Dembo M. Mechanics of neutrophil phagocytosis: experiments and quantitative models. J Cell Sci. 2006;119(Pt 9):1903-13.
118. Witko-Sarsat V, Pederzoli-Ribeil M, Hirsch E, Sozzani S, Cassatella MA. Regulating neutrophil apoptosis: new players enter the game. Trends Immunol. 2011;32(3):117-24.
119. Caudrillier A, Kessenbrock K, Gilliss BM, Nguyen JX, Marques MB, Monestier M, et al. Platelets induce neutrophil extracellular traps in transfusion-related acute lung injury. J Clin Invest. 2012;122(7):2661-71.
120. Hellebrekers P, Vrisekoop N, Koenderman L. Neutrophil phenotypes in health and disease. Eur J Clin Invest. 2018;48 Suppl 2(Suppl Suppl 2):e12943.
121. Castanheira FVS, Kubes P. Neutrophils and NETs in modulating acute and chronic inflammation. Blood. 2019;133(20):2178-85.
122. Allen C, Thornton P, Denes A, McColl BW, Pierozynski A, Monestier M, et al. Neutrophil cerebrovascular transmigration triggers rapid neurotoxicity through release of proteases associated with decondensed DNA. J Immunol. 2012;189(1):381-92.
123. Dias IH, Matthews JB, Chapple IL, Wright HJ, Dunston CR, Griffiths HR. Activation of the neutrophil respiratory burst by plasma from periodontitis patients is mediated by pro-inflammatory cytokines. J Clin Periodontol. 2011;38(1):1-7.
124. Denny MF, Yalavarthi S, Zhao W, Thacker SG, Anderson M, Sandy AR, et al. A distinct subset of proinflammatory neutrophils isolated from patients with systemic lupus erythematosus induces vascular damage and synthesizes type I IFNs. J Immunol. 2010;184(6):3284-97.
125. Pillay J, den Braber I, Vrisekoop N, Kwast LM, de Boer RJ, Borghans JAM, et al. In vivo labeling with 2H2O reveals a human neutrophil lifespan of 5.4 days. Blood. 2010;116(4):625-7.
126. Fuchs TA, Abed U, Goosmann C, Hurwitz R, Schulze I, Wahn V, et al. Novel cell death program leads to neutrophil extracellular traps. J Cell Biol. 2007;176(2):231-41.
127. Mutua V, Gershwin LJ. A Review of Neutrophil Extracellular Traps (NETs) in Disease: Potential Anti-NETs Therapeutics. Clin Rev Allergy Immunol. 2021;61(2):194-211.
128. Papayannopoulos V. Neutrophil extracellular traps in immunity and disease. Nat Rev Immunol. 2018;18(2):134-47.
129. Behrendt JH, Ruiz A, Zahner H, Taubert A, Hermosilla C. Neutrophil extracellular trap formation as innate immune reactions against the apicomplexan parasite Eimeria bovis. Vet Immunol Immunopathol. 2010;133(1):1-8.
130. Abi Abdallah DS, Lin C, Ball CJ, King MR, Duhamel GE, Denkers EY. Toxoplasma gondii triggers release of human and mouse neutrophil extracellular traps. Infect Immun. 2012;80(2):768-77.
131. Neeli I, Radic M. Opposition between PKC isoforms regulates histone deimination and neutrophil extracellular chromatin release. Front Immunol. 2013;4:38.

132. Liu C, Hermann TE. Characterization of ionomycin as a calcium ionophore. J Biol Chem. 1978;253(17):5892-4.
133. Kenny EF, Herzig A, Krüger R, Muth A, Mondal S, Thompson PR, et al. Diverse stimuli engage different neutrophil extracellular trap pathways. Elife. 2017;6.
134. Röhm M, Grimm MJ, D'Auria AC, Almyroudis NG, Segal BH, Urban CF. NADPH oxidase promotes neutrophil extracellular trap formation in pulmonary aspergillosis. Infect Immun. 2014;82(5):1766-77.
135. Li P, Li M, Lindberg MR, Kennett MJ, Xiong N, Wang Y. PAD4 is essential for antibacterial innate immunity mediated by neutrophil extracellular traps. J Exp Med. 2010;207(9):1853-62.
136. Lewis HD, Liddle J, Coote JE, Atkinson SJ, Barker MD, Bax BD, et al. Inhibition of PAD4 activity is sufficient to disrupt mouse and human NET formation. Nat Chem Biol. 2015;11(3):189-91.
137. Wang Y, Du C, Zhang Y, Zhu L. Composition and Function of Neutrophil Extracellular Traps. Biomolecules. 2024;14(4).
138. Warnatsch A, Ioannou M, Wang Q, Papayannopoulos V. Inflammation. Neutrophil extracellular traps license macrophages for cytokine production in atherosclerosis. Science. 2015;349(6245):316-20.
139. Boada-Romero E, Martinez J, Heckmann BL, Green DR. The clearance of dead cells by efferocytosis. Nat Rev Mol Cell Biol. 2020;21(7):398-414.
140. Lauber K, Bohn E, Kröber SM, Xiao YJ, Blumenthal SG, Lindemann RK, et al. Apoptotic cells induce migration of phagocytes via caspase-3-mediated release of a lipid attraction signal. Cell. 2003;113(6):717-30.
141. Greenlee-Wacker MC. Clearance of apoptotic neutrophils and resolution of inflammation. Immunol Rev. 2016;273(1):357-70.
142. Schindelin J, Arganda-Carreras I, Frise E, Kaynig V, Longair M, Pietzsch T, et al. Fiji: an open-source platform for biological-image analysis. Nat Methods. 2012;9(7):676-82.
143. Galarraga M, Campión J, Muñoz-Barrutia A, Boqué N, Moreno H, Martínez JA, et al. Adiposoft: automated software for the analysis of white adipose tissue cellularity in histological sections. J Lipid Res. 2012;53(12):2791-6.
144. Bankhead P, Loughrey MB, Fernández JA, Dombrowski Y, McArt DG, Dunne PD, et al. QuPath: Open source software for digital pathology image analysis. Sci Rep. 2017;7(1):16878.
145. Toda G, Yamauchi T, Kadowaki T, Ueki K. Preparation and culture of bone marrow-derived macrophages from mice for functional analysis. STAR Protoc. 2021;2(1):100246.
146. Lian X, Yan C, Qin Y, Knox L, Li T, Du H. Neutral lipids and peroxisome proliferator-activated receptor-{gamma} control pulmonary gene expression and inflammation-triggered pathogenesis in lysosomal acid lipase knockout mice. Am J Pathol. 2005;167(3):813-21.
147. Le Quement C, Guenon I, Gillon JY, Valenca S, Cayron-Elizondo V, Lagente V, et al. The selective MMP-12 inhibitor, AS111793 reduces airway inflammation in mice exposed to cigarette smoke. Br J Pharmacol. 2008;154(6):1206-15.
148. Buerger M, Amor M, Akhmetshina A, Bianco V, Perfler B, Zebisch A, et al. Limited Alleviation of Lysosomal Acid Lipase Deficiency by Deletion of Matrix Metalloproteinase 12. International Journal of Molecular Sciences [Internet]. **2024**; 25(20).
149. Lee J-T, Pamir N, Liu N-C, Kirk EA, Averill MM, Becker L, et al. Macrophage metalloelastase (MMP12) regulates adipose tissue expansion, insulin sensitivity, and expression of inducible nitric oxide synthase. Endocrinology. 2014;155(9):3409-20.
150. Mebius RE, Kraal G. Structure and function of the spleen. Nature Reviews Immunology. 2005;5(8):606-16.
151. De Filippo K, Rankin SM. CXCR4, the master regulator of neutrophil trafficking in homeostasis and disease. Eur J Clin Invest. 2018;48 Suppl 2:e12949.
152. Varga Z, Jacob MP, Robert L, Fülöp T, Jr. Identification and signal transduction mechanism of elastin peptide receptor in human leukocytes. FEBS Lett. 1989;258(1):5-8.

153. Varga Z, Jacob MP, Csongor J, Robert L, Leövey A, Fülöp T, Jr. Altered phosphatidylinositol breakdown after K-elastin stimulation in PMNLs of elderly. Mech Ageing Dev. 1990;52(1):61-70.
154. Senior RM, Griffin GL, Mecham RP. Chemotactic activity of elastin-derived peptides. J Clin Invest. 1980;66(4):859-62.
155. Qu P, Yan C, Du H. Matrix metalloproteinase 12 overexpression in myeloid lineage cells plays a key role in modulating myelopoiesis, immune suppression, and lung tumorigenesis. Blood. 2011;117(17):4476-89.
156. Wan J, Zhang G, Li X, Qiu X, Ouyang J, Dai J, et al. Matrix Metalloproteinase 3: A Promoting and Destabilizing Factor in the Pathogenesis of Disease and Cell Differentiation. Front Physiol. 2021;12:663978.
157. Bassiouni W, Ali MAM, Schulz R. Multifunctional intracellular matrix metalloproteinases: implications in disease. Febs j. 2021;288(24):7162-82.
158. Trojanek JB, Michałkiewicz J, Grzywa-Czuba R, Jańczyk W, Gackowska L, Kubiszewska I, et al. Expression of Matrix Metalloproteinases and Their Tissue Inhibitors in Peripheral Blood Leukocytes and Plasma of Children with Nonalcoholic Fatty Liver Disease. Mediators Inflamm. 2020;2020:8327945.
159. Kawano Y, Cohen DE. Mechanisms of hepatic triglyceride accumulation in non-alcoholic fatty liver disease. J Gastroenterol. 2013;48(4):434-41.
160. Liu S-L, Bae YH, Yu C, Monslow J, Hawthorne EA, Castagnino P, et al. Matrix metalloproteinase-12 is an essential mediator of acute and chronic arterial stiffening. Scientific Reports. 2015;5(1):17189.
161. Guan C, Xiao Y, Li K, Wang T, Liang Y, Liao G. MMP-12 regulates proliferation of mouse macrophages via the ERK/P38 MAPK pathways during inflammation. Exp Cell Res. 2019;378(2):182-90.
162. Nighot M, Ganapathy AS, Saha K, Suchanec E, Castillo EF, Gregory A, et al. Matrix Metalloproteinase MMP-12 Promotes Macrophage Transmigration Across Intestinal Epithelial Tight Junctions and Increases Severity of Experimental Colitis. J Crohns Colitis. 2021;15(10):1751-65.
163. Amor M, Bianco V, Buerger M, Lechleitner M, Vujić N, Dobrijević A, et al. Genetic deletion of MMP12 ameliorates cardiometabolic disease by improving insulin sensitivity, systemic inflammation, and atherosclerotic features in mice. Cardiovasc Diabetol. 2023;22(1):327.
164. Nenan S, Planquois JM, Berna P, De Mendez I, Hitier S, Shapiro SD, et al. Analysis of the inflammatory response induced by rhMMP-12 catalytic domain instilled in mouse airways. Int Immunopharmacol. 2005;5(3):511-24.
165. Gabrilovich DI. Myeloid-Derived Suppressor Cells. Cancer Immunol Res. 2017;5(1):3-8.
166. Zhao T, Ding X, Du H, Yan C. Myeloid-derived suppressor cells are involved in lysosomal acid lipase deficiency-induced endothelial cell dysfunctions. J Immunol. 2014;193(4):1942-53.
167. Li L, Li M, Jia Q. Myeloid-derived suppressor cells: Key immunosuppressive regulators and therapeutic targets in cancer. Pathology - Research and Practice. 2023;248:154711.
168. Le Page A, Khalil A, Vermette P, Frost EH, Larbi A, Witkowski JM, et al. The role of elastin-derived peptides in human physiology and diseases. Matrix Biol. 2019;84:81-96.
169. Fulop T, Jr., Larbi A, Fortun A, Robert L, Khalil A. Elastin peptides induced oxidation of LDL by phagocytic cells. Pathol Biol (Paris). 2005;53(7):416-23.
170. Labat-Robert J, Fourtanier A, Boyer-Lafargue B, Robert L. Age dependent increase of elastase type protease activity in mouse skin: Effect of UV-irradiation. Journal of Photochemistry and Photobiology B: Biology. 2000;57(2):113-8.

171. Smith ER, Tomlinson LA, Ford ML, McMahon LP, Rajkumar C, Holt SG. Elastin Degradation Is Associated With Progressive Aortic Stiffening and All-Cause Mortality in Predialysis Chronic Kidney Disease. Hypertension. 2012;59(5):973-8.
172. Petersen E, Wågberg F, Angquist KA. Serum concentrations of elastin-derived peptides in patients with specific manifestations of atherosclerotic disease. Eur J Vasc Endovasc Surg. 2002;24(5):440-4.
173. Szychowski KA, Gminski J. Elastin-derived peptide VGVAPG affects the proliferation of mouse cortical astrocytes with the involvement of aryl hydrocarbon receptor (Ahr), peroxisome proliferator-activated receptor gamma (Ppargamma), and elastin-binding protein (EBP). Cytokine. 2020;126:154930.
174. Szychowski KA, Gminski J. The Elastin-Derived Peptide VGVAPG Does Not Activate the Inflammatory Process in Mouse Cortical Astrocytes In Vitro. Neurotox Res. 2020;37(1):136-45.
175. Hocine T, Blaise S, Hachet C, Guillot A, Sartelet H, Maurice P, et al. Lactosylceramide induced by elastin-derived peptides decreases adipocyte differentiation. J Physiol Biochem. 2020;76(3):457-67.
176. Iyer RP, Patterson NL, Zouein FA, Ma Y, Dive V, de Castro Bras LE, et al. Early matrix metalloproteinase-12 inhibition worsens post-myocardial infarction cardiac dysfunction by delaying inflammation resolution. Int J Cardiol. 2015;185:198-208.
177. Lee PY, Wang J-X, Parisini E, Dascher CC, Nigrovic PA. Ly6 family proteins in neutrophil biology. J Leukoc Biol. 2013;94(4):585-94.
178. Jenne CN, Urrutia R, Kubes P. Platelets: bridging hemostasis, inflammation, and immunity. International Journal of Laboratory Hematology. 2013;35(3):254-61.
179. Kim WM, Huang YH, Gandhi A, Blumberg RS. CEACAM1 structure and function in immunity and its therapeutic implications. Semin Immunol. 2019;42:101296.
180. Markel G, Lieberman N, Katz G, Arnon TI, Lotem M, Drize O, et al. CD66a interactions between human melanoma and NK cells: a novel class I MHC-independent inhibitory mechanism of cytotoxicity. J Immunol. 2002;168(6):2803-10.
181. Satoh T, Nakagawa K, Sugihara F, Kuwahara R, Ashihara M, Yamane F, et al. Identification of an atypical monocyte and committed progenitor involved in fibrosis. Nature. 2017;541(7635):96-101.
182. Huang YH, Zhu C, Kondo Y, Anderson AC, Gandhi A, Russell A, et al. CEACAM1 regulates TIM-3-mediated tolerance and exhaustion. Nature. 2015;517(7534):386-90.
183. Kammerer R, Hahn S, Singer BB, Luo JS, von Kleist S. Biliary glycoprotein (CD66a), a cell adhesion molecule of the immunoglobulin superfamily, on human lymphocytes: structure, expression and involvement in T cell activation. Eur J Immunol. 1998;28(11):3664-74.
184. Nakajima A, Iijima H, Neurath MF, Nagaishi T, Nieuwenhuis EE, Raychowdhury R, et al. Activation-induced expression of carcinoembryonic antigen-cell adhesion molecule 1 regulates mouse T lymphocyte function. J Immunol. 2002;168(3):1028-35.
185. Chen D, Iijima H, Nagaishi T, Nakajima A, Russell S, Raychowdhury R, et al. Carcinoembryonic antigen-related cellular adhesion molecule 1 isoforms alternatively inhibit and costimulate human T cell function. J Immunol. 2004;172(6):3535-43.
186. Yu Q, Chow EM, Wong H, Gu J, Mandelboim O, Gray-Owen SD, et al. CEACAM1 (CD66a) promotes human monocyte survival via a phosphatidylinositol 3-kinase- and AKT-dependent pathway. J Biol Chem. 2006;281(51):39179-93.
187. Nittka S, Günther J, Ebisch C, Erbersdobler A, Neumaier M. The human tumor suppressor CEACAM1 modulates apoptosis and is implicated in early colorectal tumorigenesis. Oncogene. 2004;23(58):9306-13.
188. Ducker TP, Skubitz KM. Subcellular localization of CD66, CD67, and NCA in human neutrophils. J Leukoc Biol. 1992;52(1):11-6.

189. Gray-Owen SD, Dehio C, Haude A, Grunert F, Meyer TF. CD66 carcinoembryonic antigens mediate interactions between Opa-expressing Neisseria gonorrhoeae and human polymorphonuclear phagocytes. Embo j. 1997;16(12):3435-45.
190. Pan H, Shively JE. Carcinoembryonic antigen-related cell adhesion molecule-1 regulates granulopoiesis by inhibition of granulocyte colony-stimulating factor receptor. Immunity. 2010;33(4):620-31.
191. Hirao H, Kojima H, Dery KJ, Nakamura K, Kadono K, Zhai Y, et al. Neutrophil CEACAM1 determines susceptibility to NETosis by regulating the S1PR2/S1PR3 axis in liver transplantation. J Clin Invest. 2023;133(3).
192. Liu J, Di G, Wu CT, Hu X, Duan H. CEACAM1 inhibits cell-matrix adhesion and promotes cell migration through regulating the expression of N-cadherin. Biochem Biophys Res Commun. 2013;430(2):598-603.
193. Li M, Lin C, Leso A, Nefedova Y. Quantification of Citrullinated Histone H3 Bound DNA for Detection of Neutrophil Extracellular Traps. Cancers (Basel). 2020;12(11).
194. Fox S, Leitch AE, Duffin R, Haslett C, Rossi AG. Neutrophil apoptosis: relevance to the innate immune response and inflammatory disease. J Innate Immun. 2010;2(3):216-27.
195. Marchant DJ, Bellac CL, Moraes TJ, Wadsworth SJ, Dufour A, Butler GS, et al. A new transcriptional role for matrix metalloproteinase-12 in antiviral immunity. Nat Med. 2014;20(5):493-502.
196. Zinatizadeh MR, Schock B, Chalbatani GM, Zarandi PK, Jalali SA, Miri SR. The Nuclear Factor Kappa B (NF-kB) signaling in cancer development and immune diseases. Genes Dis. 2021;8(3):287-97.

Appendix

Figures	Licensed content publisher and granted license number
Figures 13-15 and 17-23	Permission is not required. The article is available under the terms of the Creative Commons Attributed License (CC BY 4) and I am free to share and adapt the material. The article is available under DOI: 10.3390/ijms252011001